Open your mind. LUT.
Lappeenranta University of Technology

Eidgenössische Technische Hochschule Zürich
Swiss Federal Institute of Technology Zurich

Master's Thesis in Chemical Engineering

LUT Chemistry, Lappeenranta University of Technology (LUT)

Department of Chemistry and Applied Biosciences, Swiss Federal Institute of Technology (ETH Zurich)

Large Scale Synthesis of Microdroplets for Biomedical Applications

By:

Afshin Abrishamkar

Examiners:

Prof. Tuomo Sainio (LUT)

Prof. Andrew deMello (ETH Zurich)

Supervisors:

Dr. Robert Wootton (ETH Zurich)

Dr. Katherine Elvira (ETH Zurich)

ABSTRACT

Author: Afshin Abrishamkar

Title of thesis: Large Scale Synthesis of Microdroplets for Biomedical Applications

Examiners: Prof. Tuomo Sainio (LUT)
Prof. Andrew deMello (ETH Zurich)

Faculty: Faculty of Technology (LUT)
Department of Chemistry and Applied Biosciences (ETH Zurich)

Year: 2013

Master's Thesis Lappeenranta University of Technology (LUT)
Swiss Federal Institute of Technology (ETH Zurich)
140 pages, 65 figures, 2 tables and 13 appendixes

Keywords: Microdroplet generation, bulk microdroplet, droplet breakup simulation, 3D printer, Taylor-Couette flow.

Droplet-based microfluidics is a continuously growing field of research that is emerging as an interdisciplinary branch of science due to its wide range of applications. Microdroplets are of interest as commodities in themselves for various applications such as biological, chemical, biomedical and medical systems. However, the production of large quantities of monodisperse homogeneous droplets for such processes is an area that has been always very challenging. This study focuses on two method of high-throughput generation of

microdroplets. In the first method, the bulk generation of microdroplets of water into FC-40 oil through a multi-layer microfluidic device is investigated. As a result, the best protocol for fabrication of a multi-layer PDMS device, followed by different proper designs for a multi-array microfluidic module, equipped with eight identical flow-focusing devices, are obtained. Moreover, the effective exploitation of a 3D printer in order to fabricate a multi-layer microfluidic device is represented. Whereas the second method takes advantage of Taylor-Couette flow pattern where a double-cylinder device, undergoing the aforementioned pattern, is optimized, designed and further constructed for the experimental investigations. The other accomplishment of this work lies in the exploitation of simulation to survey the droplet generation phenomenon. Consequently, the correct practical procedure for the simulation of a droplet generation system utilizing the software COMSOL Multiphysics® is studied and determined. Subsequently, a particular flow-focusing microdroplet generator is effectively simulated utilizing the same software leading to the numerical investigation on the effect of the input velocities ratio on the microdroplets size within the desired microdroplet generator.

ACKNOWLEDGEMENT

This master's thesis has been conducted as a visiting student program at Department of Chemistry and Applied Biosciences of Swiss Federal Institute of Technology (ETH Zurich), in particular, at research group of Prof. deMello. This study started in March 2013 and completed in September 2013.

First, I would like to thank God almighty for giving me the strength, courage, and health to conduct this project work. Then I am heartily grateful to Prof. Tuomo Sainio, whose promising inspirations, wise advices and encouraging supports made the accomplishment of this thesis possible to me.

Then, I am really indebted to Prof. Andrew deMello and Dr. Robert Wootton for providing me with such an extraordinary opportunity to be working along with them entering the stupendous field of microfluidics. However, I cannot express enough thanks to them for all their kind supports, peerless supervisions and unending comprehensive aids. Also, my profound appreciations also go to Dr. Katherine Elvira for all her numerous precious helps.

Moreover, many thanks are due to every single person at research group of Prof. deMello including Ms. Jennifer Gassmann, Dr. Xavier Casadevall i, Simon, Oliver, Bartosz, Tomasz, Ioannis, Anand, and Dirk to name a few, for all their valuable scientific, technical and intellectual assistances. Also, I would like to thank the staff members of ETH workshop, particularly Mr. Roland Walker for his continued technical support.

Last but not least, I would also like to acknowledge with much deepest appreciation the crucial role of my caring, loving, and supportive parents as well as two brothers, Alireza and Amin. In addition, I wholeheartedly believe that thesis would have never been accomplished without their constant encouragement and perpetual devotion.

Lappeenranta - 05.12.2013

Afshin Abrishamkar

LIST OF SYMBOLS

D	Hydraulic diameter of the Taylor-Couette cell (m)
Di	Diameter of any individual generated droplet (m)
d_p	Mean droplets diameter (m)
N	Number of generated droplets
N_{Ca}	Capillary number
N_{Re}	Reynolds number
N_{we}	Weber number
R	Rate of capturing images (fps)
r_i	Radius of outer cylinder in Taylor-Couette cell (m)
r_o	Radius of inner cylinder in Taylor-Couette cell (m)
S	Standard deviation (m)
U	Velocity of continuous phase (m/s)
Vo	Input velocity of oil (m/s)
Vw	Input velocity of water (m/s)
γ	Interfacial surface tension (N/m)
μ_c	Viscosity of continuous phase (Pa.s)
μ_p	Viscosity of dispersed phase (Pa.s)
ρ_c	Density of continuous phase (kg/m^3)

σ	Monodispersity index
Ω_i	Rotational speed (rad/s)

TABLE OF CONTENTS

LIST OF FIGURES

1 INTRODUCTION

1.1 Microfluidics Science

Fluids behavior in microscopic scale can largely differ from how fluids behave in conventional scale. Possessing over three decades of scientific background, microfluidics is a well-known science and engineering of systems that mainly investigates how these behaviors and properties are varied and how they could be manipulated for various applications under different circumstances.[1-4] Microfluidics field covers the tiny fluidic systems dealing with the small scales typically ranging from a few hundred nanometers to several micrometers.[5, 6] However, for a few particular highly specialized purposes, mainly involving nanotechnology science as well as biology and biomedical issues, a microfluidics system may deal with dramatically tiny scales down to even below 100 nanometers.[7-10] Figure 1.1 schematically depicts the diversity of scales in microfluidics:

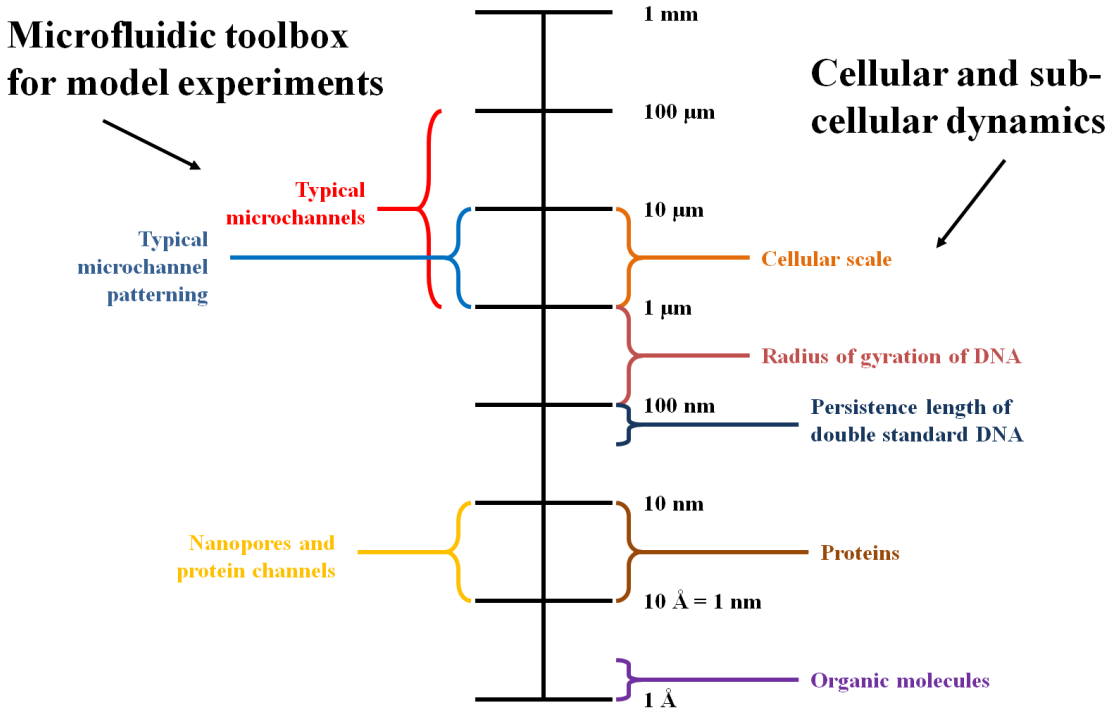

Figure 1.1. Microfluidics scales diversity through different applications.[10, 11]

Also, Figure 1.2. represents a comparative length scales for several different structures particularly for biological ones as well as popular micro-fabrication structures typically used in microfluidic processes.

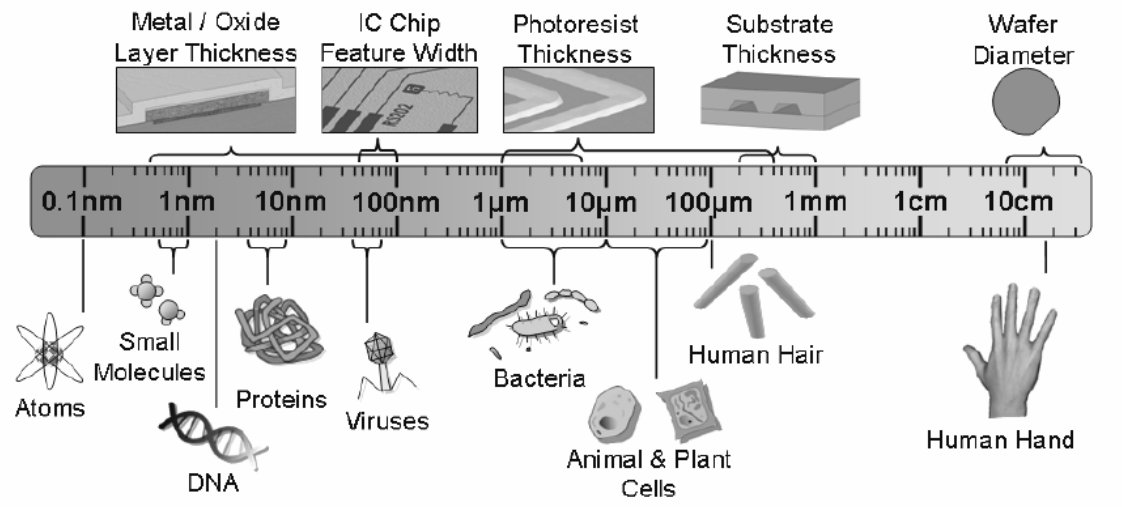

Figure 1.2. Diversity of length scales for various structures in biological as well as micro-fabrication structures.[4]

In other word, microfluidics refers to the branch of engineering for study, manipulation and exploitation of fluidic systems in terms of behavior, characteristics and properties on the nanoliter scale and below.[12, 13] At the small scales, some interesting and unintuitive phenomena are likely to happen what might not be occurred in the same scaled-up systems.[5, 14] In simple language, microfluidics is an emerging science of fluid flows in the microscopic scale with numerous established and relevant applications in various disciplines of science and technology[4, 15]; therefore, microfluidics has become an appropriate multidisciplinary platform leading to progress of several science, technology and engineering.[16]

As the matter of fact, from an historical prospective, some experts believe that microfluidics may be traced back to microelectronics industry as the root of microfluidics[4, 16]; however, some demonstrations imply that the field of microfluidics has been essentially originated from four different fields i.e. molecular biology, molecular analysis, microelectronics and biodefence.[17] Initially, microfluidics extensively appeared

in various chromatography systems such as capillary electrophoresis (CE)[18, 19], gas chromatography (GC)[20, 21], high performance liquid chromatography (HPLC)[22-24] and thin-layer chromatography (TLC)[25]. [4, 17, 26] In these particular cases, the chromatography processes are actually scaled-down to the micro scale and the processes are carried out within the microchips. Presently, microfluidics has been spread through various fields aiming to miniaturization of the systems, reduce the consumption of chemical and reagents for tests and experiments, and provide major parallelization as well as several new phenomena what are not applicable in macro-scale lab works.[17]

At the infancy, every new emerged science or technology come across many challenges to overcome and in microfluidics field, one of the major challenges has been the material selection.[5, 27] In fact, microfluidic devices are typically quite tiny and consequently relatively sensitive[28]; thus, selection of the right and appropriate material for the devices is as of high importance in microfluidics in order for systems to be properly functional toward the desired target.[29, 30] To this end, besides possessing the small scales and tiny features, microfluidic devices have to be sufficiently precise as well.[28, 31]

1.2 Microfluidic Devices

The very early microfluidic devices were predominantly based on glass and silicon substrate[29, 32] since the fabrication methods and procedure of microfluidic devices using these materials were broadly well-known and effectively enhanced.[32] Although these techniques were greatly known and developed, they were still much costly and time consuming; in addition, they require many specialized equipment and facilities to get the process accomplished.[32, 33] In order to overcome these drawbacks, exploration of an alternative for the material used for microfabrication might be drastically crucial. To this end, polydimethylsiloxane (hereinafter refers to as PDMS), an elastomeric polymer with wide range of applications, was extensively introduced as an appropriate alternative for fabrication of microfluidic devices.[4, 32, 34, 35]

Since the introduction of this field, many investigations have indicated the fabrication of microfluidic devices using various polymers (such as PDMS, PMMA, and PC) [27, 36-40]

and also some other comparative investigations were carried out assessing the applicability of various polymers to be used for fabrication of microfluidic devices.[41-43] However, the first attempts reported on the use of PDMS for a microfluidic device fabrication return to the middle of last decade of the 20th century[44-46], since then PDMS has been becoming more popular in microfluidic devices to the extent that PDMS is currently ubiquitous in almost all of the microfluidics devices.[4, 34, 42] In general, manipulation of polymers is quite easy due to their physical and chemical properties[32]; and their use as material for microfluidic fabrication possess numerous advantages such as reducing the complexity, manufacturing costs and required time as well as capability of surface modification and providing relatively wide range of physical and chemical properties.[30, 34] Particularly, PDMS as a substance which is flexible, inexpensive, abundantly available and, more important, optically transparent down to 230 nanometers has been one of the most widely used polymers in microfluidics.[32, 34, 35] Figure 1.3 depicts the schematic structure of a polydimethylsiloxane (PDMS) molecule.

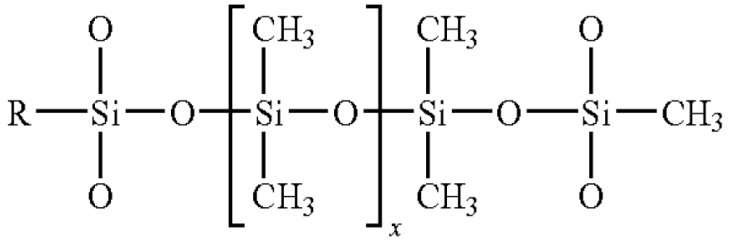

Figure 1.3. Molecular structure of polydimethylsiloxane (PDMS).[47]

1.2.1 Microfluidic device fabrication

In the most common technique of fabrication, polymer (PDMS) is initially prepared and poured over a master mold structure i.e. typically a silicon wafer consisting the inverse photoresist structure of the desired channel geometry printed on its surface using SU-8 by a certain height.[48] Subsequently, the wafer covered by sufficient amount of uncured PDMS should be placed and left into oven typically overnight until the PDMS layer is completely cured and shaped up so that it would be ready for peeling off.[4, 49] Once

casting and curing are fully accomplished, the thin slab of cured PDMS is peeled off from the wafer as is illustrated in Figure 2.4 presented in the respective part under the title of "demolding and peel off the PDMS slab" under section 0.

Figure 1.4 also schematically depicts the procedure of fabrication of a microchip using a silicon wafer, applying master fabrication and making the PDMS device.

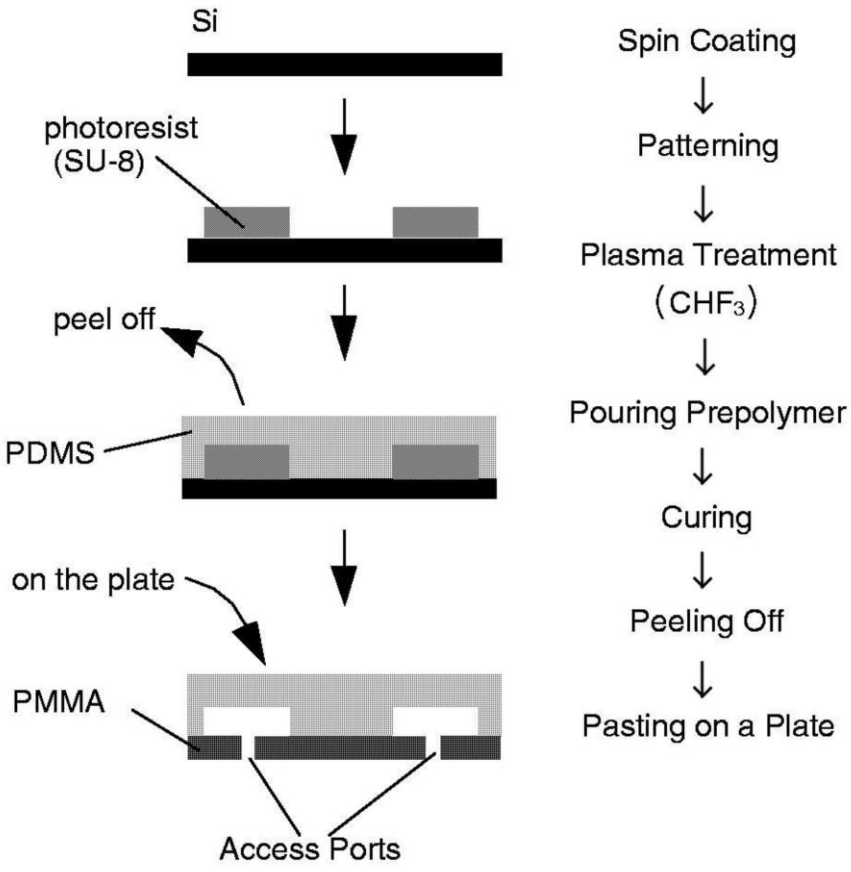

Figure 1.4. Scheme for procedure of microfluidic fabrication of a microchip.[48]

Generally, fabrication of a microfluidic device is the consequence of a multistage process presented as a flowchart in Figure 1.5 starting from a raw idea to the final implementation. However, the described procedure through the following figure is just the most regular and conventional process among the lithography-based methods. Nevertheless, there are several other methods, mostly novel, for the fabrication of microfluidic devices that will be mentioned briefly.

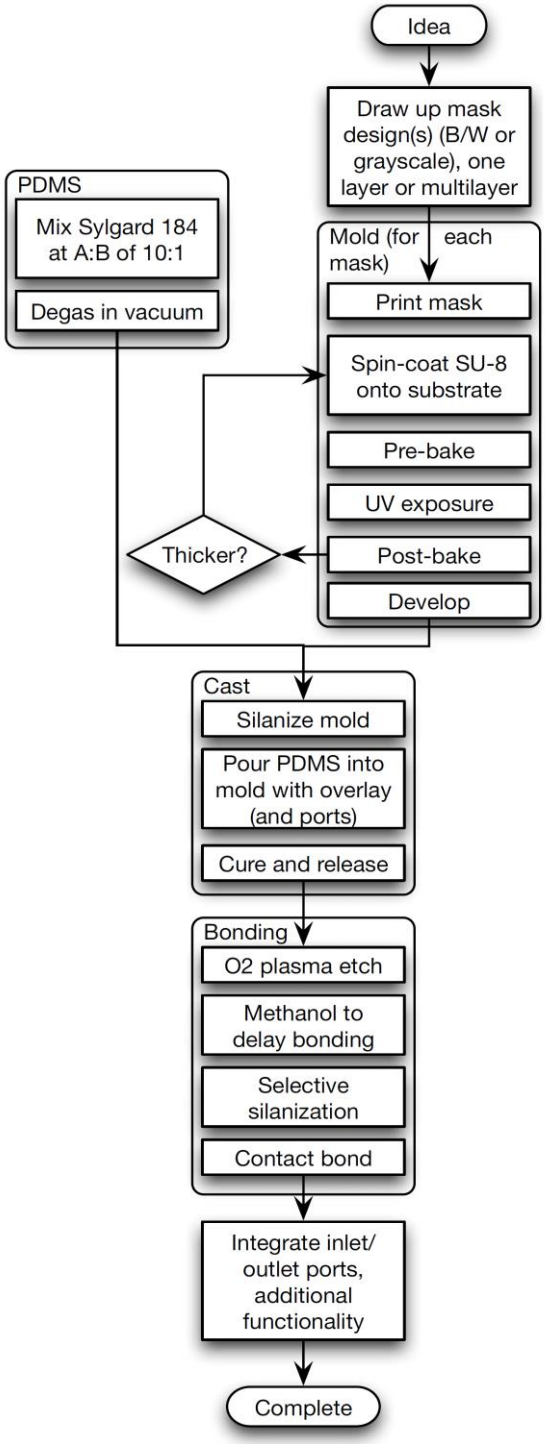

Figure 1.5. A comprehensive procedure for fabrication of a microfluidic device using PDMS from A to Z.[34]

Moreover, there have been several various investigations recently reporting the alternative methods for microfluidic device fabrication such as using wafer made of phosphor bronze

(PB) (instead of silicon wafer)[50, 51], fabrication by printing the master directly on a transparency using a novel photocopying machine[52], a wax printer[53] or even an office laser printer[54], and more interestingly fabrication of paper-based microfluidic devices[55, 56] as the novel methods.

In this process, making a PDMS device begins from an idea stating the final purpose of the task. To that end, the idea must be interpreted graphically and be drawn utilizing a computer aided drawing tool e.g. AutoCAD®.[35] Then taking the advantage of photography process, the design is printed in inverse mode on a so-called photolithography mask[57] what is later used for the fabrication of the silicon wafer undergoing some photolithography process.[39, 58] Once the wafer is fabricated under certain circumstances, PDMS is poured over, casted and cured until become a relatively rigid and stable slab. Then, the further post-processing operation (cutting, spin coating, bonding, etc.) may be accomplished.[4, 49]

The further detailed information in this regard will be provided through upcoming chapters and sub-chapters accordingly.

1.2.2 Microfluidic device design

As previously discussed, the first step to make a microfluidic device is to draw a suitable design complying with the desired target of the device, which is supposed to be fabricated. To that end, taking into account the physical and chemical properties of the systems and materials to be used, a design is typically created and fulfilled according to the demands of the microfluidic system and is further drawn utilizing various types of computer aided program e.g. AutoCAD®.[34, 35] The layout of mask could be technically modified and revised whenever later on as well; though, that will be subject to replication of all the fabrication stages (including mask preparation, master fabrication, PDMS casting, device making and post-processing operations) once again. Therefore, the more precise and proper the mask is designed, the less effort and iteration will be needed afterwards, and consequently, the less time and cost will be spent.[59] The layouts are normally drawn as the two-dimensional objects and accordingly, the photolithography masks are also printed

as the two-dimensional sheets. Then later, the two-dimensional designs are actually extruded to a certain thickness (i.e. the height of the microchannels) while fabricating the master (wafer) using the photolithography mask that leads to a three dimensional structure.[39, 48]

Figure 1.6. Fabrication steps of a PDMS microfluidic device from initial layout to master fabrication and eventually making PDMS device.[60]

1.2.3 Mask preparation

The second step in fabrication of a microfluidic device is to prepare a photomask out of a layout drawn by AutoCAD®.[35, 61] A photomask is a high-resolution opaque plate or film that contains dark and unalterable solid-state holes and transparent features that further allow light to shine through during the fulfillment of photolithography process.[32, 62, 63] Furthermore, these photomasks are also useable for several other applications in many different industries.[64-67]

There are three sorts of different base material what might be used to make photomasks i.e. soda lime glass[68], fused silica (Quartz)[69] and polyester film[70]. The first two are more widely used to make photomasks; whereas, soda lime is the most common substrate

due to its quality and economic superiority. The typical masks size may vary in the range of 15-45 square centimeters.[71]

Mask preparation is typically fulfilled in specialized companies equipped with the required facilities by which the photomasks are made with the precision of down to 10 micrometers or even less. Figure 1.7 illustrates a typical photolithography mask coming out of the printing facility right after being made.[71] Mask preparation is a vital step in microfluidic fabrication process since even any very tiny mistake, whether originated from design or in publishing procedure, will later lead to a defective master and the entire microfabrication process is subject to be repeated all over again from the scratch![59]

Figure 1.7. A commercial photomask printer while printing a photolithography mask.[71]

Also, Figure 1.8 depicts a layout drawn by AutoCAD® for several simple tiny microfluidic devices and the appropriate fabricated photomask according to the drawn layout. The plus-like signs appeared on the layout, and consequently on the photomask as well, are called alignment marks.[61, 72] These alignment marks are drawn at the same positions of different layers of a multilayer microfluidics device, at where the different layers are supposed to be placed over each other. Subsequently, these marks along with the

microchannels appear on the surface of the further cured PDMS slab facilitating the alignment process particularly in the sensitive cases or when high precision alignment is needed.[73, 74]

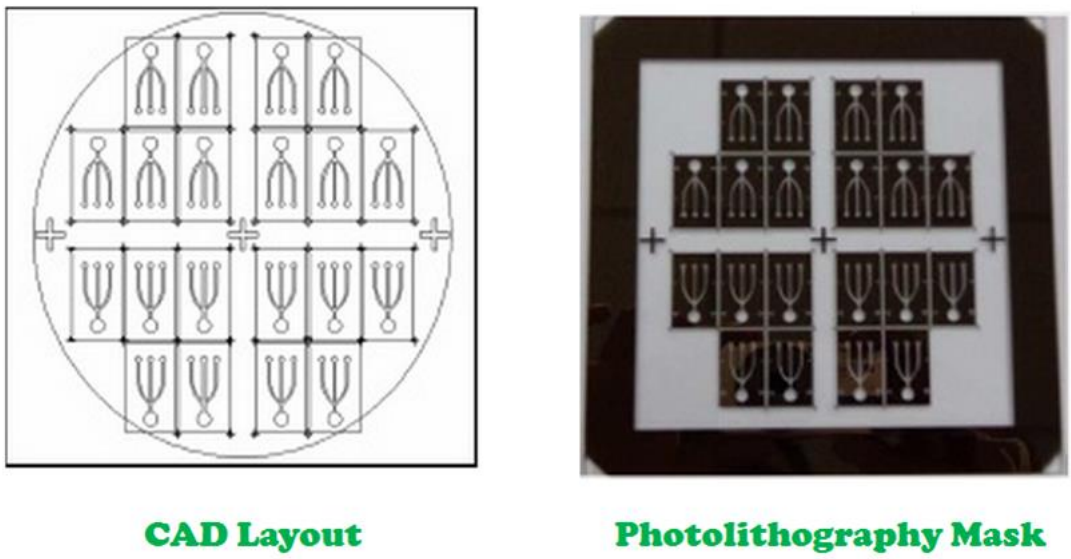

Figure 1.8. A drawn CAD layout for microfluidic devices and the photomask fabricated accordingly.[61]

1.2.4 Master fabrication

Once the photomask was prepared, the master should be fabricated according to that utilizing the specialized facilities through high precision processes up to the clean room standard. Master (wafer) is referred to a metallic micromold, which is fabricated based on a photolithography mask (photomask) and used to make polymeric devices.[42, 48] To that end, there are different possible methods of fabrication whether lithography-based techniques or non-lithography ones, which are mainly based on laser e.g. “laser micromachining, microwelding and molding (LCWM)”[75, 76] and “laser micromachining, hot embossing and molding (LHEM)”[77]. Moreover, there are a couple of various techniques known for lithography process such as photolithography[34, 35], extreme ultraviolet lithography[78], soft-lithography[39, 58], magnetolithography[79], and nanoimprint lithography[80, 81]. Also, in another alternative non-lithography method,

utilizing a 3-D printer and having the device designed in 3-D in AutoCAD®, the master will be printed and fabricated directly with no need for a photomask.[32, 82, 83]

The most widely used technique in this regard is photolithography, also known as UV lithography or optical lithography.[58] As Figure 1.9 depicts in a very simple way, the photolithography is a process applied in microfluidic in order to transfer a geometric pattern from a photomask to a substrate coated with a light-sensitive material and remove some parts from a thin film.[4, 58, 84] However, there have been also several attempts on accomplishment of lithography without any photomask i.e. so-called maskless lithography[85] that are mainly based on use of multiple electron beams.[84, 86]

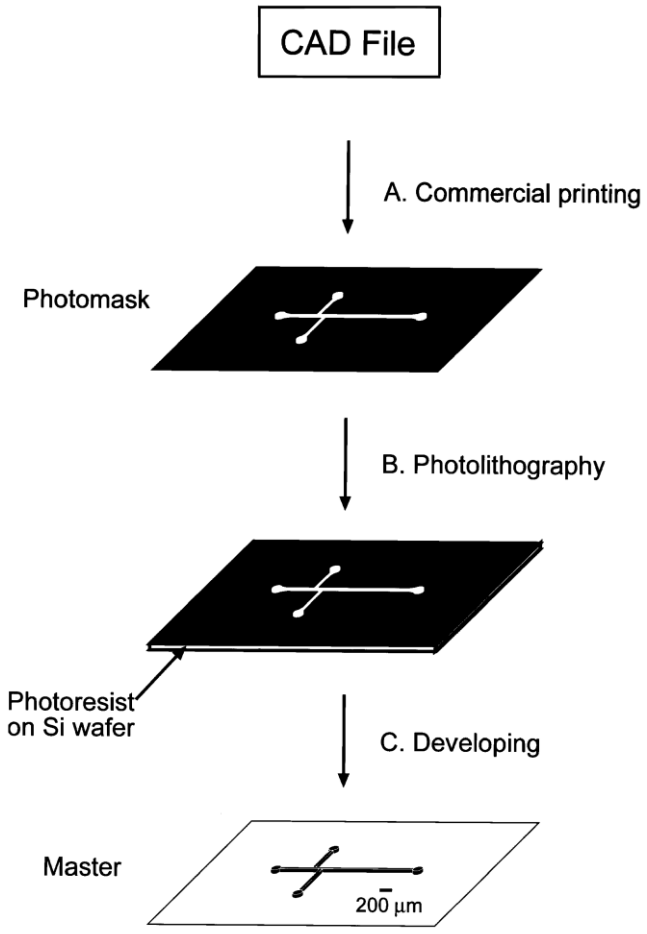

Figure 1.9. A simple scheme for fabrication stages of a microfluidic master.[39]

In other words, photolithography process may be divided into four steps i.e. pre-exposure bake, exposure, post-exposure bake and development. In photolithography process, a silicon wafer (as the most commonly used platform) is used as the substrate.[58] Figure 1.10 schematically illustrates the consecutive stages for master fabrication.

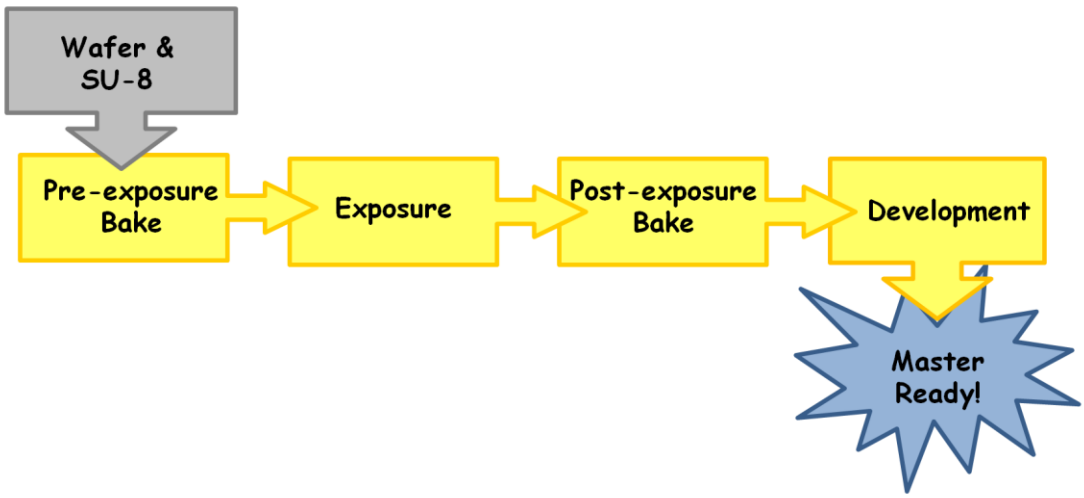

Figure 1.10. Master fabrication stages from scratch toward final step.

In the pre-exposure stage, a photo-sensitive material so-called photoresist is poured over the wafer gently (to avoid bubble production) and is initially heated up to a certain temperature. This heating helps to remove any remaining solvent and also facilitates the spreading procedure of the photoresist material over the entire surface of silicon wafer due to the high viscosity of the photoresist.[87] SU-8 is a commonly used material as the photoresist which is divided into several different grades possessing slightly different properties.[34, 35, 88] In terms of material properties, SU-8 is a very viscous polymer and an epoxy-based negative photoresist, meaning that makes a negative mask of the original mask (refer to Figure 1.11).[58, 88]

Then, the heated wafer containing photoresist material over its surface undergoes a high precision spin coating process to make sure SU-8 layer is fabricated evenly on the surface of silicon wafer and according to the desired height.[88, 89] The rotational speed and the

specifications of spin coater as well as the grade of SU-8 to be used vary from case to case according to the desired height for the target master.[89, 90]

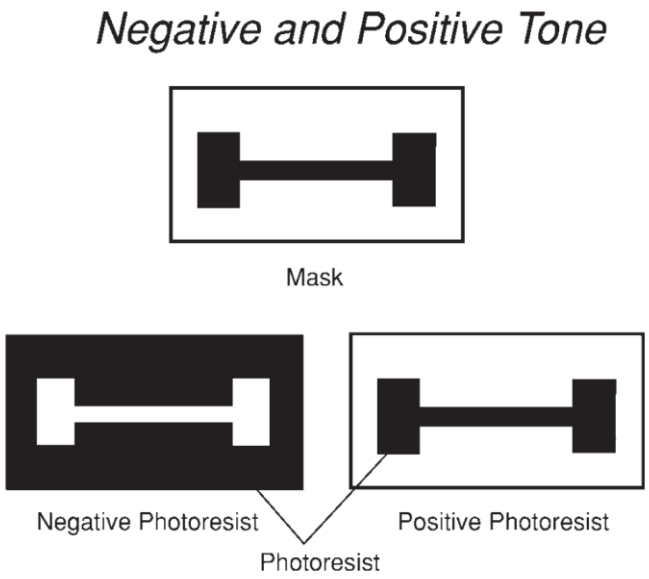

Figure 1.11. Remaining pattern after exposure and fuifillment of development of a positive and negative photoresist.[58]

After spin coating and pre-exposure bake, the coated wafer must be slowly cooled to room temperature in order to be ready for exposure.[91] After that, the appropriate photomask is attached over a glass plate and placed into the exposure machine as well as the wafer with SU-8 coated surface, so that the photomask would be placed between the exposure source and the wafer.[4, 34, 91] Subsequently, the exposure is accomplished and the lights shine through the mask toward the wafer. The exposure time may also vary based on the desired thickness for the master.[92] Since SU-8 is a negative photoresist; the exposed areas will cross-link and permanently remain after the development stage.[4, 87, 93]

After the exposure, the wafer must be heated up again over a hot plate for several minutes so that the patterns start to stand out and stabilize. During this process, the film may be bubbly; however, the bubbles are never placed on the structures and are between them and therefore, there is no need to be worried about the bubbles at this stage. This stage is called post-exposure bake.[34, 87]

At the final step i.e. development, the wafer is placed into the bath of a SU-8 developer for a few minutes. The most widely used SU-8 developer is propylene glycol methyl ether acetate (PGMEA).[91, 92] After a few minutes, the patters on the wafer appear and become visible gradually. Then the wafer is just rinsed in developer and dried by blowing air and eventually the appropriate master is fabricated.[87, 88, 92]

Figure 1.12 shows a complete process flow for a basic photolithography technique for a process in which the photoresist is a permanent part of the final desired device.

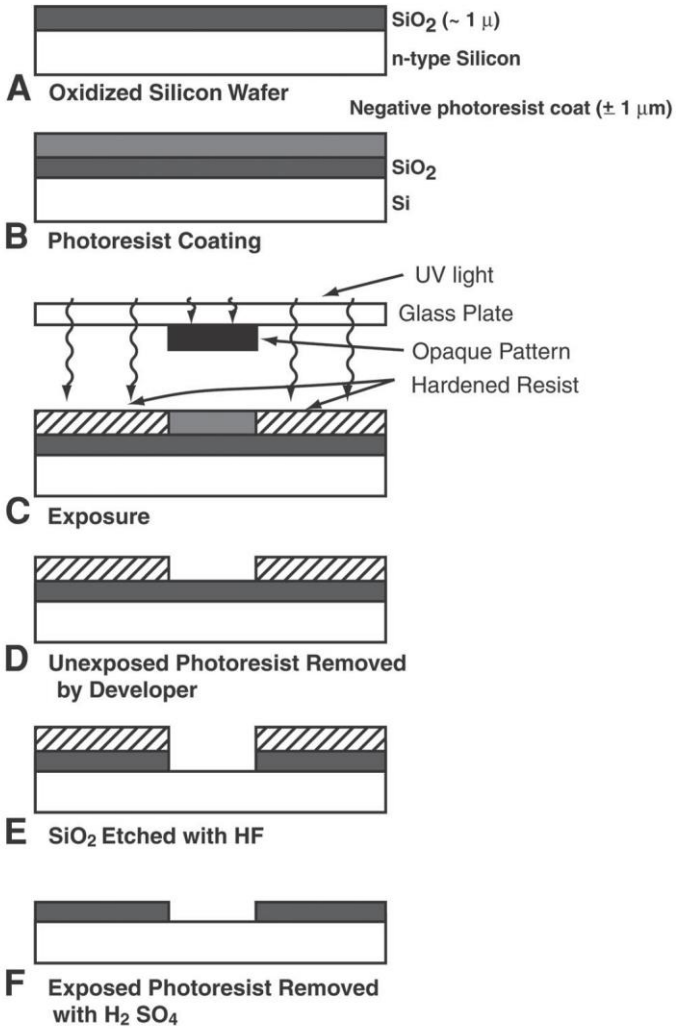

Figure 1.12. Detailed process flow of a complete photolithography for the case at which photoresist is a permanent element of the final device. (A and B) pouring photoresist material (SU-8) over wafer, (C) exposure, (D, E, and F) development. [58]

1.3 Purpose of the work, methods and limitations

In this work it has been endeavored to generate microdroplets at high-throughput rates through study and implementation of two different methods of generation. To that end, two different methods of droplet formation were taken into account that in first method the droplet generation takes place through a well-known and advanced designed microfluidic device undergoing flow-focusing technique.[94]

To accomplish this method, a multi-layer PDMS module is required to be designed and fabricated. In terms of fabrication procedure, the imprinted photomask is used to make a silicon master utilizing a microfabrication process. Then, the PDMS devices are casted against the fabricated masters and finally the multi-layer module is fabricated as a result of accurate bonding of the fabricated PDMS devices. Due to the massive size of the PDMS chips (devices), it is not possible to perform the bonding process by oxygen plasma bonding, and instead, the corona discharge device is utilized. All the necessary techniques regarding the fabrication of a PDMS microfluidic device will be extensively described through chapter 2. Also, the massive size of the design resulted in another limitation factor that was complexity and difficulty of microfabrication of the silicon master out of the desired photomask since its features and microchannels were much likely to be removed during the fabrication process or post exposure development process. Due to the safety issue, the light intensity of the high-speed camera is always retained at the lowest available rate (i.e. 30% intensity).

The second method concerns the formation of microdroplets utilizing a concentric double-cylinder undergoing Taylor-Couette flow pattern, where the inner cylinder is rotatable and driven by a motor while the outer one is fixed and transparent. The droplets are formed using rotational force within the gap area between two cylinders.[95] This topic will be also explained broadly in section 5. For that method, two pumps and a motor have been ordered and purchased according to the need and the double-cylinder device was modelled and optimized. Subsequently, based on the obtained optimized dimensions, the whole assembly was designed and further constructed for the experimental investigations.

Noteworthy that unless otherwise mentioned or cited, all the pictured from laboratory equipment and the experiments used in this thesis have been taken at the laboratory of Prof. deMello group at ETH Zurich.

2 PDMS DEVICE FABRICATION AND DROPLET FORMATION

2.1 PDMS Device Fabrication

When the master is fabricated, a polymeric device should be made by casting out of the fabricated master. As previously discussed, the most popular polymer for fabrication of microfluidic devices is PDMS.[4, 34, 42] Several different stages are involved in preparation of a microfluidic device i.e. enlisted as below in the chronological order of fulfillment in the experiment:

- Gas phase silanization of surfaces
- PDMS preparation and dispense
- PDMS degassing
- PDMS curing
- Demolding and peel off the PDMS slab
- Hole punching
- Plasma bonding
- Spin coating
- Post-bonding treatment

Majority of the above mentioned stages are essential and have to be carried out; however, a few of them i.e. “spin coating” and “post-bonding treatment” are optional and are accomplished just in the cases that are needed. Moreover, PDMS degassing may also be done either before dispensing over the wafer [41, 74], or after doing so [96], or even at both turns to make sure there is no bubble left [92] depending on the individual preference. The stages and techniques are further explained in details.

2.1.1 Gas phase silanization of surfaces

To begin the fabrication of PDMS device, the first task to do is the surface silanization of master. Silanizing the master is crucial since a silicon surface typically shows high adherence to polymers, particularly PDMS, that result demolding and peeling off the cured PDMS would be more difficult afterwards.[93, 96] The process of silanization helps to prevent PDMS sticking to the master and is normally carried out at room temperature and either under vacuum or at atmospheric pressure. There are a couple of different silane chemicals suitable for this purpose (i.e. surface silanization) which allow passivation of the surfaces such as dichloromethylsilane [97, 98], chlorotrimethylsilane [93, 99], hexamethyldisilazane [100], and dimethyloctadecylchlorosilane[34, 101].[58] However, the most common one among them is "Trimethylsilyl Chloride" also known as "Chlorotrimethylsilane" with the molecular formula of $(CH_3)_3SiCl$ (usually abbreviated as Me_3SiCl)[102] i.e. a highly corrosive and toxic liquid substance which causes skin burns and is respiratory irritant![103] Thus, its handling must be done with extreme caution under the fume hood.

Silanization process starts by placing the master into a desiccator located inside a fume hood. The complete protocol for silanization is as follow:

1. Place the master(s) into the desiccator located inside the fume hood;
2. Pour a few drops of chlorotrimethylsilane (~50µl per master) in the specific vessel and place it in the desiccator;
3. Close the lid of desiccator and turn on the vacuum;
4. Leave the system to be under vacuum for about one hour;
5. After one hour, equilibrate the pressure in desiccator slowly;
6. Open the desiccator and take out the master(s).

Prior to place the masters in the desiccator, they might be air blown or even, for more precision, cleaned by isopropanol and air dried. During the silanization process, chlorotrimethylsilane covers and coated all the exposed surfaces within the designated area that concerns the entire interior volume of desiccator. This surface coating makes the surface of master hydrophobic and reduces the adhesion of PDMS to the silicon surface as well as the SU-8 patterns fabricated on the master.[41, 96] Bear in mind that chlorotrimethylsilane has relatively low vapor pressure at ambient temperature and therefore vaporize at room temperature under slight negative pressure easily and as mentioned earlier, must be used only under the fume hood. Figure 2.1 also depicts the different stages of gas phase silanization process as is accomplished empirically in the laboratory.

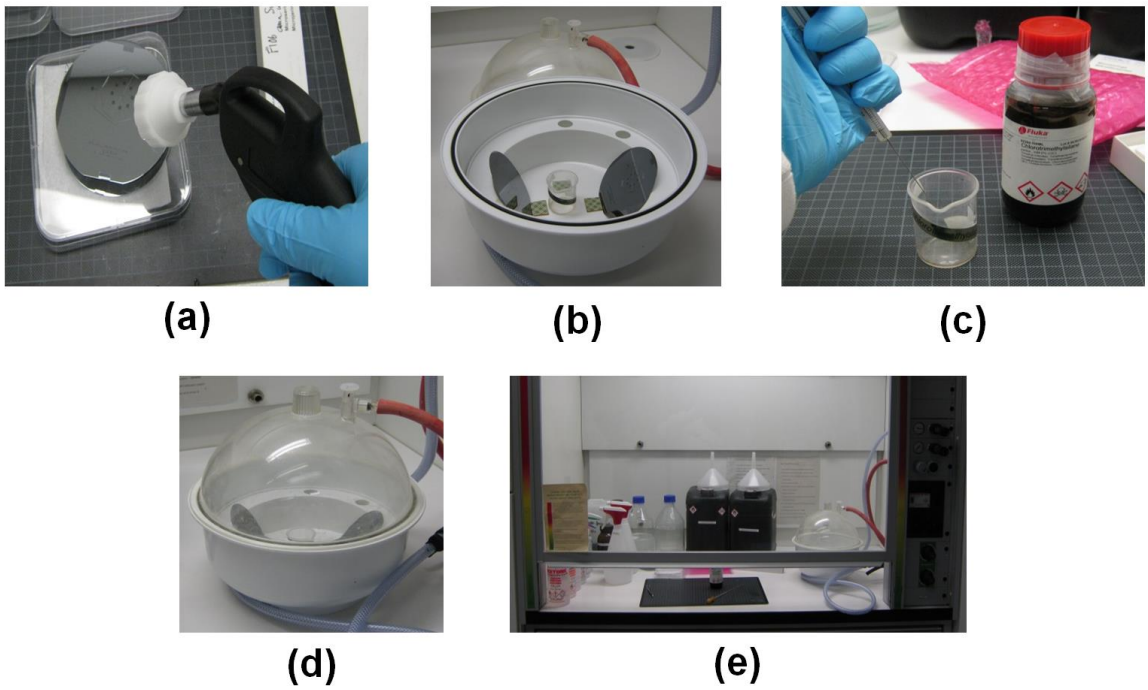

Figure 2.1. Different steps of gas phase silanization of surfaces. (a) Cleaning the master by blowing air, (b) placing the cleaned masters in the desiccator, (c) pouring desired amount of chlorotrimethylsilane into the assigned beaker, (d) placing the beaker inside and closing the lid of desiccator, and (e) turning on the vacuum and leaving the desiccator inside a fume hood.

2.1.2 PDMS preparation and dispense

Taking into account that PDMS cures even at ambient temperature; though slowly, PDMS is typically available as a two-component kit containing two substances including a prepolymer (base) and a cross-linker component (curing agent) which must be mixed together to produce PDMS. [58, 104] The most commercially available two-component kit is Sylgard-184® consisting of a package of silicon elastomer (prepolymer) and a bottle of silicon elastomer curing agent (cross-linker) manufactured by Dow Corning Corporation©. The kit normally contains one kilogram of prepolymer and 0.1 kilogram of curing agent. In order to prepare the PDMD polymer, prepolymer and curing agent might be mixed through different ratios; however, this preparation process normally undergoes the ratio of 10:1 by weight (ratio of prepolymer to curing agent) according to the supplier procedure[105]; though, other ratios such as 3:1[106], 5:1[70] and 8:1[91] have been also reported for some other specific conditions. Here below is the procedure of PDMS preparation using a two-component kit of Sylgard-184®:

1. Prepare an empty plastic cup and weigh it using a balance,
2. Pour a certain amount of prepolymer (Sylgard-184) substance into the cup rather off the balance,
3. Replace the cup containing the prepolymer on balance and take a note of total weight of cup containing prepolymer,
4. Remove cup from the balance and add required amount of curing agent (calculated according to the desired ratio such as 10:1 and 5:1),
5. Take a note of the final weight of cup plus substances,
6. Mix the two compounds with a spatula vigorously for a few minutes until the polymer become ready (that will be recognizable by appearance as well),
7. PDMS is now ready to use!

Noteworthy that, all the above mentioned steps have to be fulfilled under the laminar flow cabinet (ventilated fume hood) in order to avoid entering the particles into the mixture. Although the tasks of adding materials (whether prepolymer or curing agent) could be done either off the balance or on that, the first method (off the balance) is always recommended.

Also, in terms of quantity and as a rule of tongue, about 40 grams of Sylgard-184 is sufficient for one master (what will lead to a PDMS slab of 4-5 mm thick)[58]; however, any other amounts within a reasonable range could be also used in cases a certain amount of polymer is required for a specific application. Stirring the mixture for around one minute or two is usually enough for preparation of polymer provided that the mixing is accomplished with a reasonably high speed.

When the polymer becomes ready, the next step is to dispense it over the desired master. To this end, a previously silanized master is placed and strictly fixed into a Teflon ring (made of PTFE). The master and its ring are placed horizontally on the table and PDMS is poured over the surface of master. Dispending the polymer at the center of the master from a low altitude as well as proceeding the process slowly will lead to minimization of the possibility of bubble formation in the polymer; though it could be degassed afterwards.[58, 87]

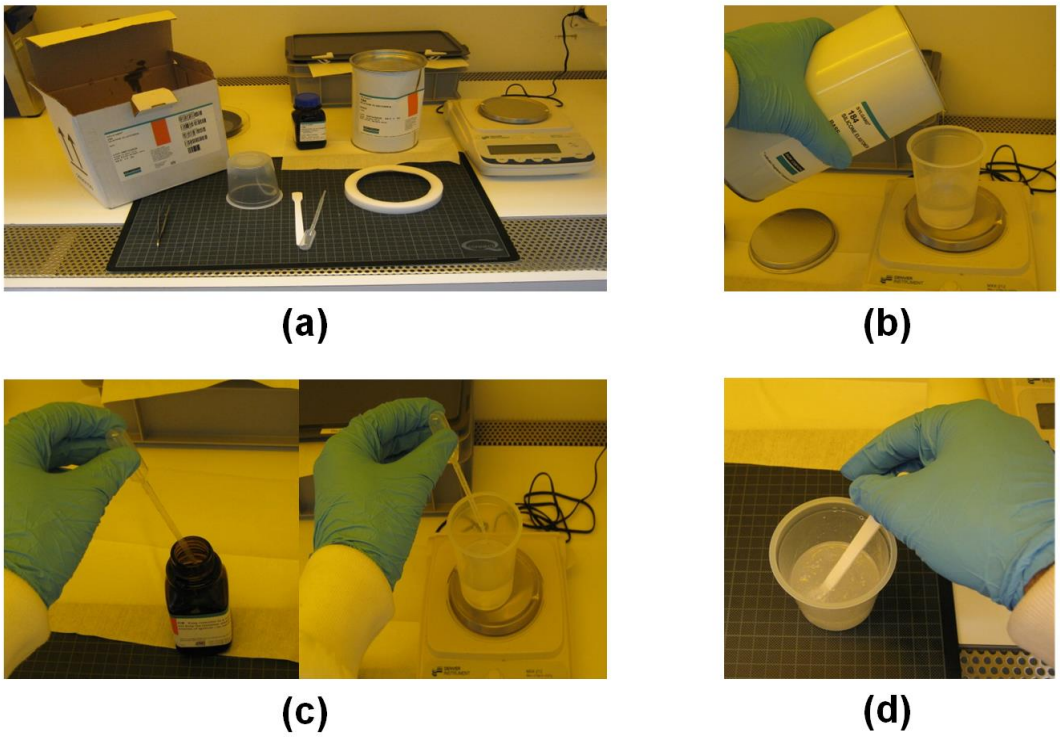

Figure 2.2. Steps for PDMS preparation. (a) Prepare the required substances and facilities, (b) pour prepolymer (Sylgard-184) into the plastic cup, (c) take the required amount of curing agent and add to prepolymer, and (d) stir the mixtue.

When the PDMS is thoroughly poured over the master, the entire molding assembly (ring, master and poured PDMS) might be tilted at a low angle slowly facilitating the spreading of PDMS to make sure PDMS is dispensed evenly throughout the master.[87] Once the polymer covered throughout the master evenly, the entire system might be placed into a desiccator for degassing.

Figure 2.2 and Figure 2.3 depict the different steps of PDMS preparation process and dispensing process followed by a degassing, respectively.

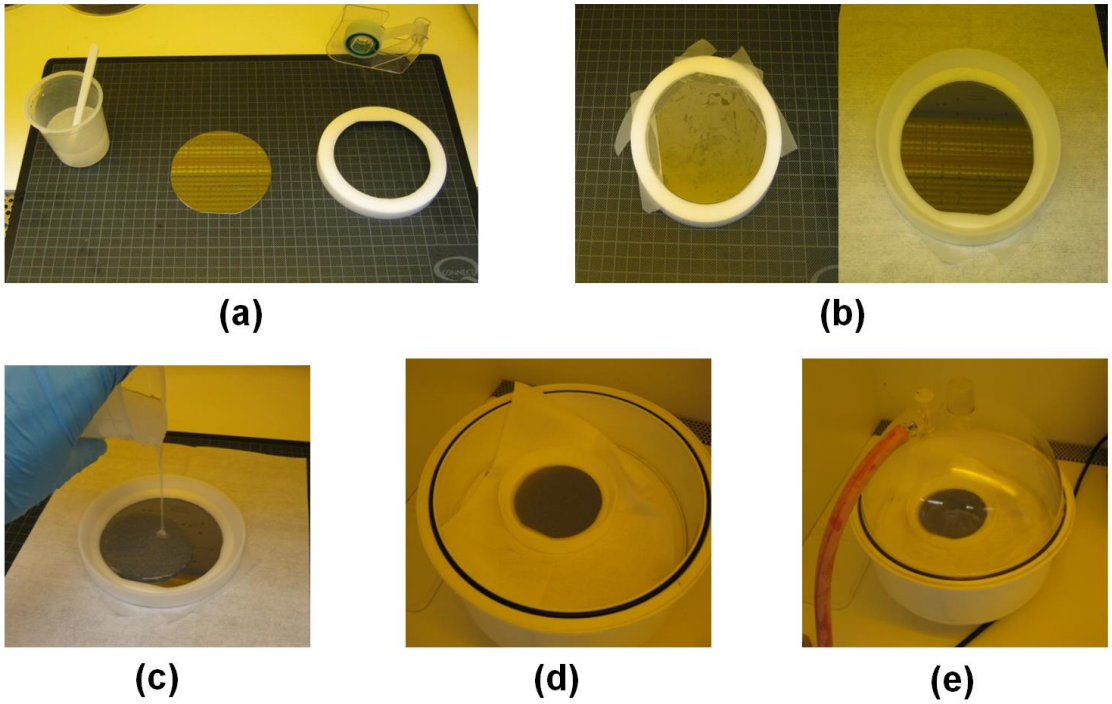

Figure 2.3. Procedure of dispensing PDMS followed by degassing. (a) Prepare the required items, (b) place and fix the master into the ring and turn it around, (c) dispense PDMS over the master, (d) place inside a desiccator, and (e) close the lid and put the desiccator under vacuum.

2.1.3 PDMS degassing

After the mixing, the polymer will be full of air bubbles with different sizes; therefore, needs to be degassed. As previously mentioned, PDMS degassing can be done either before

dispensing over the master [41, 74], or after doing so [96], or even at both turns. This is done by simply placing the entire molding system inside a desiccator under vacuum (to speed the degassing process[96]) and room temperature (Figure 2.3 parts “d” and “e” illustrate the process simply through two pictures). During this degassing process, the bubbles from all over the polymer mixture initially come up to the top surface of mixture and subsequently vanish. The sufficient amount of time should be passed to make sure there is no bubble left on the surface of dispensed PDMS. When the polymer is clear and transparent, the degassing is completely done. Degassing process normally takes around one hour depending on the amount of polymers used for molding and also the pressure of desiccator.[87]

2.1.4 PDMS curing

Sylgard-184 is a heat curing material and cures at even room temperature (~ 25 ºC) up to until around 150 ºC.[87, 105] Once the polymer was completely degassed and is clear and transparent, the mold containing master and PDMS should be placed inside an oven for at least a few hours at around 70 ºC; however, the easiest and most convenient method is to let the PDMS cure inside an oven or at the room temperature for a certain time or even overnight.[51, 74, 77] The required time for curing PDMS may vary according to the slab thickness.[93]

Furthermore, different conventional methods of curing have been reported, which vary according to the desired application. As such, curing at 70 ºC for 48 hours[91] or putting in the first oven at 60 ºC and subsequently in the second one at 95 ºC each for 30 minutes[96] or a combined method i.e. curing in an oven at 95 ºC for 30 minutes followed by curing at room temperature for 24 hours[104]. Also, another research has extensively investigated on the rate of curing and as a result has introduced a novel heated micro-indentation setup for rapid curing of PDMS for microfluidic devices to reduce the required time.[107]

Although the polymerization process begins as soon as both components (prepolymer and curing agent) get in contact together for mixing; heating up the mixture speed up the polymerization process. After the curing, the cured PDMS is recommended to be cooled

off initially prior to peel off.[16, 93] This could be done by just simply leaving the master and PDMS at room temperature for a few hours to cool down gradually that will cause a reduction in the possibility of damage while peeling off. Furthermore, cooling the PDMS will prevent buckling what might be as of important in cases that the microfluidic device possesses an unusual and specific geometry.[81]

2.1.5 Demolding and peel off the PDMS slab

When the cured PDMS cooled down sufficiently, the PDMS slab should be peeled off gently. At that point, having the adequate tools the PDMS slap is easily peeled off and cut. The required tools for this purpose are at least a tweezers, a sharp blade (or a scalpel), and possibly a plastic spatula. There are numerous various types of protocols applied for peeling off the PDMS slab from the master what might be used as long as they take essential considerations into account.

As an example, the entire borders of PDMS slab all around the setup might be detached (or even totally released) from the mold ring slowly within the common area only between PDMS and mold ring using a tweezers (with extreme care not to enter and the area in contact with master and scratch the surface). And holding the detached edge of PDMS slab from any point (by fingers or using a plastic spatula) and applying a slight upward force, the PDMS slab is peeled off gently and gradually starting from a corner and proceeding toward the counterpoint on the opposite side of the slab.[49, 87] Figure 2.4 illustrates a cured PDMS slab while is getting peeled off.

Regarding the direction for peeling the slab away, it is extremely recommended to do so in the direction of channels of microfluidic devices available in the PDMS slab as much as possible, and thereby the tiny features of microfluidic devices are more likely to be removed properly and without damage. Noteworthy, the entire manipulation regarding this step has to be accomplished under the laminar flow cabinet.

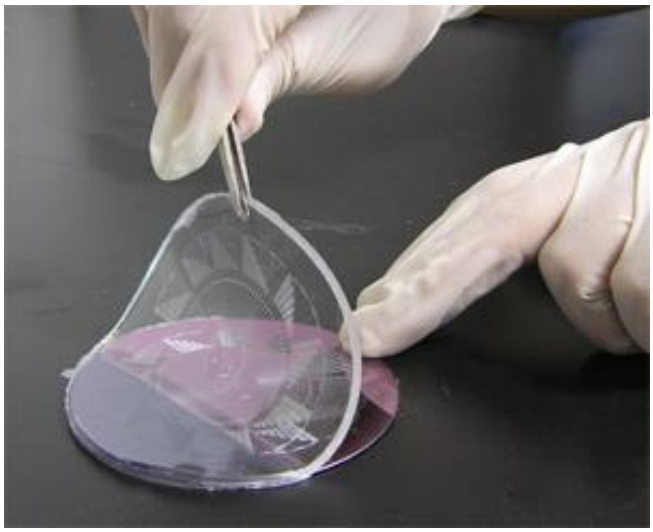

Figure 2.4. Peeling off the cured PDMS slab including the microchannels.[49]

The surface of PDMS slab which consists of the microchannels and features must never be touched. Moreover, throughout the surface of the peeled PDMS slab or at least the area consisting of microchannels and features must be immediately covered by tape after peeling off in order to avoid being touched as well as deposition of any particles on the casted features.[93]

Finally, the PDMS slap might be cut into the smaller desired features (according to the designated area to each section) with extreme care. These smaller target features, cut from the cured PDMS slab, are often called as microfluidic devices of microfluidic chips. In fact, each master (and consequently each PDMS slab) typically includes different numbers of microfluidic devices ranging from one (for a relatively big device) to some (for more tiny devices).

2.1.6 Hole punching

In order to have access to the microchannels, features and patterns of microfluidic device from outside of the PDMS device afterwards, some access ports are needed to be improvised into the PDMS device. Thus, inlets and outlets positions are normally marked, along with the other features, from the early stage of fabrication i.e. drawing the layout of the device. Consequently, they will further appear in the master and also further in the

PDMS slab casted out of the same master. These inlets and outlets are manually punched after demolding using a proper device perpendicular to the surface of PDMS slab and also to the directions of microchannels.[41, 84]

These holes will play the role of access ports (or access holes) and any connection tools (tubing, pin, and etc.) can be inserted into them to connect any external system (located outside of the PDMS device) to the microchannels and features of PDMS device. These access ports are normally placed at the terminals of microchannels. These holes are used to handle the fluids from pumps or manually into the microchannels and from there toward out.[12, 27] The holes might be punched using either hole-punching machine or manual puncher. As an alternative for punching method, the holes may be also made through drilling using a micro-drill machine.

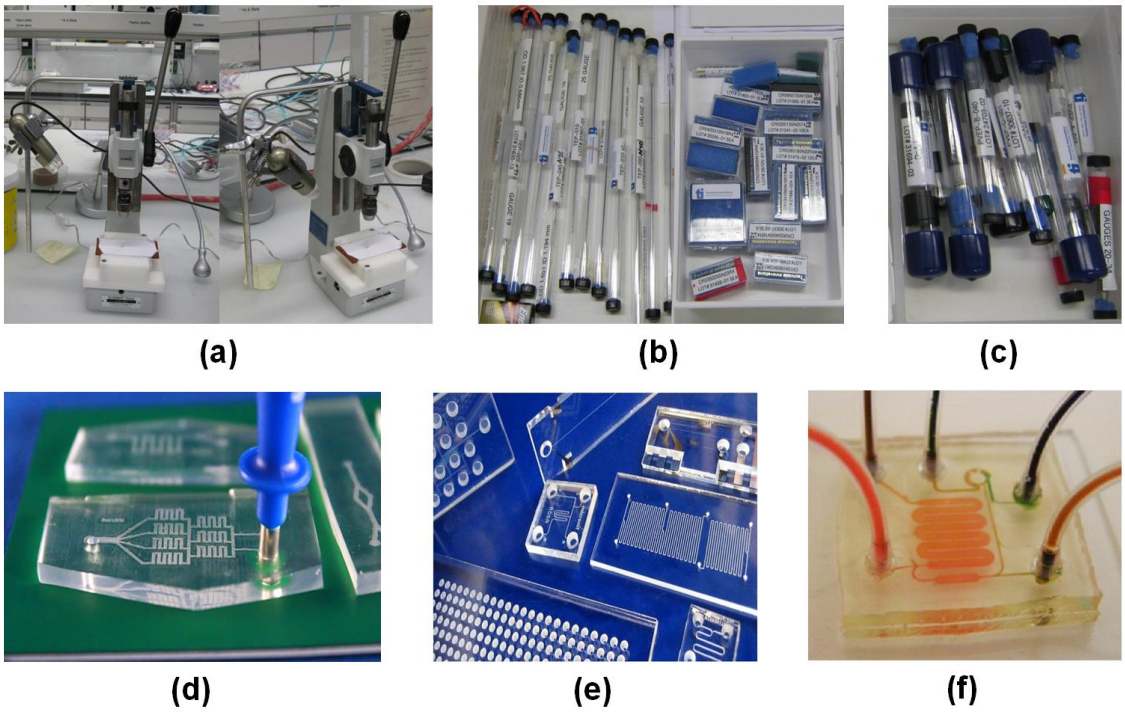

Figure 2.5. Hole punching in PDMS microfluidic devices. (a) A hole-punching maching equipped with a light source, (b) required accessories for hole-punching machine i.e. gauge or ejector (left) and punching pins (right), (c) manual puncher with accessories, (d) a microfluidic device getting hole-punched[108], (e) samples of punched microfluidic chips[109], and (f) a microfluidic device under operation with tubing inserted into the punched holes[110].

The procedure of punching is as easy as making a simple hole in the PDMS slab using any tool provided that the proper ejector and punching pin, in terms of both type and size, is selected. The size of ejector and punching pin is typically selected according to the specifications of the tubing which is supposed to be inserted through the intended hole.[111] The volume which is removed from the PDMS slab by punching is a cylinder-like PDMS piece with the diameter and height equal to outer diameter of used punching pin and thickness of slab, respectively. The evacuated volume will be a vertical channel which is the desired access port (inlet or outlet).

Due to the softness and flexibility of the PDMS slab even after curing, using a slight downward force, the punching tool easily penetrates through that and makes the hole by removing the designated volume. Bear in mind that in order to increase the quality of punching, the microfluidic device must be placed under the punching tool with the microfluidic on top and also covered by tape. This consideration helps the holes to have sharper and smoother edges in the end.

Alignment of the chip under the puncher to locate the exact position, at where the holes are supposed to be punched, as well as punching the hole vertically straight all the way through is as of high importance in this procedure since punching any off or tilted hole is likely to cause the entire microfluidic device be totally useless! In that case, the microfluidic device will be subject to be fabricated all over again and all the steps from PDMS preparation to PDMS casting has to be replicated again. To this end, an investigation has introduced a new method facilitating the exploration of exact location for intended hole by putting a ring of light source underneath of the PDMS device. In this method, due to the fact that the microchannels scatter the light, the positions of inlets and outlets will be clearly observable.[112]

2.1.7 Plasma bonding

The PDMS devices what are casted using a master normally have their features and microchannels semi-open from one side at which they were in contact with the master. Thus, in order to get them applicable for flowing fluids into them, they should be sealed

against a flat surface making the hollow microchannels and features as schematically shown in Figure 2.6. To this end, the PDMS device may be bonded to another PDMS slab[113], or a glass[70], or a thermoplastic polymer such as PMMA[43, 114], or silicon[87], or also other materials[115]. The most popular types of bonding are PDMS-glass and PDMS-PDMS bonding. However, nowadays the polymers are becoming important substrates for the bonding thanks to their less cost and disposability property, as well as their wide applicability for rapid prototyping method and mass production technologies.[116]

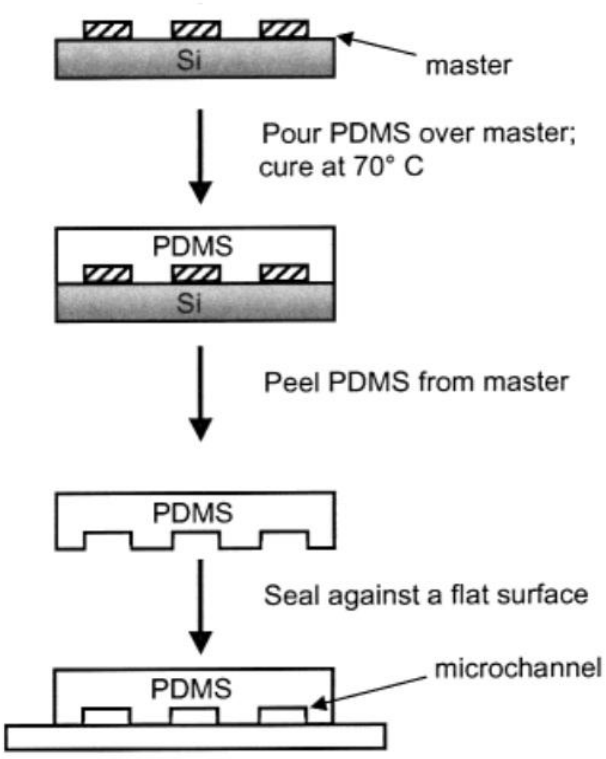

Figure 2.6. Schematic of casting PDMS device and bonding the device against a flat surface forming the microchannels.[32]

In fact, PDMS loose its adhesion property after casting; consequently, does not stick to any other surfaces and also the surface of PDMS is strongly hydrophobic.[34] In order to accomplish the bonding, the PDMS surface must transform to a hydrophilic surface. There have been several investigations on different physical methods and techniques enhanced

for this purpose; however, the technique of “oxygen plasma surface treatment” is the most frequently used one.[113, 117]

In this technique, the lab air is used to activate the surfaces of PDMS devices i.e. mainly made of PDMS or glass. The plasma preparation also incorporates the oxygen atoms available in the surface of PDMS device and as a result, the hydrophobic property of the surface will change leading to transform the surface to hydrophilic and also become very reactive.[87, 114] As the matter of fact, using this method (oxygen plasma surface treatment) the bond consistency is increased by oxidation of the surface. Noteworthy that, due to its nature of this technique and also talking into account the reported experiences, this technique provides the opportunity to bond the PDMS to other surfaces as well, provided that those surfaces are also plasma treated.[82, 113]

The bonding is accomplished by simply placing the pre-cleaned specimens into the plasma-chamber of the oxygen plasma instrument which is located under a laminar flow cabinet as shown in Figure 2.7. Prior to start the process, all the related settings of the instrument (coating time, pressure, plasma current, and etc.) must be checked to be properly regulated. Then, closing and fixing the lid of the chamber, the process is initiated which typically takes a few minutes. During the process, the surface to be bonded is exposed to oxygen plasma and transform to hydrophilic. The researches have demonstrated that a longer oxygen plasma time will result to a smoother surface.[117]

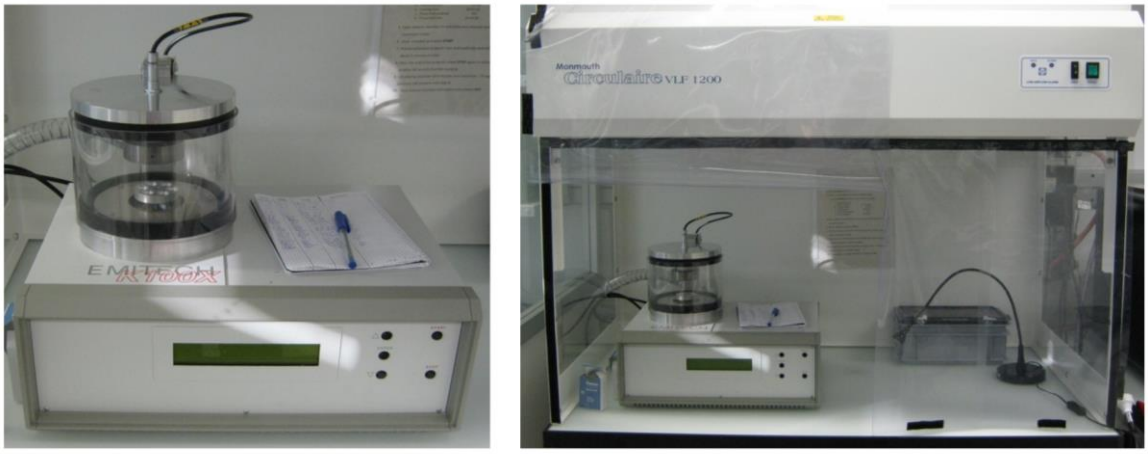

Figure 2.7. A typical oxygen plasma device located into a laminar flow cabinet.

Once the process is finished, the specimen must be taken out from the chamber and bonded against the intended surface as soon as possible within a minute. The faster the bonding process would be taken place, the better quality will have. At this stage, although the bonding is thoroughly fulfilled, the bonded device is recommended not to be used for the experiments right away after bonding. For strengthening the bonding, the bonded device is advised to be heated (either by placing inside an oven or putting over a hot plate) for at least an hour.[113] Heating might be accomplished by placing either into an oven or on a hot plate. It should be always taken into account that an oven heats up the device evenly from all sides; however, a hot plate transfers the heat to a PDMS device only from a single side (bottom) and in some cases the unidirectional heating might result in damage or deforming the PDMS device. Heating the bonded device will also make the device become hydrophobic again. Moreover, another method to obtain the better result while bonding, is to drip a drop of water between the two surfaces which are about to be bonded. This will evaporate prior to finishing the bonding and allows longer time for adjustment and also provides the more consistent bond in the end.[93] When the bonded device was heated (cured) for a sufficient time, the device is ready to use after a short cooling operation to reach room temperature. At that point, the bonding is quite stable and strong and the device could be actually used.

This technique has some disadvantages. As such, the applicability of the oxygen plasma instrument is limited to the size of its chamber; therefore, the relatively bigger devises cannot fit into the chamber. An alternative technique to overcome this drawback is so-called “corona discharge treatment” which is a hand-held equipment with the same concept as of oxygen plasma surface treatment (for surface activation), that may be implemented to bond even several layers together.[113, 118] The equipment is designed so that the high voltage is applied to its sharp electrode tips and plasma is formed at the end of the tips. This plasma is used for bonding process the same way as utilizing oxygen plasma method. Usually the treatment time of around 10-15 seconds is sufficient, depending on the size of the devise.[115]

Noteworthy that, due to many advantages over the conventional oxygen plasma treatment such as portability, minimizing the chance of contamination and also possibility to cover the larger devices (with surface up to more than 7 cm), corona discharge seems much more useful and applicable.[118, 119] Though, the investigations have demonstrated that the substitution of the corona discharge with a uniform oxygen plasma surface treatment instrument will result in the improvement of reproducibility of the system.[114]

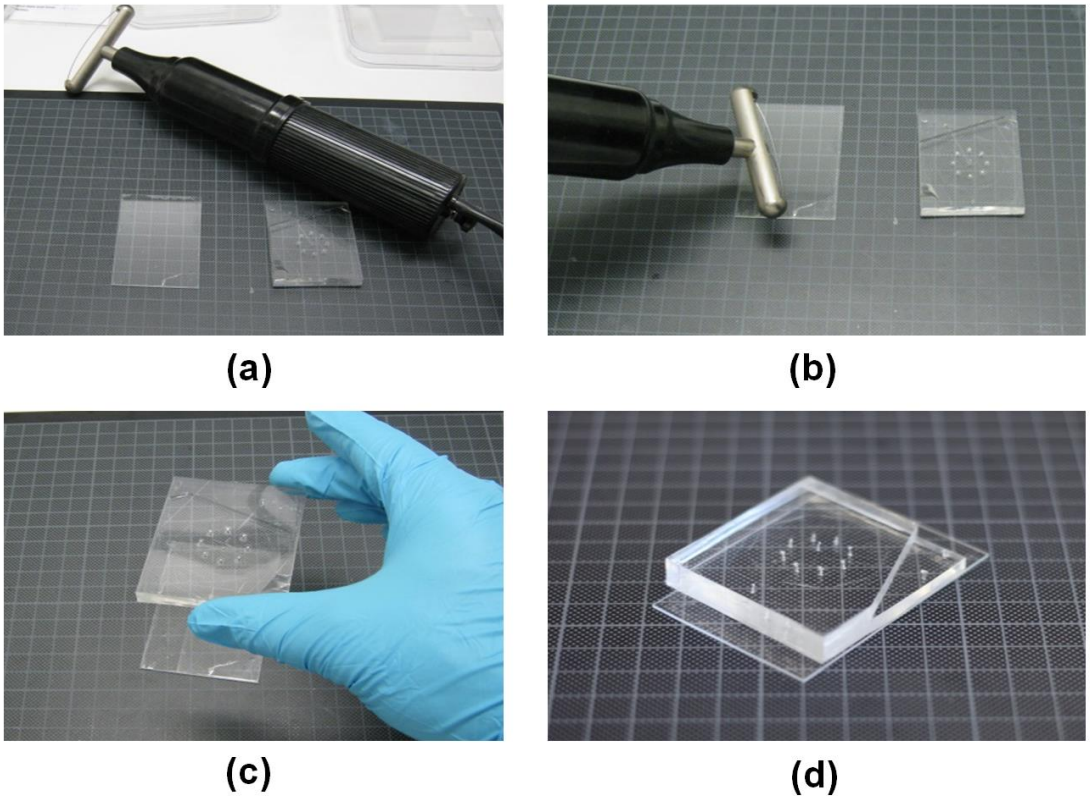

Figure 2.8. Steps of plasma bonding utilizing corona discharge treatment. (a) Prepare the required items, (b) keep the wire electrode at 2-5 mm from the top of the surfaces to be bonded and move it repetitively for 10-15 seconds, (c) place the two surfaces in contact and gently press one against another, (d) the device is bonded.

Due to the generation of high voltage, corona discharge should not be operated close to electronics or, in general, electric devices. Moreover, corona discharge produces Ozone (O_3) which is an absolutely toxic gas; therefore, all the safety consideration should be taken into account and the corona treatment process must be always performed under the fume hood. Also, the bonding performed by corona discharge are reversible in the first few

minutes meaning that it is possible to separate the bonded surfaces and bond again in case the bonding was not initially performed properly or from the correct location. This feature might be as of high importance and very helpful for alignment of multi-layer microfluidic devices.

Also, in order to bond a very precise and sensitive multi-layer device, it is always tricky and risky to get them aligned exactly from the place they were expected to by naked eye. To that end, a stereoscope is typically utilized assisting the alignment process for bonding. In addition, to fulfill the alignment of multi-layer devices, which must be super accurate, some alignment assisting protocol could be taken into account. As such, the alignment marks may be also drawn in the photolithography mask that will consequently further appear on the PDMS devices as well[61], or a sort of transitional spacers might be used for bonding[94] or even a kind of accurate alignment assisting device may be utilized. This alignment device can potentially be incorporated into a stereoscope as well for more careful and accurate bonding.

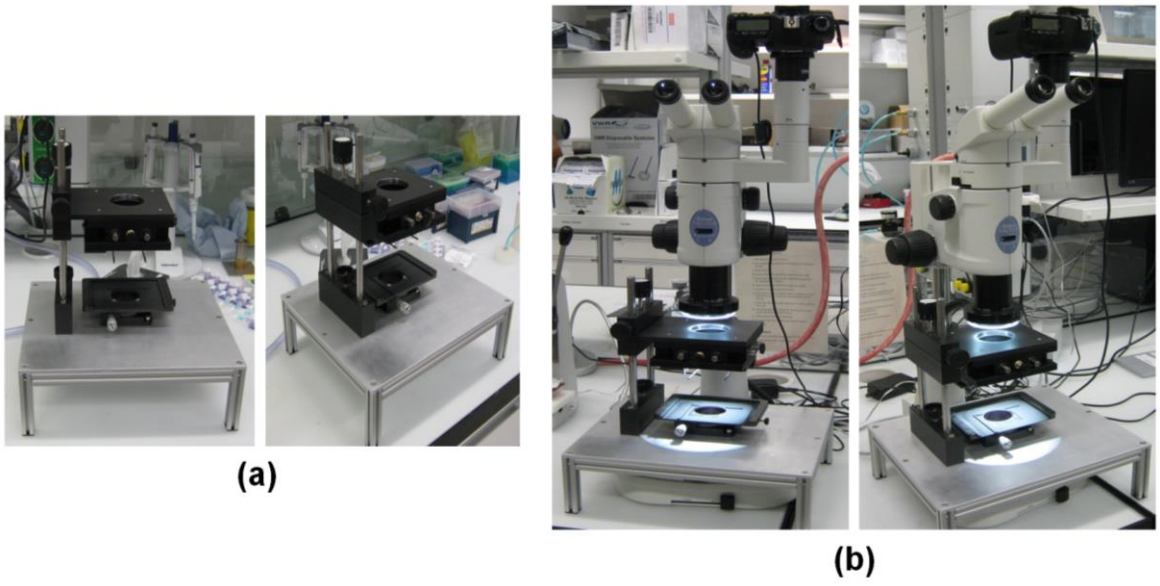

Figure 2.9. (a) An alignment assisting device, (b) an alignment assisting device incorporated into a stereoscope.

2.1.8 Spin coating

As it was also explained earlier, the bonding of PDMS-PDMS is more consistent as well as more hydrophobic than PDMS-glass bonding. Therefore, instead of bonding the PDMS chips right against a glass slide, it is recommended to initially bond the PDMS chip against a thin blank slab of PDMS and then bond the two-layer PDMS device against the glass slide (from the surface of blank PDMS slab)[120]. Another alternative to this approach is to spin coat a very thin layer of PDMS over the surface of the glass slide first, and then the PDMS chip is bonded over the spin coated surface of the glass slide.

To this end, a little amount of PDMS is prepared through the same protocol as PDMS preparation for device fabrication. Then, the settings of spin coater machine are regulated according to the desired thickness and purpose of the intended coated layer and the glass slide is placed into the machine with the surface to be coated on top. Subsequently, the prepared amount of PDMS is gently poured over the glass slide trying to pour it in the center as much as possible. Finally, the spin coating process is operated by turning on the machine which takes only a few minutes. At the end, the coated layer of PDMS is required to be cured; thus, the coated glass is placed over a hot plate or inside an oven for a couple of hours to be cured completely. Once the coated layer of PDMS is fully baked, the coated glass is then ready to be used as the substrate for the bonding of a PDMS chip. Noteworthy that, the spin coater machine is located inside a laminar flow cabinet; thus, the entire process is also operated inside the cabinet.[104]

2.1.9 Post-bonding treatment

Once the PDMS chip is fabricated and further bonded, the PDMS device is ready to be applied for the experiments. However, in order to achieve even better and more proper results in the experiments, the PDMS device may undergo some sorts of treatment leading to better quality of experiments afterwards. As such, the approach of surface treatment of PDMS microchannels by Aquapel™ may be noted as one of the most widely used technique for the chemical surface treatment of the PDMS channels after activation by oxygen plasma surface treatment and bonding.

Aquapel™ is a commercial glass treatment substance i.e. a hazardous and toxic chemical what may cause several different health injuries to the person dealing with that; therefore, its handling should be done carefully and thoroughly under the fume hood.[121] Treating the microfluidic device with Aquapel™, the surfaces in contact with Aquapel™ get fluorinated and thus the device and, in particular, its microchannels become more hydrophobic. To fulfill that, a drop of Aquapel™ is dripped over one of the inlet of the PDMS device where enters the device by capillary force, and is also pulled through the device, whether manually or using a pump, making sure all the channels are filled with Aquapel™. Then, the channels are let to stay filled for one or two minutes and finally, the device and channels are flushed with air.[122, 123]

After flushing, the device is recommended to be filled with oil to be used and store in oven at around 70 ºC for at least half an hour. Although it must be thoroughly endeavored to evacuate the entire amount of Aquapel™ from the device and its microchannels, remaining a trace amount of it inside the microchannels is negligible.

2.2 Microdroplets Generation

Microfluidics is a wide branch of science consisting of several subcategories and one of its most important and applicable subcategory is “droplet-based microfluidics” also known as “digital microfluidics”.[124, 125] Droplet-based microfluidics is a continuously growing field of research that is becoming an interdisciplinary branch of science due to its wide range of applications.[126] The droplets manipulated in microfluidics science are normally sub-nanoliter droplets usually referred to as microdroplets, which offer a wide range of opportunities thanks to their wide potential applications.[127, 128] These microdroplets are technically the relatively unstable and deformable droplets of a liquid which are suspended in a flow of a carrier immiscible liquid.[129]

In other words, the manipulation of droplets in microfluidic channels is an immensely useful emerging technological platform for various applications in many different scientific fields. As such, different applications have been reported in whether biological fields such as biology science[130], biomedical studies[131], single cell analysis[132], and drug

discovery[133], or chemistry-related fields like chemical synthesis[127] and biochemical screening[134], or even more interestingly chemical reactions[14, 135] and synthesizing functional micro- and nanoparticles[136, 137] at where the droplets are mainly the carrier media serving the systems in different manners.

The microdroplets are generated through a two- or even multi-phase systems dealing with the immiscible phases. This is typically fulfilled by combining two or more flow streams of immiscible fluids (normally a sort of oil and water) at a joint area and producing a shear force on the dispersed phase which causes it to break up into certain discrete volumes generating the droplets.[126] In fact, in contrast to continuous phase microfluidics, droplet-based microfluidics mostly concentrate on creating the discrete volumes.[125] Also, in comparison with continuous phase microfluidics, droplet-based microfluidics provides a broad range of advantages including possibility of compartmentalization[138] and encapsulations[126], improvement of mixing[139], accomplishment of highly parallelized experiments[140], fulfillment of monodisperse particle generation[141] and resulting in higher sensitivity in digital analyses[142].

There are different chemical and physical parameters involved in characterization of a microdroplet generation system. As such, the surface tension, as a key mechanical property of fluids, is a crucial factor in determination of microdroplet behavior regarding the relatively large surface-to-volume ratio of microdroplets.[143] Also, unlike the normal applications of continuous flow microfluidics, another key factor to achieve the stable microdroplet generation in droplet-based microfluidics is the wettability of the channels walls which has a direct influence on forming oil-in-water (O/W) or water-in-oil (W/O) droplets.[13, 126] In addition to “Reynolds number”, another dimensionless number so-called “capillary number (N_{Ca})” is defined in order to predict the droplet formation and its behavior which is calculated as

$$N_{Ca} = \frac{\mu_c \cdot U}{\gamma} \tag{1}$$

where μ_c (Pa.s) and U (m/s) are the viscosity and the velocity of the continuous phase, respectively and γ (N/m) is the interfacial surface tension between the two immiscible phases.[16] Capillary number can be used for control the generation, break-up and coalescence of droplets.[124] In practice, the droplet break off; and consequently, the droplet formation takes place above a certain capillary number called "critical capillary number". This dimensionless number is system dependent and highly depends on the geometry of the channels; therefore, different values and ranges for that have been reported in the literatures such as $0.001 < Ca < 0.15$ [144], $Ca \approx 0.01$ [145], and even larger values up to $1.2 \leq Ca \leq 1.7$ [146].[31, 125]

The formation of microdroplets within the microfluidic channels is a spontaneous phenomenon that is normally a consequence of shear force as well as interfacial surface tension and is required to be initiated. That might be accomplished using either micro-injectors[147], or the needles[148], or even the electric fields[149] as well as applying pressure as the driving force aiming to generate uniform microdroplets[143].[127, 150]

2.2.1 Methods of microdroplet generation

Initially, the generation of microdroplets through spontaneous process was reported as a generation process in the capillary format[151] through the technique so-called "co-flowing streams"; though, it was implemented later in many other microfluidic devices including "geometry-dominated devices"[152], "flow-focusing devices"[135] and "T-junctions"[139]. Among those various methods, flow-focusing devices and T-junctions are two well-established and most frequently used techniques for generation of monodisperse microdroplets in microfluidics, while co-flowing streams and other methods are rarely used.[128, 143, 150]

Figure 2.10 schematically illustrates three techniques for formation of microdroplets. In co-flowing flow, the capillary having the disperse liquid is located inside and concentrically of a wider capillary having the continuous liquid flowing in. Once the disperse liquid leaves the capillary get in contact with continuous liquid and due to the pressure and shear force forms discrete plugs or droplets.[129, 150]

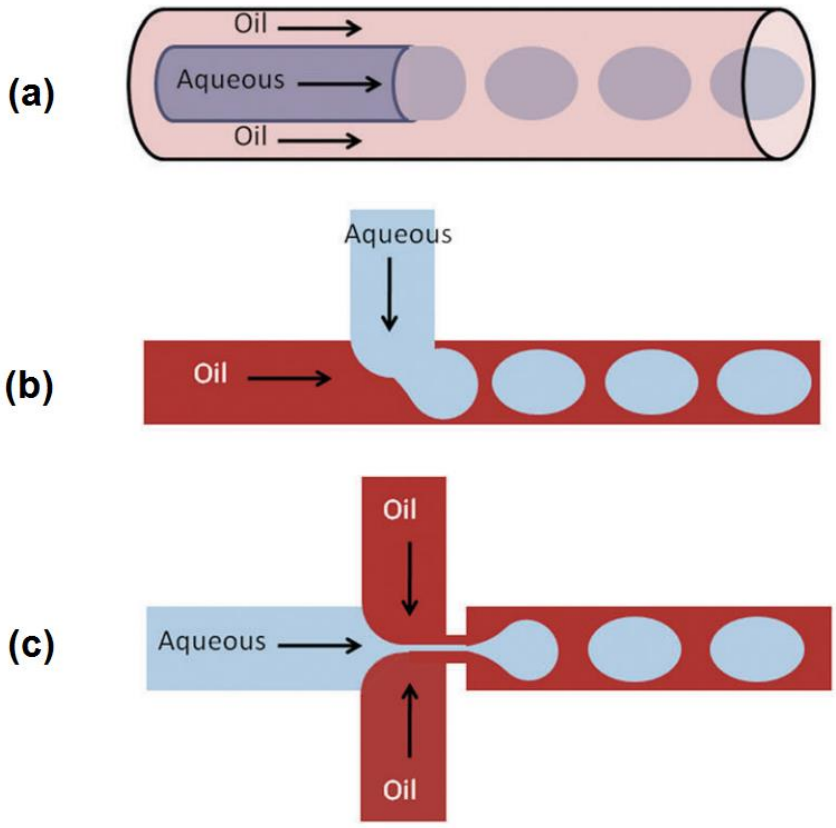

Figure 2.10. Different techniques for formation of microdroplets of aqueous phase into continuous oil phase. (a) Co-flowing streams, (b) T-junction, and (c) flow-focusing device.[150]

As it was previously noted, T-junctions and flow-focusing devices are the most widely used techniques for generation of microdroplets through channels; therefore, we describe these two methods only with emphasizing on flow-focusing devices as the selected method for this work as well. In fact, in a T-junction device, the aqueous phase is injected into the continuous phase perpendicularly and as a result, microdroplets are formed in consequence of the shear force between the two phases.[127, 153]

However, the flow-focusing devices undergo a different pattern in which a liquid (i.e. liquid A) flows in a middle channel and an immiscible liquid (i.e. liquid B) flows in two other channels located both sides of the middle channel. The both channels of liquid B reach the middle channel, having liquid A, perpendicularly at where both liquids from all

three channels are induced to enter a narrow orifice as the entrance of another channel located at their downstream. Then, liquid B applies pressure and viscous stress to liquid A and as the result, liquid A is driven to a narrow strand and subsequently is broken down through the orifice forming the droplets.[127, 154]

Through a certain device the capillary number is only a function of the velocity of continuous flow since the viscosity and interfacial surface tension are the constant for a certain device undergoing the same condition. Therefore, manipulating the velocity of velocity of the continuous phase (and consequently the capillary number), when the velocity of disperse phase remains the same, the system might undergo various flow regimes. Figure 2.11 illustrates the various flow regimes for different droplet generation techniques.

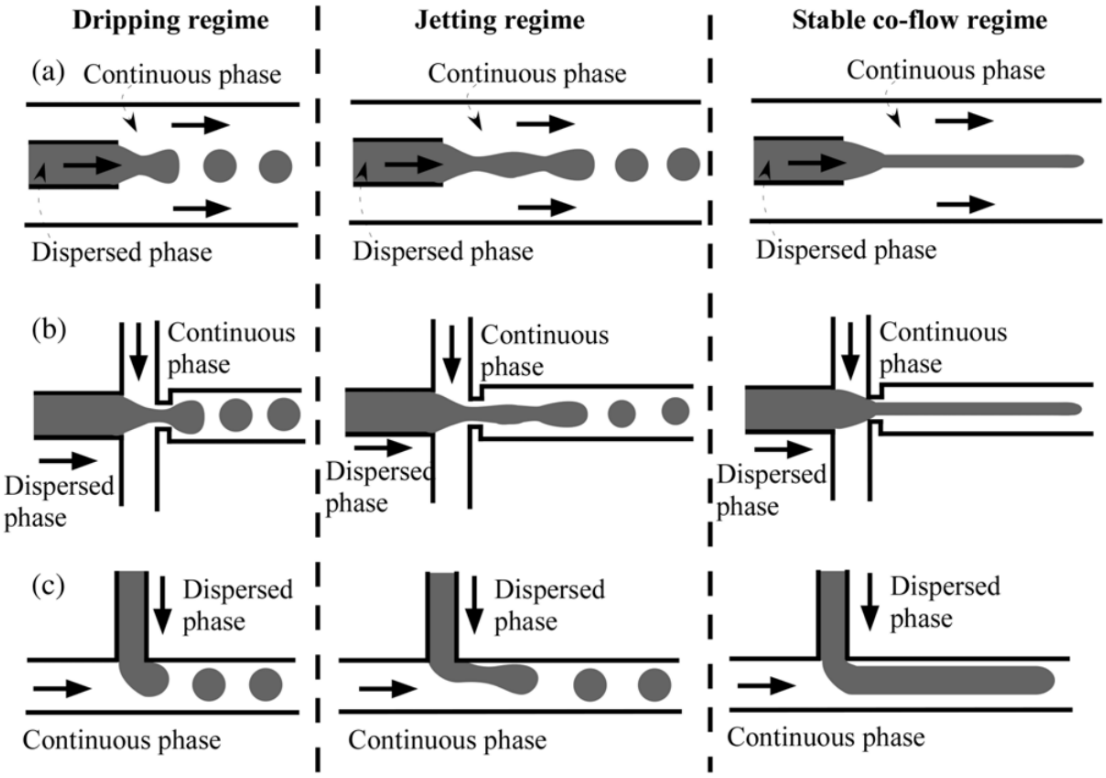

Figure 2.11. Schematic illustration of three different flow regimes in three main techniquies for droplet generation. (a) Co-flowing streams, (b) flow-focusing device, and (c) T-junction. The velocity of contnuous phase, and consequently the capillary number, increases from left to right. (lower velocity for dripping, higher for jetting and even higher for stable co-flow)[155]

On the above critical capillary number, the droplet formation starts. On the moderate velocity of continuous flow, the droplet breakup and formation takes place normally and the droplets are pinched off close to the orifice or capillary tip. This regime is so-called "dripping regime". Increasing the velocity of continuous phase up to a certain extent, the droplet formation still occurs; however, the droplets are pinched off from an extended thread downstream of the orifice or capillary tip. This regime is known as "jetting regime" and increasing the velocity of continuous phase even more, the system reaches the condition at where no more droplet formation occurs and instead a film of each phase flows through the post-orifice or downstream channel.[129, 155]

As it might be seen at the previous figure, the phenomenon of droplet formation takes place only through the first two regimes that are dripping and jetting regime. Figure 2.12 also depicts the images of droplet formation in the real experiments through either of these two regimes (dripping and jetting).

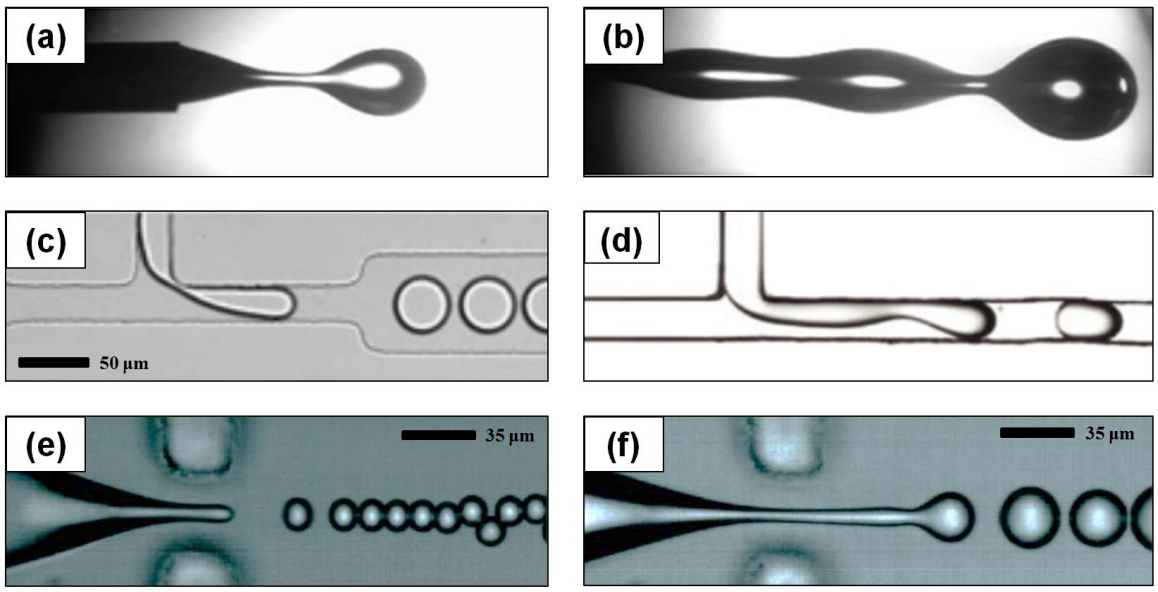

Figure 2.12. Droplet formation in a co-flowing stream device (through (a) dripping and (b) jetting regime)[156], a T-junction (through (c) dripping[157] and (d) jetting[155] regime), and a flow-focusing device (through (e) dripping and (f) jetting regime)[146].[129]

As it might be simply understood, the droplet break-up and consequently the droplet formation phenomenon only occurs within a certain range of viscosity of continuous flow that has to do with the ratio of the input velocities of two phases as well as the physical and chemical properties of the liquids like surface tension and obviously the technique of droplet generation and the geometry of the device. This will be further investigated in the coming chapters.

2.2.2 Bulk synthesis

As it was described before, microdroplets are of interest as commodities in themselves for various applications such as biological, chemical, biomedical and medical systems; however, the production of large quantities of monodisperse homogeneous droplets for such processes is an area that has been always very challenging. On the other hand, the bulk emulsification process, in particular, shear induced emulsification, has been broadly investigated through many researches in which the large quantities of emulsions are produced for different purposes like cosmetic, food industries and drug delivery [126, 158, 159] and also in some researches the control over their size range has been reported to be improved [160-162]. That approach is a suitable method for production of large quantities of emulsions as long as the monodispersity of the emulsions is not critical and important. Also, a general bottleneck of all high-throughput systems is compartmentalization.[126, 127]

However, the main bottleneck of this type of processes is the monodispersity and to overcome both drawbacks of monodispersity and compartmentalization, the droplet-based microfluidics is an appropriate technique.[143, 154] Although the microfluidic devices have shown utility to generate the droplets in different sizes and also can be controlled to optimize the monodispersity, low production rate of these systems confines the applicability of these devices for clinical and biomedical applications.[94] In fact, the droplet-based microfluidics which has provided a wide range of applications, particularly biomedical applications, ranging from typical point-of-care diagnostics[163] to enhanced molecular screening [164] and genetic testing [165] is an emerging and promising platform

to overcome the aforementioned drawback as well as for high-throughput systems.[166, 167]

To that end, many different techniques and methods have been developed for high-throughput generation of microfluidic devices for example utilization of multiple modular microfluidic (M^3)[168], adoption of continuous flow microfluidic formats [169, 170], implementation of a multi-array microfluidic module[94, 166], and even high-throughput generation of microdroplets through the highly advanced designed microfluidic devices[164, 171-173]. Basically, the generation of microdroplets through a microfluidic device consisting of microchannels can be easily obtained at rate of up to couple of kHz even with control over microdroplet size and monodispersity.[150, 174] Moreover, undergoing the same concept along with improvement of the design and scaling-up the assay is so likely and unsurprisingly to result in fabrication of a microfluidic device capable of formation of microdroplets at high rates even up to more than million hertz (microdroplet generated per second).[150, 175]

In this work it has been endeavored to generate microdroplets at high-throughput rates through study and implementation of two different methods of generation. To that end, two different methods of droplet formation were taken into account that in first method the droplet generation takes place through a well and advanced designed microfluidic device undergoing flow-focusing technique.[94] The second method concerns the formation of microdroplets utilizing a concentric double-cylinder in which the inner cylinder is rotating and the droplets are formed using rotational force within the gap area between two cylinders.[95]

2.2.3 First method: Multi-Array Microfluidic Module utilizing Flow-Focusing

In the first method, a microfluidic device consisting of eight symmetric modules is used. Each module is equipped with a flow-focusing device playing the role of a separate microdroplet generation device; however, all the eight modules are connected to each other from upstream of the connecting channels for oil and aqueous phase. The device is actually a multilayer device aligned and bonded over each other. The method and appropriate

attempts, results and achievements will be described further in the coming chapter. A published investigation[94] was used as the benchmark of this method; however, the investigations were thoroughly accomplished separately and independently from layout design, to mask preparation, to implementation and carrying out the experiments. Figure 2.13 illustrates the multi-array microfluidic module consisting of eight symmetric microfluidic flow-focusing devices used as the benchmark for this method for further investigations.[94, 166] This method will be extensively discussed in chapter 3.

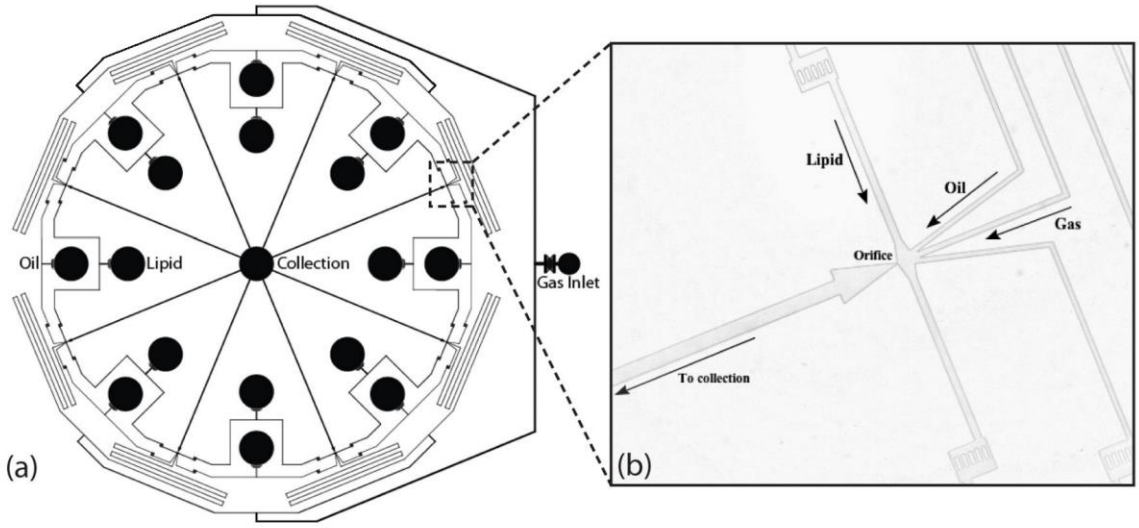

Figure 2.13. The multiarray microfluidic module used as the benchmark. (a) the entire module and (b) one of the eight flow-focusing device.[94]

2.2.4 Second method: Taylor-Couette Flow pattern using Rotational Force

In the second approach, the droplet generation is investigated through a concentric double-cylinder undergoing Taylor-Couette flow pattern. As the matter of fact, the main aspect of this device is based on the rotation. Regarding its principle, the device contains two concentric cylinders located one into another that depending on their orientation, they are categorized as horizontal and vertical devices.[176] The outer cylinder, which is typically made of a transparent substance, is fixed and the inner one is rotatable. The gap area between two cylinders is initially filled with the fluid (continuous phase) and the inner cylinder starts rotating to reach the desired rotational speed. Then, at that point, the second

fluid (disperse phase) is injected to the gap and the droplets are formed along the cylinders axis heading to the outlets.[95] Figure 2.14 illustrates the schematic of a Taylor-Couette cylindrical device. Chapter 5 will broadly cover this method.

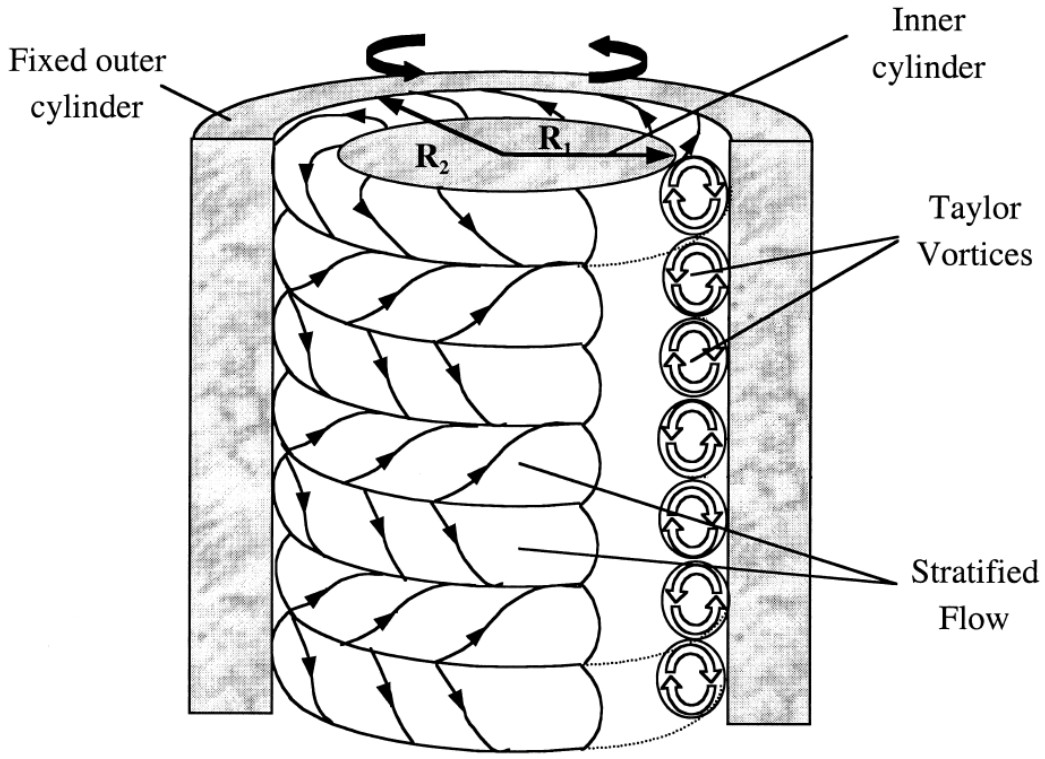

Figure 2.14. Schematic of a double cylinder undergoing Taylor-Couette flow pattern.[177]

3 EXPERIMENTAL INVESTIGATIONS

3.1 Multi-Array Microfluidic Module utilizing Flow Focusing Technique

As it was explained before, a multi-array microfluidic module that might be a multi-layer device is a potentially appropriate method for enhance and improvement the production of microdroplets aiming to reach the higher production rates. There are various investigations accomplished on this area fulfilling this purpose. Take for instance; a published research has indicated the usage of a 128-channel array investigating the increased production of liquid-in-liquid droplets in a multichannel microfluidic device up to 1.4×10^3 droplets per second which is not very significant.[178] Also a similar work have reported the usage of a three-layer radial module consisting of 64 parallel channels generating the droplets with 33 gradient concentrations at the production rate of around 10^3 droplets per second.[179] Although these are not very high-throughput modules, another investigations have demonstrated the high-throughput generation of microdroplets within an extensive production rates ranging from lower rates such as $\sim 2.8 \times 10^3$[164], $\sim 12 \times 10^3$ [180], $\sim 14 \times 10^3$ [181] and $\sim 30 \times 10^3$ [182], up to higher rates like $\sim 3.7 \times 10^5$ [166], $\sim 1.3 \times 10^6$ [171], and $\sim 3.4 \times 10^6$ [183] droplets per second.

Another investigation in this field [94], which was taken as the benchmark for this section of the present work, have developed two four- and eight-channel microfluidic modules presenting a system capable of production of microdroplets at high generation rate for drug delivery using flow focusing method. Through that investigation, the production rate of 1.34×10^5 droplets per second was obtained in an eight-channel module that is about 50-100 times greater in comparison with the generation rates demonstrated in the previous similar attempt using a single-channel module.[94] Therefore, the mentioned published investigation was selected as the benchmark. Figure 2.13 shows the design of the desired eight-channel microfluidic module. In this approach, the key targets are the throughput (production rate) and the monodispersity of the droplets, while the actual size of the droplets is of less importance and is enough to be within a reasonable range. Therefore, the

design mainly aims to increase the throughput and improve the monodispersity of generated droplets.

This module is a multi-layer microfluidic device made of PDMS consisting of two main PDMS layers with different applications. For each layer a separate layout design is required what further is used for photomask preparation as the platform for subsequent stages of master and finally PDMS fabrication. The upper PDMS device of the multi-layer stands for the main chip when the droplets are supposed to form and the inner(s) are the distributing channels from the main inlets into several symmetric channels.

3.2 Mask Design by AutoCAD®

Given the layout design of the benchmark investigation (presented in Figure 2.13) the appropriate chip was designed aiming to include eight symmetric flow-focusing droplet generator devices. The PDMS chip is supposed to undergo the two-phase processes where water and FC-40 oil are used as dispersed and continuous phases, respectively. This main chip will be placed and bonded over another PDMS chip (hereinafter referred to as "bottom layer") playing the role of distribution channels for continuous phase (oil) from main inlet into eight evenly distributed microfluidic channels.

Utilizing AutoCAD®, the layout of the main chip might be designed carefully. The procedure of design is accomplished through a four-stage procedure illustrated in Appendix I. The module has the radial design with the inner diameter of 33 mm. The aqueous phase (water) passes through the 35 μm wide serpentines and channels, while the channels for oil phase (FC-40) have the width of 50 μm. Oil is fed to the bottom PDMS layer (that will be explained later) where the a single main flow of oil is distributed evenly into eight identical and equal flows which further pass through the eight vertical channels connecting the bottom layer to main chip (upper layer) at the positions of oil inlets. Both phases reach the flow-focusing area and enter a 25 μm wide orifice and pass through an expansion area in order to form the droplets by shear force along the expansion. Following the droplet generation at orifice, microdroplets flow through a wider post-orifice channel which is 60 μm wide and about 16 mm long connecting post-orifice expansion area to the outlet of the

device. Figure 3.1 indicates the initial drawn layout including whole design (on the left) as well as the flow-focusing droplet generation section (on the right). The details of the drawn design including the width of each channel have been represented in Appendix II.

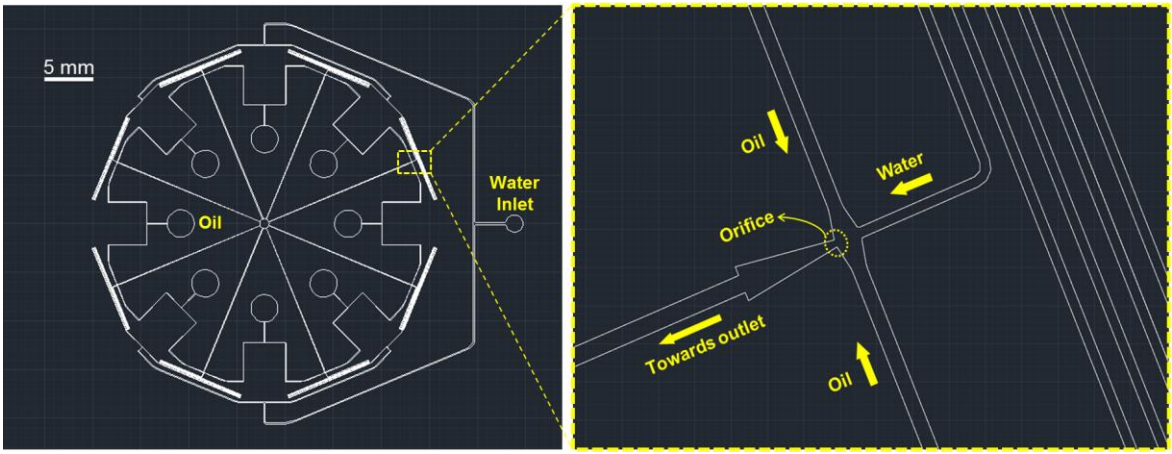

Figure 3.1. The initial layout for the main chip (upper layer) of the mult-array module drawn by AutoCAD®.

3.3 Photomask, Master and Chip Fabrication

Based on the above mentioned drawn layout, an appropriate photolithography mask (photomask) might be printed by Micro Lithography Services Limited© which will be further used to fabricate the master accordingly through the photolithography process. For the first try, the height of the master was decided to be 25 μm so that subsequently the PDSM device (which will be casted and made out of the due master) will include the microchannels of 25 μm high. Both printed photomask and fabricated master are illustrated in Figure 3.2.

All the masters used for the fabrication of PDMS devices during this project work were fabricated at the newly established clean room unit at research group of Prof. deMello in ETH Zurich. Though, due to the various typical unpredictable errors (that normally appear at any newly established clean room unit), there were some fabrication issues with a few of first fabricated mastersin the aforementioned clean room. Therefore, a few of the first tries for master fabrication for the main chip led to production of partly damaged and useless masters. Appendix III represents the closed-up images of two of those masters indicating

the fractions and other failures on the masters. Although there were still a few fractions observed over the final proper fabricated master, it was heated up on a hot plat at 150 ºC for a just about five minutes. This was accomplished twice and after that, the fractions seemed to vanish to some extends.

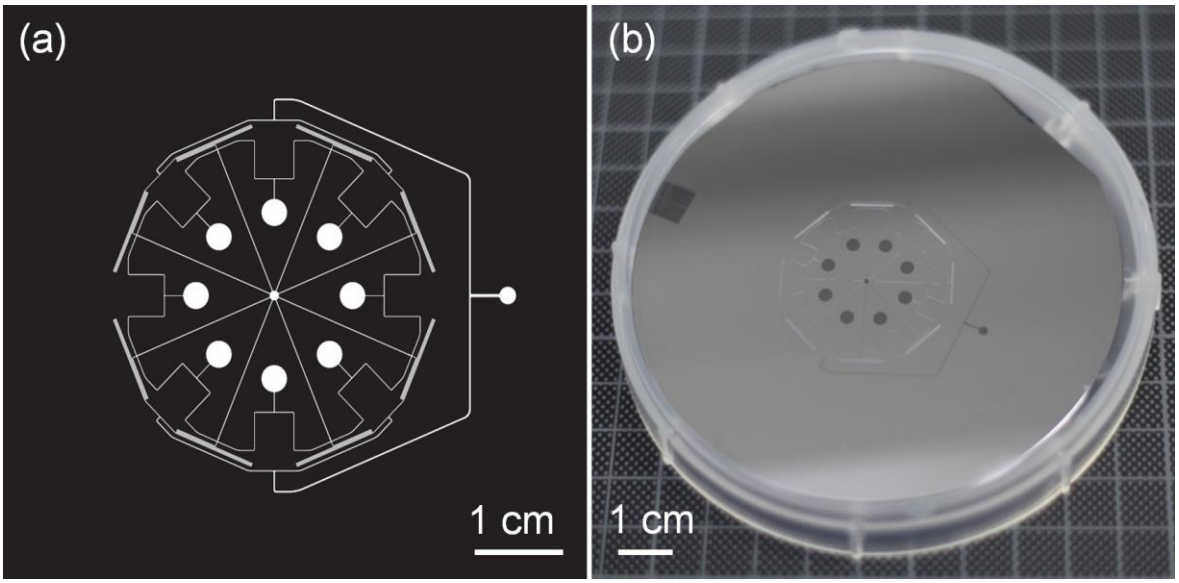

Figure 3.2. (a) The photomask printed according to the initial drawing, and (b) fabricated silicon master according to the printed photomask.

Moreover, another drawing is needed for the bottom layer which is actually a normal PDMS chip to split the main flow of oil into eight equal flows. The positions of the eight oil inlets in the main chip should be the same as those on the bottom layer since both PDMS layer are supposed to be bonded together and so the eight vertical channels of the bottom layer must be placed exactly underneath of the eight oil inlets of main chip. Thus, the design of bottom layer is not sophisticated; however, it should be perfectly symmetric ensuring that all the eight flow-focusing are operating under the same and identical flow rates. The height of the microchannels for the bottom layer is also the same as that of main chip which is 25 μm for the initial try. The drawn layout for bottom layer has been illustrated in Figure 3.3 (a). The same way as for main chip, the desired photomask and master may be fabricated for the bottom layer as well. (Figure 3.3, (b) and (c))

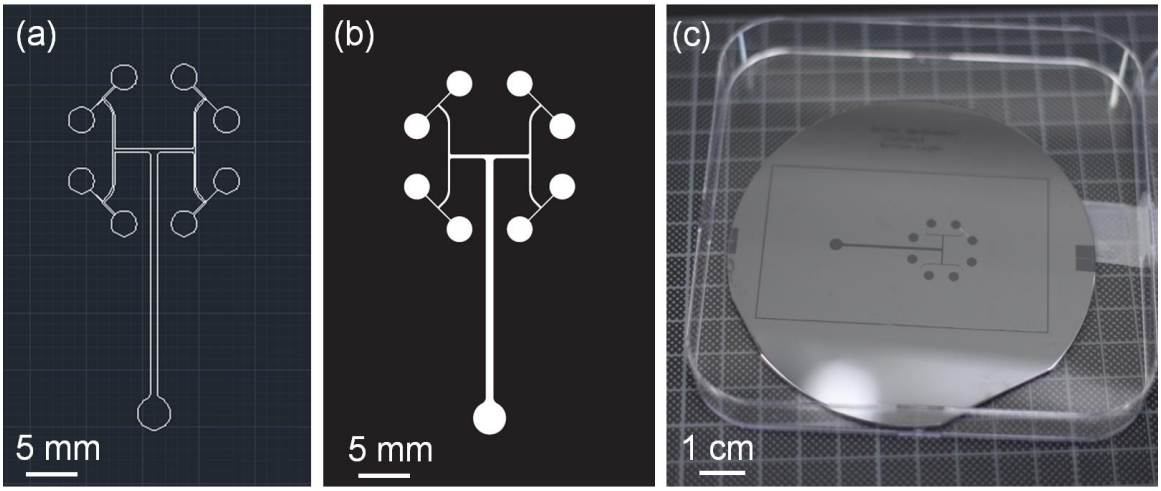

Figure 3.3. Bottom layer of the mult-array module. (a) Layout drawn by AutoCAD®, (b) photomask printed based on the layout, and (c) fabrictaed master according to the photomask.

Once both of the masters are fabricated and ready to use, the PDMS device may be casted. To that end, as it was extensively explained in the section 2.1, the PDMS devices are casted against both masters previously silanized using 200 µl of chlorotrimethylsilane. For making PDMS, the ratio of 10:1 for prepolymer to curing agent is used. Around 40 g of PDMS is initially consumed for each master meaning that each PDMS device is fabricated using about 40 g of PDMS. When the casting and curing is over, the PDMS devices are cut into the desired pieces for bonding.

Prior to bonding, all inlets and outlets (water inlet and main outlet in main chip and main oil inlet in bottom layer) are punched using the 0.89 mm diameter pin. While, the eight oil supply inlets in the bottom layer are punched using 1.40 mm diameter pin. The bonding is accomplished as Figure 3.4 shows i.e. main chip is bonded against the bottom layer (obviously to the opposite surface of which contains microchannels) and subsequently two bonded PDMS slabs are bonded against a substrate from the side of the bottom layer which contains the microchannels and patterns. In terms of substrate, the first alternative is to bond over a blank PDMS slab which has been casted against a blank master (wafer). Due to the high accuracy required to get all of the eight oil inlets precisely aligned over the corresponding eight oil channels of bottom layer for bonding, the alignment assistance

device is incorporated into a stereoscope (both presented in Figure 2.9) and the bonding process is accomplished utilizing in order to obtain more accurate results in bonding.

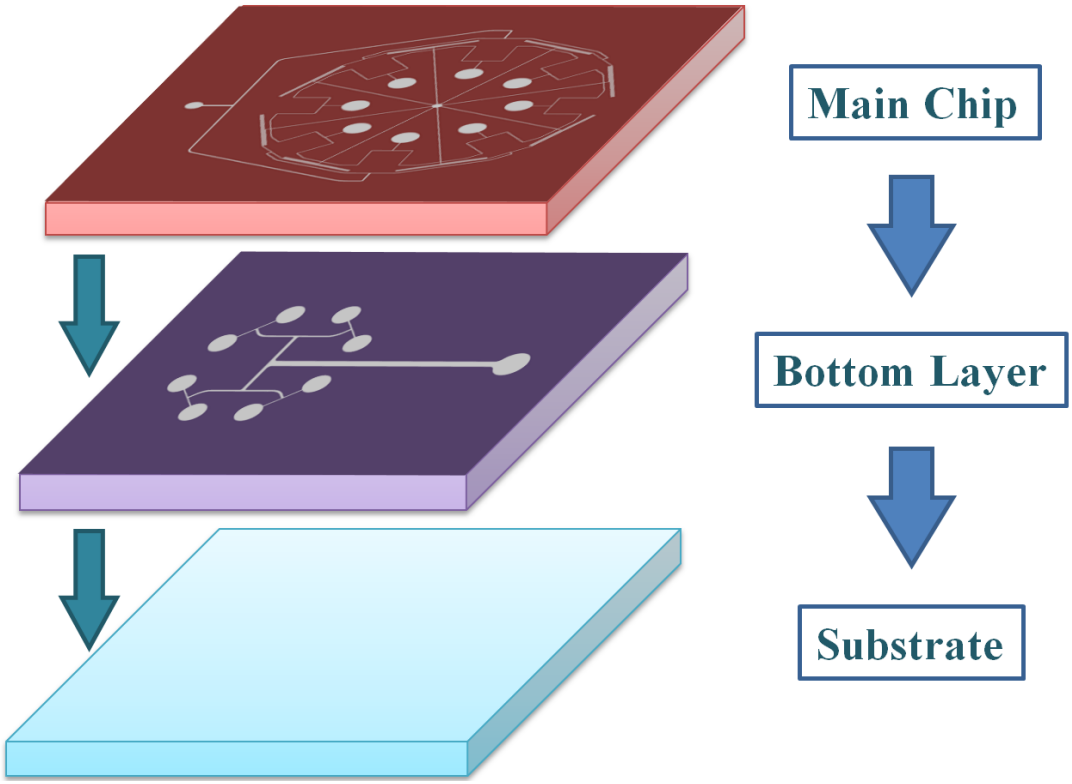

Figure 3.4. Fabrication of a multi-layer PDMS device consisting of main chip, bottom layer and a substrate.

Once the three-layer PDMS device is fully bonded, the whole three-layer PDMS device might be also bonded against a glass slide giving the device more possibility and stability to be safely placed underneath of the microscope and cameras for capturing the droplet generation process. In fact, in this case a PDMS slab is used as the substrate for bonding the bottom layer against it, and the glass slide then has no special functionality in terms of a substrate or a layer of the multi-layer design and is only used to give more stability to the device. Thus, the glass slide is not obligated to be physically bonded and is enough even just to place it underneath of the three-layer PDMS device and will stick to the bottom of the substrate (PDMS slab) due to a slight natural adhesion property of PDMS.

3.4 Droplet Generation

3.4.1 Solutions preparation

The continuous and dispersed phases for all the experiments are FC-40 oil and water, respectively. Prior to inject any fluids into the PDMS device, whether FC-40 oil, or water, or any other sort of liquids (like Aquapel™), the liquid is filtered through a sufficiently fine filter avoiding the entrance of any particle or contaminant which might further cause a blockage or failure in operation of the device. In practice, the liquids are filtered through a 0.2 µm CHROMAFIL® Xtra PET-20/25 or CHROMAFIL® Xtra RC-20/25 that are disposable syringe filters made of polyester and regenerated cellulose respectively having the pores which are 0.20 µm in diameter.[184, 185]

In order to produce more stable microdroplets, a surfactant may be added to the continuous phase (FC-40 oil). In fact, the surfactant is an agent which lowers the interfacial surface tension between the continuous and dispersed phase leading to facilitation of surface deformation what will result in formation of more stable microdroplets and avoiding the merging between the generated microdroplets.[186, 187] Therefore, a locally synthesized surfactant is added to the continuous phase for all the experiments with the concentration of %2 by weight and firmly mixed. The mixture of FC-40 and the surfactant might be filtered also prior to injection into the device.

3.4.2 High-speed camera

Due to the high-throughput of the microfluidic device in terms of numbers of generated microdroplets, a normal camera or microscope would not be rapid enough to capture all the generated microdroplets. Therefore, a high-speed camera is required to fulfill this need. In this work, a high-speed camera is used which is capable of capturing extremely large number of frames up to 9000 frames per second, with the minimum exposure time of 1 µs and adjustable exposure time ranging from 1 µs up to a couple of thousands microseconds. This high-speed camera is equipped with different objectives of 10X, 20X and 40X;

though, due to the massive size of the appropriate PDMS device in this work the objective of 10X is normally used and the objective of 20X is also used merely for the very sensitive and tiny features of the device. The camera stage is precisely controlled for the best position of the device by a joystick which is also programmable. The desired rate at which the images are expected to be capture in the system can be varied through the LabVIEW program installed on the connected computer what allows the user to have control over almost every key variable and parameter of the experiment such as numbers of required frames to be captured, rate of capturing, and image contrast. A detailed picture of the high-speed camera as well as its related belonging and sections has been presented in Appendix VI.

To this end, the sample (multi-layer PDMS device) is placed over the sample stage of the apparatus and fixed with the proper holder. Also, in order to feed the fluids (oil and water) into the PDMS device, two pumps are required. In this work, two similar syringe pumps from Harvard Apparatus so-called “Pump 11, Pico Plus Elite”[188] are used. Two 5 ml plastic syringes are filled with either of the fluids. Each of them is placed and carefully fixed on the syringe pumps. The connection tubing connects each syringe to the desired inlet of the PDMS device. In order to connect the tubing to the PDMS device, a metal pin is used which has the outer diameter as large as the inner diameter of the punched inlets holes in the PDMS device. When all the tubing are properly installed, the pumps are initiated to run by pressing the power option ensuring that all microchannels are thoroughly filled with the fluids and also the droplet generation phenomenon is effectively taking place within the microfluidic device.

Once the pumps and fluidic system of the module are properly installed and in use, the desired objective is mounted underneath of the device and then the focus and light intensity of the camera as well as the position of the device are regulated to reach the appropriate statue giving the best resolution according to the need. Utilizing the connected computer as well as the LabVIEW program, the number of required frames, the capturing rate and other key parameters are also properly manipulated. When all the parameters of operation are fully regulated and all the accessories are installed (as illustrated in Figure 3.5), the pumps

are let running and so the droplet generation starts to take place which is continuously observable on the screen. The capturing might be initiated at any time by either simply pressing the “record” button on the LabVIEW program or even pressing the external trigger. Once pressed, the high-speed camera immediately records the defined number of frames with the determined rate and subsequently, the video file might be saved in the directory. Due to the high resolution and high frequency of the camera, the generated video files are usually quite massive. The captured videos can be used further for analysis and result exploration.

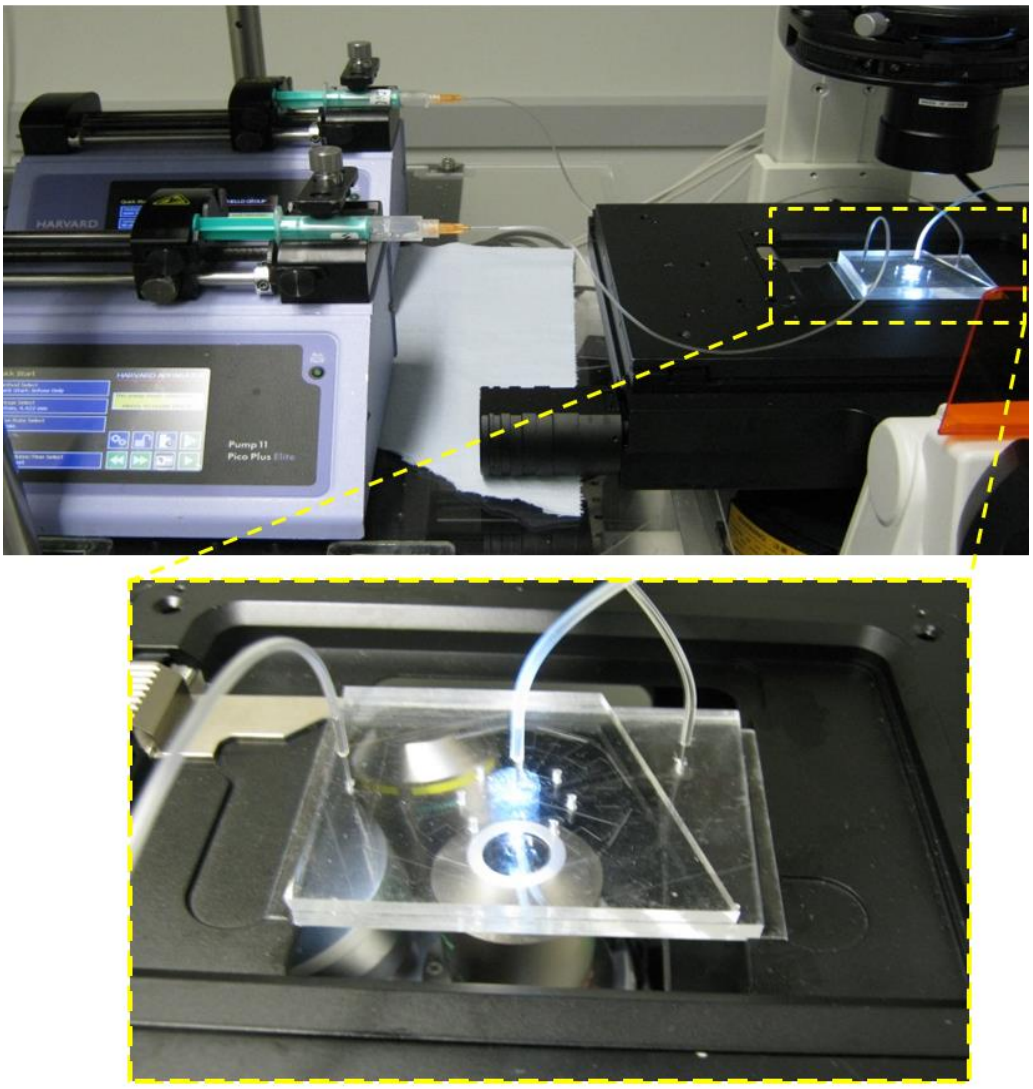

Figure 3.5. A device properly ready for capturing by high-speen camera with pumps, syringes of fluidc, and connection tubing effectively installed.

3.4.3 Data analysis by ImageJ®

The captured videos by high-speed camera are the raw videos and need to be analyzed. To that end, the videos are further imported to a freely available analyzer software so-called "ImageJ®" (Image Processing and Analysis in Java)[189] and get manipulated. In fact, a video is imported to ImageJ® and may be opened whether through a range of specific frames of the video or the entire frames (whole video). In order to facilitate the image processing as well as increase the accuracy, the threshold is applied to the image(s) to be analyzed sharpening the borders and edges to be more detectable and consequently, gives more reliable and accurate results. Figure 3.6 depicts two different types of threshold on an image which is getting processed by ImageJ® as well as the original image before threshold.

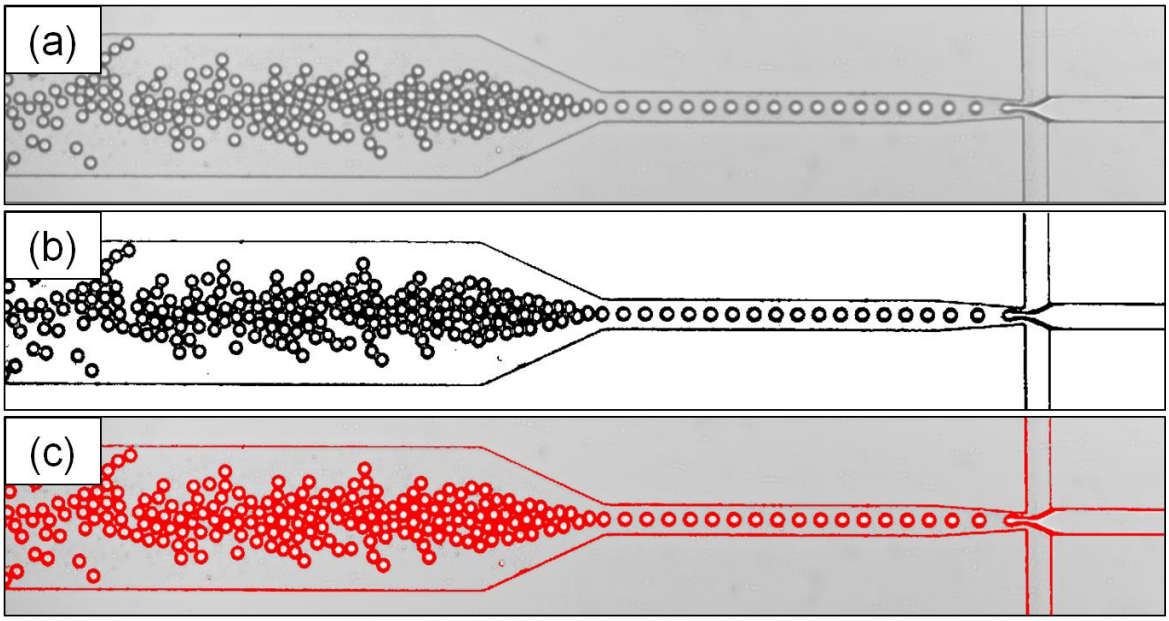

Figure 3.6. An image to process by ImageJ®. (a) The original image before threshold, (b) after applying black/white threshold, and (c) after applying red threshold.

Utilizing ImageJ®, it is possible to take any number of the frames ranging from a single to all the captured frames as the input for analysis. Also, ImageJ® is capable of providing various analysis results such as counting the number of the generated microdroplets, calculating the standard deviation as well as the area of each microdroplet, and also

drawing the desired population charts based on the area of microdroplets. For instance, a simple ordinary flow-focusing device is taken for droplet generation experiment with water and oil as the dispersed and continuous phase, respectively. The experiment is accomplished successfully and in total 100 frames is captured with the rate of 500 frames per second (fps) utilizing the high-speed camera. Analyzing the recorded 100 frames long video by ImageJ® (as the drawn charts are presented in Figure 3.7), the total number of generated microdroplets is calculated to be 1378.

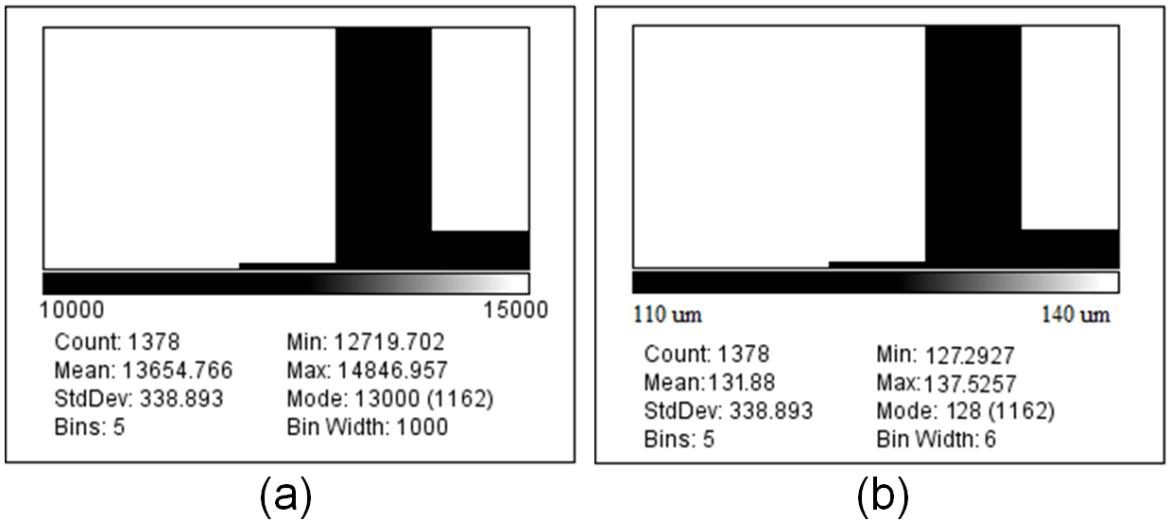

Figure 3.7. A sample of analysis results provided by ImageJ® which is (a) based on the surface area of the microdroplets and (b) based on the diameter of the microdroplets.

Moreover, the area of each generated microdroplet is also calculated by ImageJ® and given in a table. Based on the area, the diameter of each droplet is then easily calculated and the standard deviation might be calculated as

$$S = \left(\frac{1}{N}\sum_{i=1}^{N}(D_i - d_p)^2\right)^{0.5} \quad (2)$$

where S (m), N, and d_p (m) are standard deviation, number of generated droplets and mean droplets diameter, respectively and D_i (m) stands for the diameter of each generated droplet. Thus, having the total number and the diameter of the generated microdroplets, the

standard deviation for the generated microdroplets is easily found out. Subsequently, monodispersity index might be calculated as

$$\sigma = \frac{S}{d_p} \times 100 \tag{3}$$

where σ is monodispersity index. In the aforementioned example, the mean microdroplets diameter was calculated to be 131.88 μm and given the number of generated microdroplets which is 1378, the standard deviation and as a result, the monodispersity index are simply calculated using just mentioned equations and found out to be 1.63 μm and 1.2%, respectively.

In addition, having the number of the generated microdroplets, as well as the specifications of the captured video (number of total frames captured and rate of capturing), the throughput (or production rate) of the module would be easily calculated which shows the number of microdroplets generated within the device in every second. The throughput might be calculated as

$$Throughput = N \times \frac{Total\ Frames\ Captured}{R} \tag{4}$$

where R (fps) is the capturing rate of the high-speed camera. As previously mentioned, in total 100 frames are captured in this case while the camera undergoes the rate of 500 fps. Therefore, having the number of generated microdroplets, the throughput is simply calculated which is 6890 droplets per second that is not considered as a high-throughput process.

Having the required solutions prepared, the protocol for microfluidic device fabrication clear and the high-speed camera ready to use, different devices might be fabricated through the best protocol which gradually undergoes the required revisions and amendments accordingly.

3.5 Attempts and Troubleshooting

3.5.1 Collapsing problem and solutions

Based on what was described in the section 3.3, the multi-layer device could be fabricated. Accordingly, the first three layer PDMS device is fabricated with a PDMS slab as the substrate (shown in Appendix I) and is further experimentally tested aiming the droplet generation using water and FC-40 oil as dispersed and continuous phase. However, during the experiment, it is turned out that there is one main drawback observed with this fabrication protocol. In fact, the main channel of the bottom layer is collapsed through the length leading to partially or completely blockage of the channel and consequently non-applicability of the entire PDMS device.

To overcome this drawback (i.e. collapsing issue), the initial guess for the reason of the problem would be the extra pressing force while bonding; therefore, the simplest solution to that is to accomplish the bonding other way around meaning that start from bonding the bottom layer to the substrate followed by bonding the bonded two layer device to the main chip. Also, another technical solution is to make some amendments to the designed layout for bottom layer in terms of adding some regular supporting pillars in the middle of the channels toward the length as illustrated in Figure 3.8.

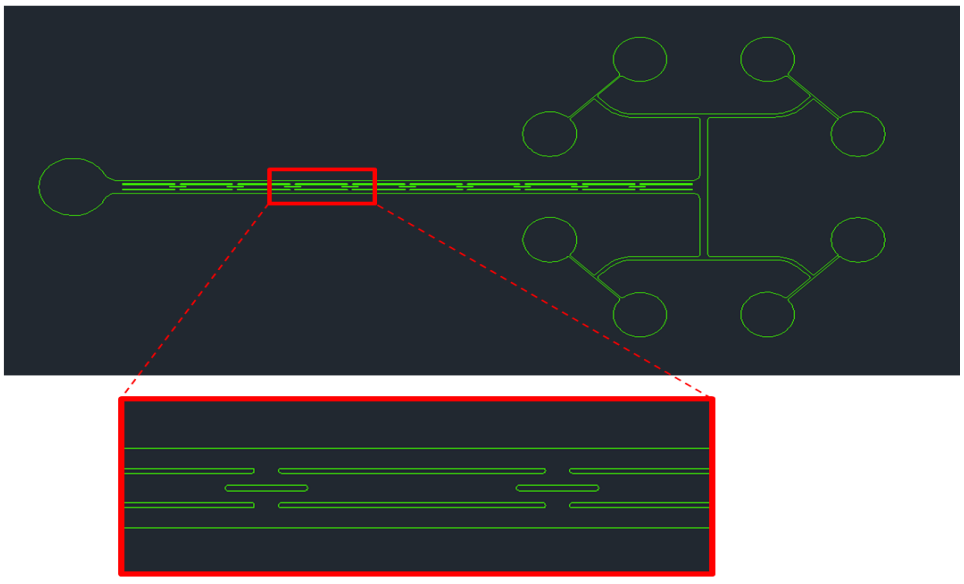

Figure 3.8. The layout of bottok layer enhanced with supporting pillars.

3.5.2 Thickness drawback and appropriate solutions

Once the problem with collapsing is solved, the next drawback just appears that is the large thickness of the multi-layer device! The large thickness of the three-layer device exceeds the maximum applicable thickness for functionality of the high-speed camera in which it can regulate the focus to capture the image or video and is around 8 mm. Therefore, the features and microchannels on the top layer (main chip) were not possible to be captured due to the position of the objective that is underneath of the device.

To overcome this drawback, there are two alternative methods that both concern the substrate. First protocol is to remove the PDMS slab (which was the substrate) and instead, bond the two-layer PDMS device (consisting of main chip and bottom layer) directly against a previously spin coated glass slide as shown in Figure 3.9 (a). And the second is to bond a very thin layer of PDMS over the glass slide and bond the main two-layer PDMS device (consisting of main chip and bottom layer) against the very thin layer of PDMS which has been bonded against the glass slide as illustrated in Figure 3.9 (b). Undergoing these protocols, prevent the problem of thickness and all the features and microchannels will be observable by high-speed camera provided that the thickness of the two PDMS layer of main chip and bottom layer is within a reasonable range.

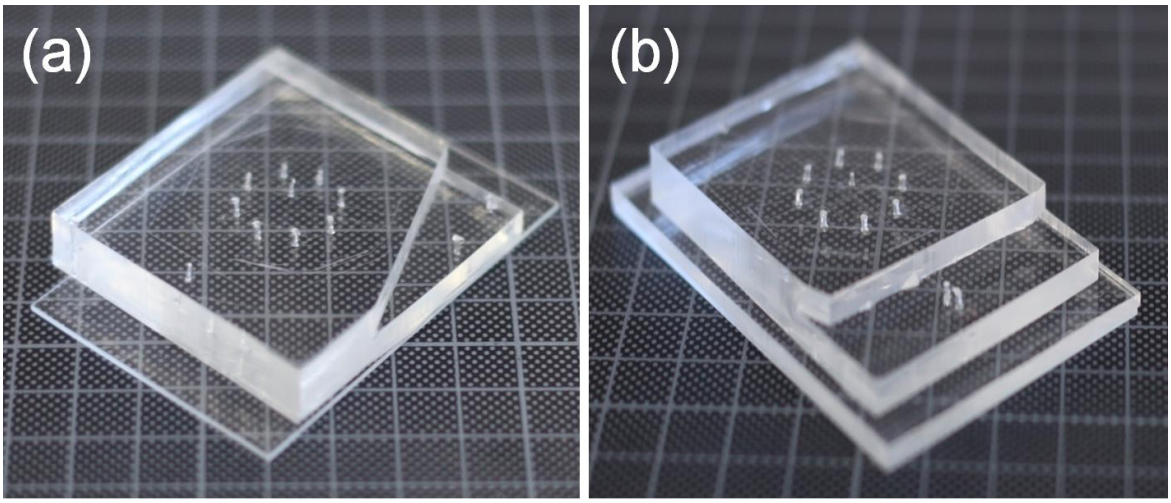

Figure 3.9. Two protocols to overcome the problem of limited applicable thickness. (a) Using a spin-coated glass slide as the substrate, and (b) using a glass slide with a thin layer of PDMS bonded its against as the substrate.

3.5.3 Instability of the inlets and proposed Solutions

Noteworthy that, due to more simplicity the devices are fabricated through the first mentioned protocol in previous section, meaning that a spin coated glass slide is used as the substrate for all the next attempts for fabrication of multi-layer microfluidic device. In fact, solving the problem with thickness facilitates carrying out the experiments with the fabricated devices. However, another problem happens during carrying out the experiments which cause the inlet pins and connection tubing to be thrown out of the inlet holes!

The first hypothesis is the human error during the fabrication process; however, fabricating two new devices through the same protocols with extreme care rejects this hypothesis when they both undergo the previous problem. As an alternative, making the inlet holes using microdrill machine instead of hole-puncher is also tested what provides the same result. Therefore, the final definitive solution is to fix the pins into the holes. To that end, two alternatives might be applied as represented in Figure 3.10 i.e. either apply a trace amount of uncured PDMS around the pins and inlets, or use a strong glue to fix the pins and subsequently use the uncured PDMS over the dried glue. The glue which is used in this work is so-called "Araldite® Rapid"[190] which is a strong two-component epoxy that completely dries in just less than five minutes.

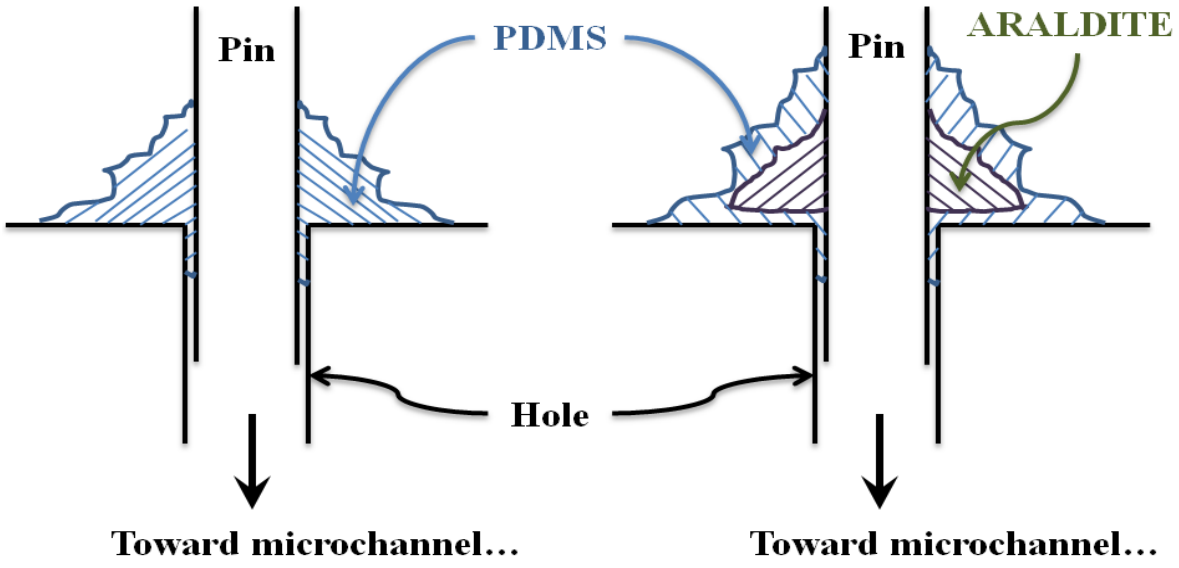

Figure 3.10. Solutions for fixing the pins and tubing into the inlets holes.

Following the mentioned protocols for stabilizing the inlets pins into the holes, the new microfluidic multi-layer devices are fabricated without any of the previous problems (neither collapsing, nor thickness issue, nor removing the inlets pins and tubing). Therefore, the experiments are carried out all over again using the new devices and the experiments are tested as previously explained i.e. trying to generate the microdroplets in a multi-layer microfluidic device having water and FC-40 oil as the dispersed and continuous phase. The tip is that initially the whole volume of the microchannels of the device is filled with oil phase for the better result and then the water is started to be injected using a syringe pump. The flow rate of two pumps is manipulated separately in order to achieve the situation in which the droplet generation happens. The essential point is that the flow rate of continuous phase is always higher than that of dispersed phase; otherwise there will be impossible for the droplets to form.

3.5.4 Back Pressure and Alternative Methods

The two pumps and desired syringes are checked prior to connection to the device ensuring there is no problem before the fluid enters the device. The microchannels are thoroughly filled with oil while the pump for water is fully regulated and temporarily paused. Once the system is stable, the pump for water is initiated and water enters the desired microchannels and passes through until reaches the flow-focusing area and enters the orifice. At there, due to the shear forces between two phases the droplets form. Therefore, the ratio of the flow rates is a critical parameter in this regard.

Given all the mentioned criteria and instructions for the experiments and despite of fabrication of the multi-layer device according to the latest defined protocol (with stabilized pins and tubing), a new problem arises in the experiment when all the channels are filled with oil and the pump for water is initiated! Unlike what is expected, there is no water flowing into the inlet and microchannel! The first scenario is this regard is the blockage within the inlet; however, it is soon rejected by replicating the experiment iteration with the same specifications. The next and the most probable hypothesis is the back pressure issue which avoids water to flow in. The problem may happen due to the

significantly long length of the microchannels relative to theirs small height. Therefore applying some remarkable modifications to the designed layout of main chip seems necessary.

To this end, as the first step two new masters are fabricated out of the same photomasks (for both main chip and bottom layer) with the microchannels height of 50 μm that is two times larger than the previous ones. The microfluidic device fabricated out of these new masters with larger height also shows not very significant and promising improvement in terms of flowing water into the device. Further, as the second alternative, the same layout is actually used for the main chip; however, with the channels enlarged in width for 1.6 times. This method requires photomask preparation and master fabrication as well and provides a lower ratio of length to width of the microchannels; however, the problem with water flowing is not resolved in the microfluidic device fabricated as the result of these new layouts as well.

And as the third option, the serpentines in the path of water microchannels is considered as an unnecessary element taking into account the current circumstances of the experiments. Therefore, they might be reduced or even totally eliminated so that the distance which water flow should travel from inlet to the flow-focusing section significantly decreases. Applying this modification leads to two new designs with short- and no-serpentine as is illustrated in Figure 3.11 (a) and (b). This is supposed to facilitate the situation with back pressure. Moreover, in order to split down the back pressure, a new set of layout is drawn in which the main water channel splits into four channels either fully symmetric, or semi-symmetric right after the main water inlet as shown in Figure 3.11 (c) and (d).

These all new layouts are subject to photomask imprint and consequently master fabrication prior to be able to caste PDMS device against them. These masters might be also fabricated for the height of either 25 μm or 50 μm; however, in order to be on the safe side, the height of 50 μm is selected for the masters. Nevertheless, the PDMS devices fabricated out of the main chip with no serpentine as well as min chip with symmetric splitter are experimentally tested where not that much improved manner is observed in terms of water flow! Though, increasing the flow rates, a weak droplet generation

phenomenon happens within the microfluidic device, but it is not the symmetric and expected desired high-throughput process.

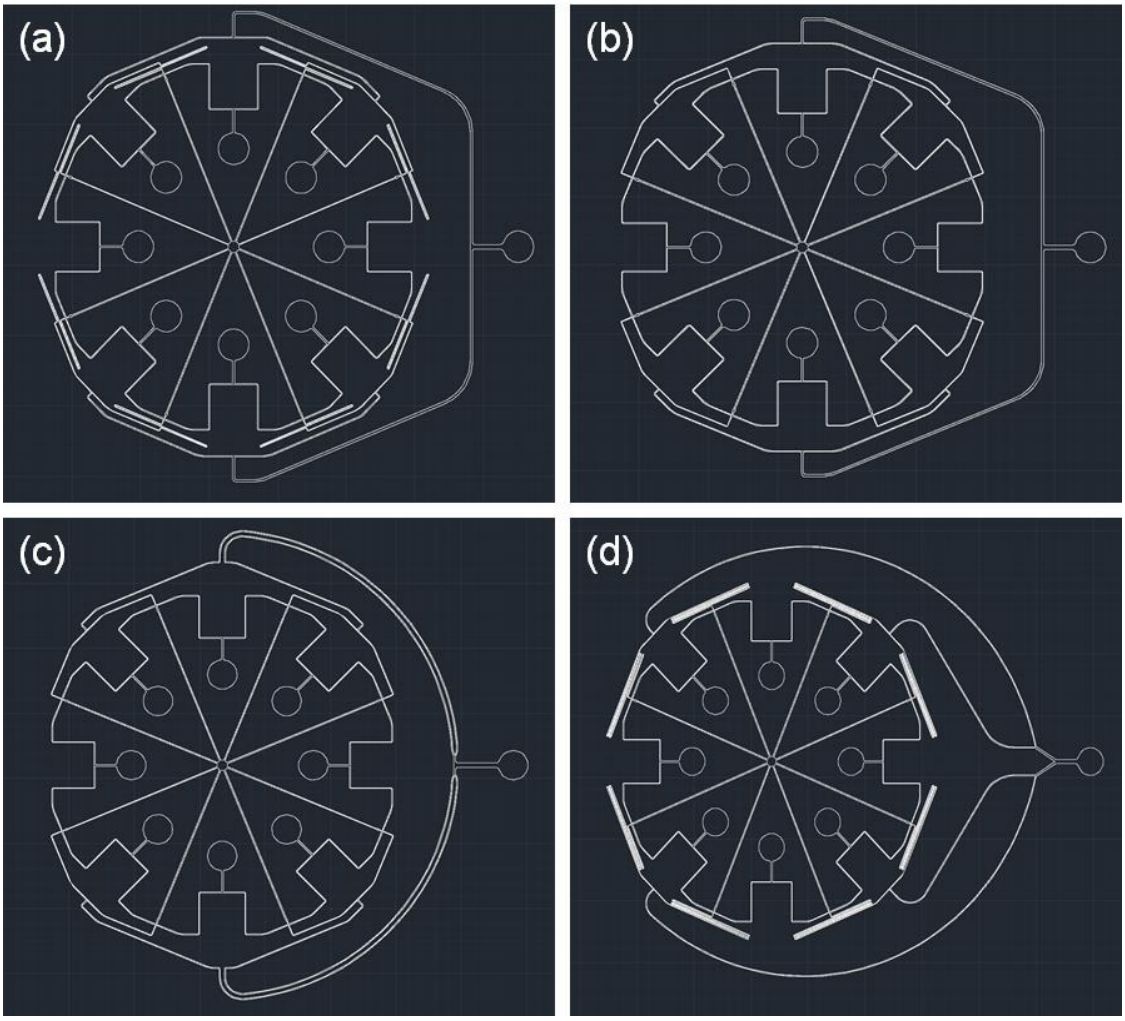

Figure 3.11. New drawn layouts aiming to solve the problem with back pressure. Main chip with (a) short serpentine and (b) no serpentine, and using (c) fully symmetric and (d) semi-symmetric splitter at main water channel of main chip.

3.6 Exploitation of a 3D Printer

Considering the difficulties and drawbacks with handling of the PDMS devices as well as long time required for some fundamental and basic microfabrication processes, incorporation of the utilization of a 3D printer into the microfluidic fabrication and microfluidic device preparation is a highly promising platform. The 3D printer has been

extensively used in different industries mostly to manufacture the design prototypes; however, the exploitation of a 3D printer in for microfluidic applications is a relatively emerging issue providing large numbers of opportunity within microfluidic technology.[191-194]

As the matter of fact, incorporation of a 3D printer into the fabrication process might lead to the better and perhaps easier methods. Therefore, two different tries with the objective of utilizing 3D printer might be carried out that is either three-dimensional printing of a 3D designed holding frame for the previously fabricated PDMS device or more interestingly three-dimensional printing of a whole microfluidic device designed in 3D including all the microchannels and tiny features.

3.6.1 3D Holding Frame

In order to solve the problem with instability of the inlets pins as well as the drawback with back pressure, a sort of holding frame might be used to fix the inlets stronger. To this end, exploitation of a 3D printer may bring a useful alternative. Thus, a high-definition 3D printer so-called “ProJet™ HD 3000” is utilized.[195] Noteworthy the aforementioned 3D printer is capable of proper printing of the straight features and straight microchannels with the precision of down to about 100-150 µm. Also, the twisty and curved microchannels with the precision of down to around 200 µm are likely to be printed out properly and completely.

As the first try, a holding frame is designed in three-dimensional domain in order to further contain the previously fabricated multi-layer PDMS device. To that end, the CAD drawing files for main chip (which is the upper chip) is considered and the positions of the inputs are precisely taken into account for the accurate design of the holding frame. Then, two slightly different designs for the holding frames are drawn in which one of them has fixed bars and another moveable bars (as shown in Figure 3.12). Moreover, in order to ensure the positions of inlets of the PDMS device are punched properly and are exactly at the corresponding positions of the predicted places at the bars of the holding frames, some

assisting sheets are also designed and fabricated by 3D printer what could be used for cutting the PDMS slab after curing and prior to bonding (as illustrated in Figure 3.13 (b)).

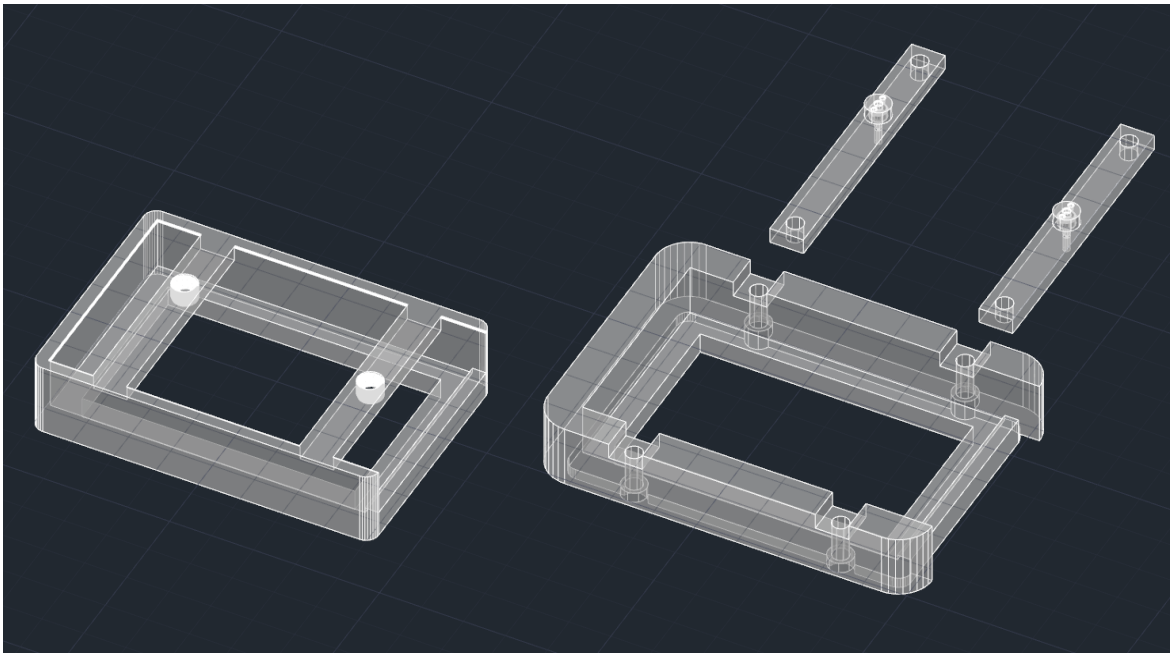

Figure 3.12. Designs for a holding frame to be printed out by a 3D printer.

In addition, a special type of fitting is designed to enhance the stability of the inlets in which three holes are located next each other including the main inlet hole in the middle and two smaller holes in the sides. The two smaller holes are internally connected and have surrounded the main hole to which the tubing is inserted. Another class of PDMS that Sylgard-184® is applied for this purpose which has more hardness after curing and is black in color. This PDMS is also available as a two-component kit so-called Sylgard-170®[196] which is used to fill the two sided holes completely. This PDMS is prepared by mixing the two components with the same quantity for prepolymer and curing agent and before usage; it should be degassed like Sylgard-184®. The two sided holes are connected and have surrounded the main inlet hole in which the tubing is previously placed. Then, they are filled with prepared Sylgard-170® thoroughly and subsequently the PDMS should be cured in the oven; however, it needs shorter time for curing in comparison with Sylgard-184®. Figure 3.13 (a) depicts a simple fitting block and an enhanced fitting module to be placed over the bars of the holding frame.

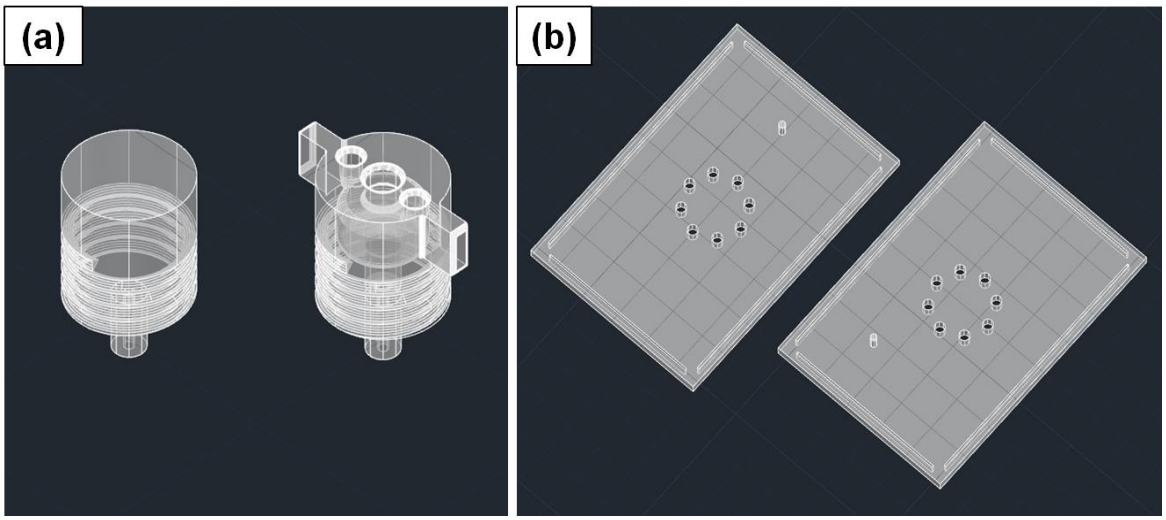

Figure 3.13. Designs for (a) fitting to be installed on the bars of the holding frame, and (b) measuring sheets to cut the PDMS slabs according to the hoding frame structure.

A few different types of holding frames are designed and tested until finally the best design which has the moveable bars is taken for the experiment investigations. A small problem observed with the tiny tail of the fitting (as shown in Figure 3.13 (a)) so that due to the small diameter, they are very likely to break off while installing on the PDMS device (illustrated in Appendix VIII (c)). To that end, their outer diameter might be designed to be larger and obviously the diameter of the punched holes in the PDMS device should be wider accordingly. Figure 3.14 shows a 3D printed holding frame in which the multi-layer PDMS device has been installed for the experiments.

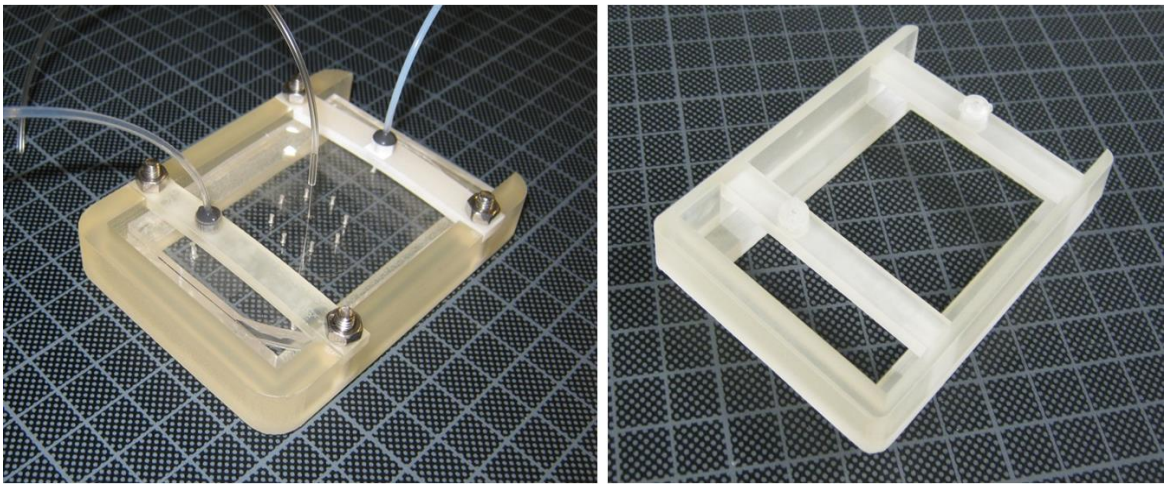

Figure 3.14. A 3D printed holding frame alone as well as with PDMS device installed.

The primary results out of this method demonstrate a promising future for application of these kinds of holding frames; however, due to the lack of time they could not be investigated and experimentally tested extensively.

3.6.2 3D Microfluidic Device

Another application of a 3D printer is to go even beyond this and design a whole microfluidic device in three-dimensional domain and print the whole device in 3D. To that end, both designs of the main chip and the bottom layer are applied to generate a new three-dimensional design of the entire microfluidic device. The 3D design is drawn in AutoCAD® and converted to the appropriate format which is readable by the 3D printer (that is a ".stl" file).

Noteworthy that due to the resolution of the 3D printer, the small features of the design such as the microchannels that are 50, 80 and 100 µm as well as the orifice geometry with the entrance width of 40 µm are likely to be printed uncompleted or even damaged and corrupted; therefore, all the tiny geometric sizes like the mentioned ones are resized and scaled-up for three times. Thus, the corresponding microchannels will have the width as large as 150, 240, and 300 µm respectively and the orifice entrance will be 120 µm wide. Once the three-dimensional design is fully drawn and saved according to the desired format, it could be sent further to be printed by 3D printer.

Required time for the printing of a 3D printed device varies according to the size, complexity and the tiny features of the design. In this case, printing every one of the 3D microfluidic device takes around 8-10 hours. Adding the required time for post-processing such as cleaning, polishing up and more importantly, removing the wax from the engraved features of the printed device, will lead to the time of about one day per every printing, which still far less than corresponding time required for the fabrication of a microfluidic device through photolithography mask preparation, master fabrication, and PDMS device fabrication with bonding, post treatment and other related tasks. Therefore, this method could be potentially a suitable alternative for fabrication of the microfluidic device; though it is subject to limitation of material, size and also cost. Figure 3.15 represents the complete

3D design for the desired microfluidic device drawn utilizing AutoCAD® to be sent forward to a 3D printer.

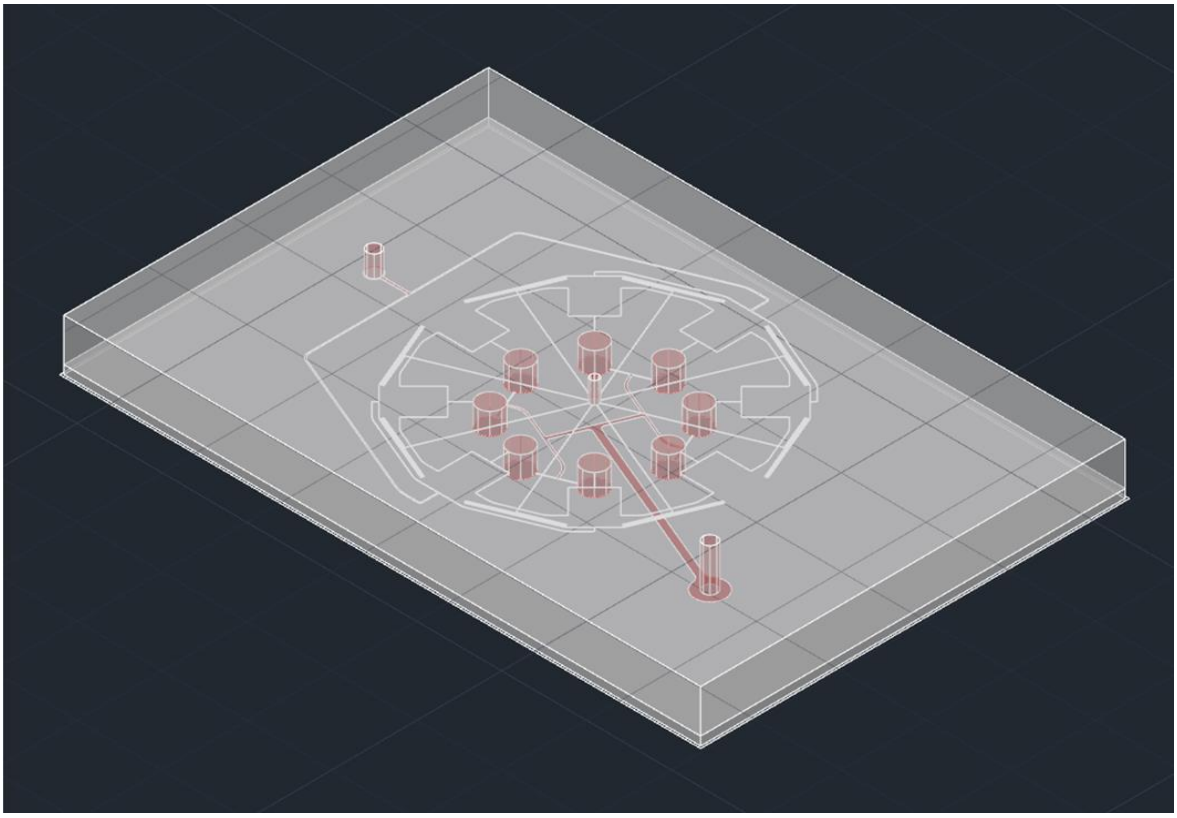

Figure 3.15. A 3D design of a multi-layer microfluidic device drawn by AutoCAD® to be printed by a 3D printer.

Unsurprisingly, the first few tries out of the 3D printer are semi-damaged with missing or improperly printed microchannels. Manipulating the geometries of the microchannels and design as explained before, the proper dimensions and geometry is figured out. Moreover, for more stability of the inlets and also to prevent the licking at the inlets, the same fitting design as shown in Figure 3.13 (a) is integrated into the 3D design on the upper part of the inlets so that the tubing might be further inserted and fixed by applying Sylgard-170® into the sided holes.

However, another key issue in this regard is removing the wax from the printed design. Since in this case, there are many long and relatively narrow microchannels particularly in the upper section of the design (corresponding to the main chip of the microfluidic device),

the process of removing wax becomes very vital; otherwise, remaining a little amount of wax inside the device might cause the printed device would be inapplicable. This process is normally accomplished by sonication. Thus, the printed device is placed into a sonicator bath for a few hours until the wax would be completely removed from the microchannels. It could be checked by a stereoscope time by time. Once the process of removing wax is completely fulfilled, the tubing may be installed into the inlets holes and fixed by applying Sylgard-170® around that and obviously curing afterwards. After that, the 3D printed device might be used for the experiments as Figure 3.16 represents a sample of 3D printed device before and during the experiments.

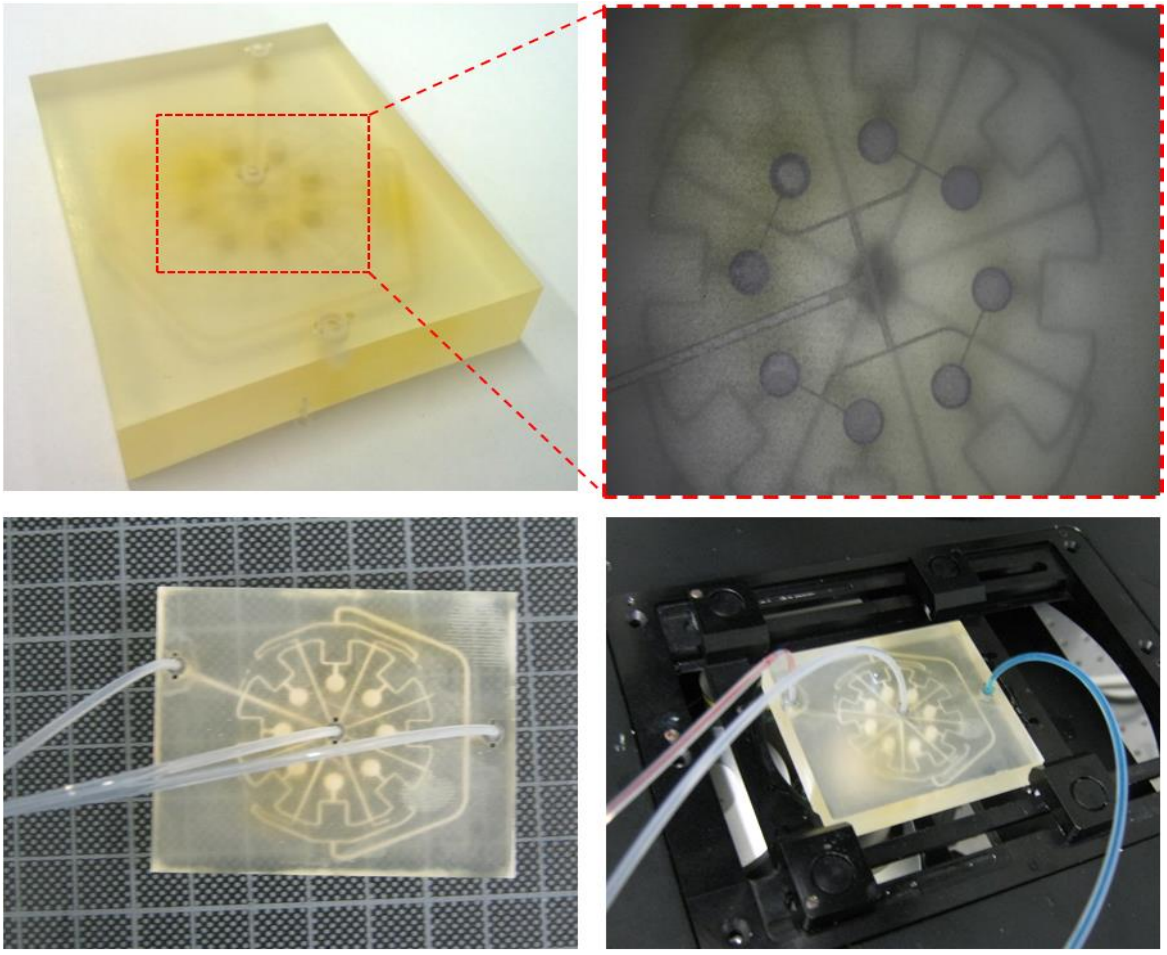

Figure 3.16. A 3D printed microfluidic device alone, with installed tubing and during experiment with colorful fluids.

The only small drawback in this regard is capturing inside the printed module since due to the used material for printing, the surface as well as whole device is not transparent. Although, applying the polishing process on the surface the transparency will be enhanced, it is not completely sufficient for imaging. To this end, the solution is to apply a strong polishing process on the surface or alternatively, image the microdroplets off chip so that the microdroplets are generated inside the 3D printed microfluidic device and then leave the device from the outlet and pas through a transparent capillary where they could be captured. Also, adding dye in the fluids (particularly in the continuous phase) will lead to be easier distinguishable as well as generating more elegant images. Due to the lack of time, this method is also left for future researchers to be further and more extensively investigated.

4 SIMULATION

The manipulation of droplets in microfluidic channels is an immensely useful technological platform for applications in many scientific fields such as biology, biomedical studies, chemical synthesis and drug discovery. There have been many investigations experimentally researching the process of droplet generation in a microfluidic device in terms of the role of geometries [197], the effect of viscosities [198] and the influence of flow-rates [199] on droplet formation. However, the experimental and empirical researches are usually subject to spend much amount of time, efforts and facilities as well as they typically undergo a high chance of failure particularly at the initial stages. Therefore a numerical study of microdroplet generation can play a crucial role in providing a model for predicting the effect of different parameters on a droplet generation module. There are many different numerical studies carried out dealing with the field of droplet formation.[200-204] These models may be able to forecast the performance of a module precisely in terms of droplet size and frequency, as well as the functionality of the entire system. Moreover, this will lead to a better understanding of the phenomenon of droplet generation.[201, 205, 206]

Thus, a reliable simulation may be a suitable method in order to reduce the required time for achievement of the optimized characteristics of the systems also to forecast the consequence of modifications in the process. In this work, the effect of flow rates of both phases and their ratio on the size of generated droplets is investigated. The simulations are carried out utilizing a well-known specialized software for various engineering fields including computational fluid dynamics (CFD) so-called COMSOL Multiphysics® (hereinafter referred to as only COMSOL®). This software takes advantage of an enhanced library specifically and solely to model and simulate the droplet formation systems.

4.1 Geometry and Initial Data Description

Generally, the simulation of droplet breakup in COMSOL® is a complicated and to some extents, difficult process. Thus, the aim of this section is firstly to obtain the right

procedure for simulation of droplet generation by COMSOL. And secondly, to completely simulate a specific flow-focusing droplet generator as well as investigate the effect of input velocities ratio on droplet size in a microfluidic device. To this end, a typical flow-focusing device which is shown in Figure 4.1 illustrating the geometry dimensions and computational mesh is taken as the case. As it might be observed on the figure as well, the diameter of the input channels for both phases (continuous and dispersed) is the same and equal to 50 µm. Both phases enter a 30 µm wide orifice and pass through an expanding area where the droplets are formed due to the shear force which is 200 µm long. Finally, the fluids move along a post-orifice channel which is 70 µm in width and 340 µm in length. Although in the real device, the length of channels are significantly longer, in the simulation they are cut into the shortest possible length to reduce the required time for the software to solve the simulations.

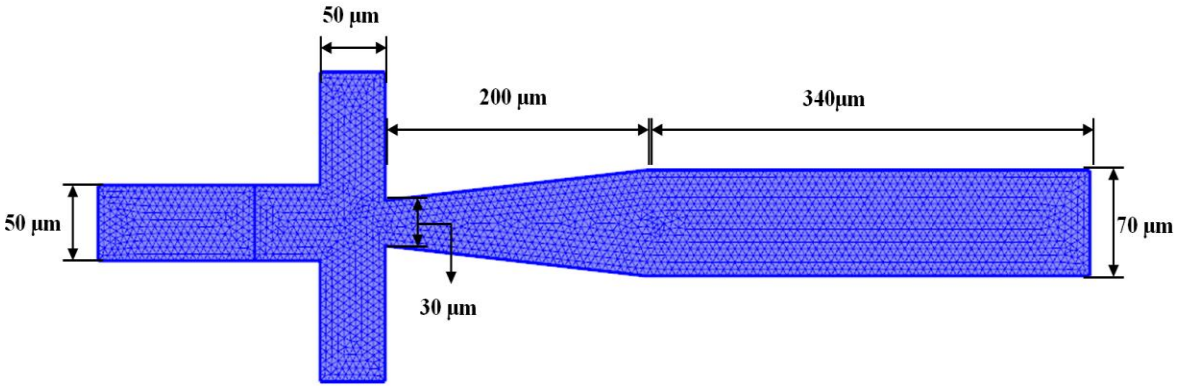

Figure 4.1. The geometry dimensions and computational mesh of the used flow-focusing device for the simulations.

The same as the experimental parts, FC-40 and water are used in the simulation as the continuous and dispersed phase, respectively. Water is already defined among the available materials of COMSOL®; however, FC-40 is not available in the material library of COMSOL®; thus, is required to be defined manually. Definition of a new material in COMSOL® can be accomplished through manually defining the density and dynamic viscosity of due material.

4.2 Carry Out the Simulations

In this work, the process of droplet generation using water as the dispersed phase and FC-40 oil as the continuous phase in a microfluidic device is numerically investigated. In particular, COMSOL Multiphysics® version of 4.3a is utilized. In fact, the simulations are accomplished within the module of "Microfluidics" and in particular, the library of "Droplet_Breakup". All the simulations are carried out in a two dimensional domain through a flow-focusing droplet generator which is illustrated in Figure 4.1 along with the geometric dimensions and the computational mesh. In fact, the geometry is firstly designed and drawn in AutoCAD® and is further simply imported into COMSOL®. Also, in order to be further able to define two different phases (materials), the design should be apparently divided into two compartments. To that end, an extra line is drawn in the channel of dispersed phase (water) which causes the flow-focusing design would be divided into two separated compartments. However, in the section of physics, this separating line is defined as the initial interface at where two phases start to get in contact to each other. Over time, this interface deforms and bends along the axis toward the orifice at where the formation of droplets begins.

Initially the simulations are run through normal mesh to obtain the result faster. Once the proper parameters for droplet generation are determined, the iteration is carried out through fine mesh to achieve more accurate and reliable results. In terms of study mode, all the simulation runs are defined to be "time dependent" and to have a better sense of the actual experiment and also in order to minimize the required time for computing the simulation, each run is accomplished over a very short period of time i.e. 0 to 0.01 second, with the time span of 0.0005 second.

The simulations are fulfilled through the physics of "laminar two-phase flow, Level set" with the channel walls specified as wetted. In order to define the walls as wetted walls, the key parameter to define is the contact angle to which the droplet generation system is so sensitive and dependent. To that end, having the typical range for contact angle extracted from literature review and also an extensive trial and error through much iteration, finally

the optimum contact angle between water and FC-40 oil for droplet generation is determined to be 0.349 radian.

4.3 Simulation Results

The simulation tries are carried out through two different categories, one with a varying oil velocity at constant water velocity and the other with a constant oil velocity and varying water velocity taking into account that the velocity ratios are the same in both cases. And the effect of the velocity ratio between the aqueous and oil phases on droplet size was studied using two sets of simulations. Initially, running a few iterations, the applicable range for the velocity of phases at which the droplet formation takes place is determined and different ratios within the determined range are considered as the desired velocity ratio for each set of simulation.

For the first set of simulations, the oil inlet velocity is varied between 0.0449 m/s to 0.36 m/s in eight steps while the water inlet velocity is kept constant at 0.04 m/s giving the water to oil velocity ratio (Vw/Vo) of 0.11, 0.22, 0.33, 0.44, 0.44, 0.55, 0.66, 0.77, and 0.88. However, it is observed that there is no droplet generation phenomenon taking place in the first two ratios (0.11 and 0.22); therefore, these two ratios are left out of the applicable ratios and only the remaining six ratios are taken for the actual simulation. Therefore, the oil inlet velocity is varied between 0.0449 m/s to 0.12 m/s and the applicable ratios are from 0.33 to 0.88.

Since software COMSOL® is not capable of parallelizing the simulations, each simulation is run separately and averagely takes a couple of hours depending on the mesh size and also the configurations of the computer on which the computing is accomplished. Finally, all the six simulations for the first set (that is called constant water velocity) are successfully accomplished and droplet generation is clearly observed in all of them. With the same water velocity of 0.04 m/s, all of the six results might be collected together and compared to each other. Figure 4.2 represents the simulation results of this set of simulations. As expected, droplet formation phenomenon occurs in all of them. Moreover, given the same

water velocity (as the dispersed phase), the size of generated droplets decrease by increasing the oil velocity (as the continuous phase).

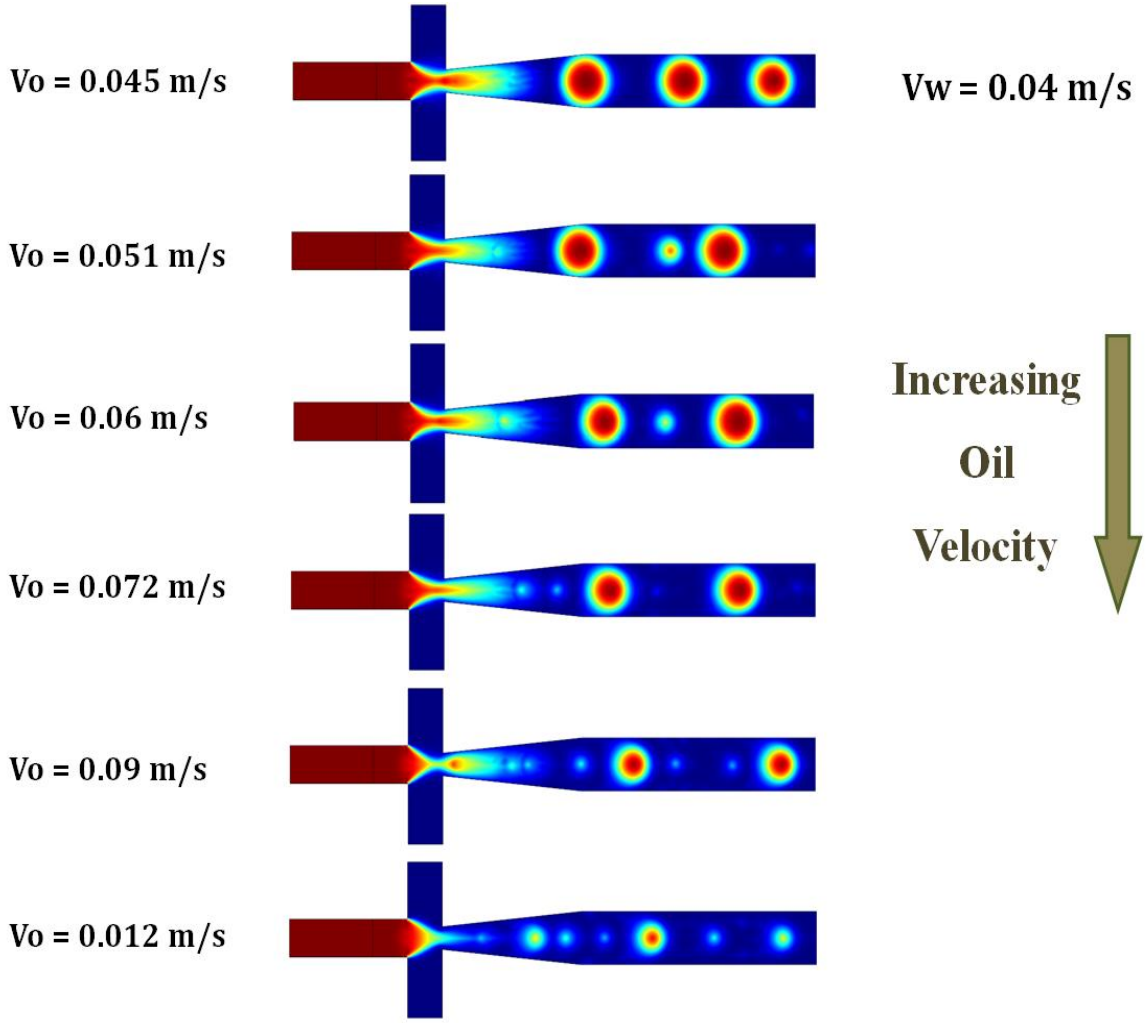

Figure 4.2. Simulation results for constant water velocity. Vw and Vo denote water and oil input velocities respectively.

For the second set of simulations which is called constant oil velocity, also the same velocity ratios as for the first set are applied. In them, the six ratio of 0.33 to 0.88 are used when the oil inlet velocity is held constant at 0.09 m/s; and consequently, the water inlet velocity is varied between 0.03 m/s and 0.08 m/s in six stages. Figure 4.3 depicts all the simulations in this set. As it might be seen from the figure, droplet sizes are increasing by

increasing the water input velocity at constant oil velocity at 0.09 m/s and this is what is expected from any flow-focusing device in terms of droplet generation.

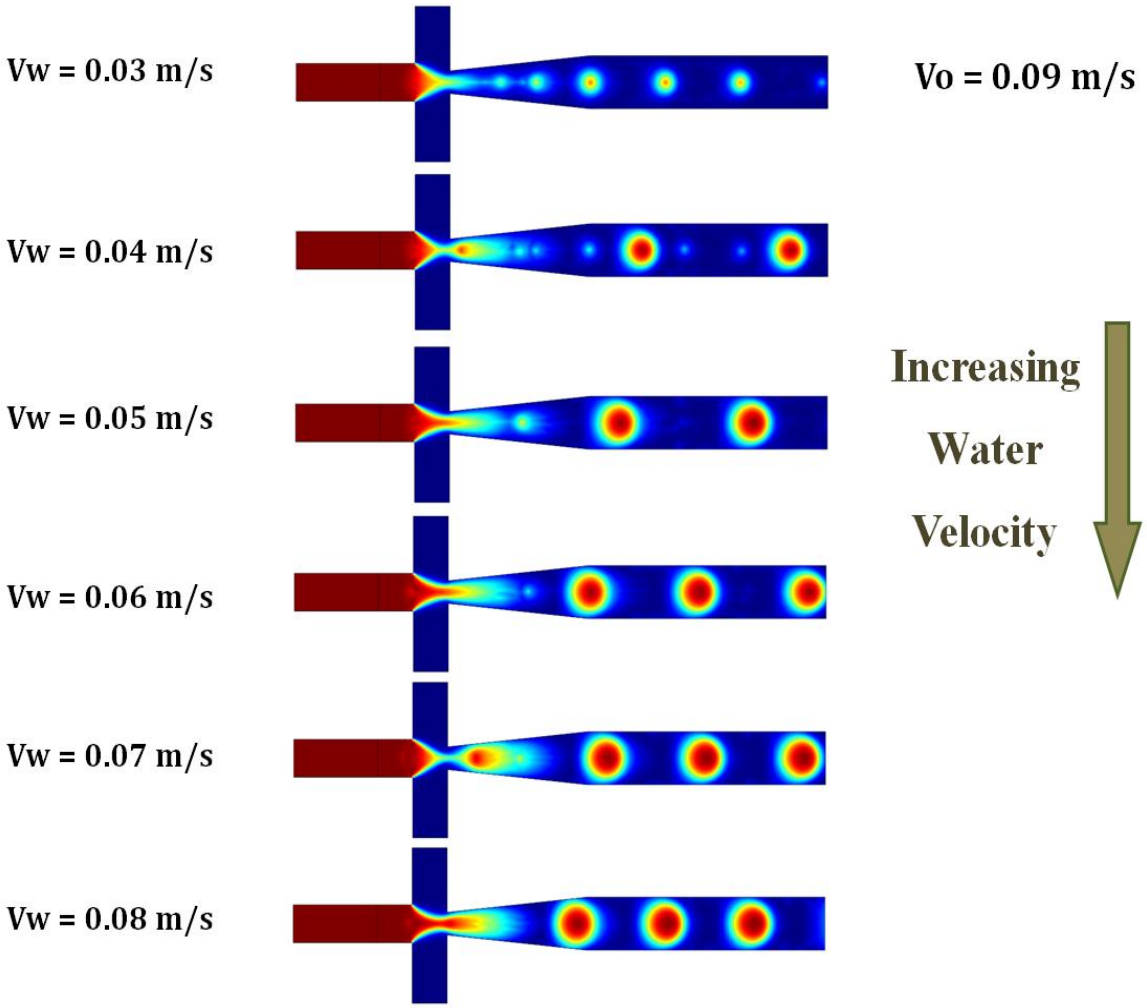

Figure 4.3. Simulation results for constant oil velocity. Vw and Vo denote water and oil input velocities respectively.

The obtained results out of these two sets may be compared to each other; thus, the size of generated droplets must be measured. To that end, mean droplets size is measured based on 3-4 measurements in each simulation case and the standard deviation is also calculated. In order to achieve a comparative diagram, the results of both sets of simulations are plotted on a same graph in which the droplets size is plotted with respect to water to oil velocity

ratio (Vw/Vo). Figure 4.4 represents the drawn graph indicating the mean size of generated droplets with respect to the ratio of input velocities.

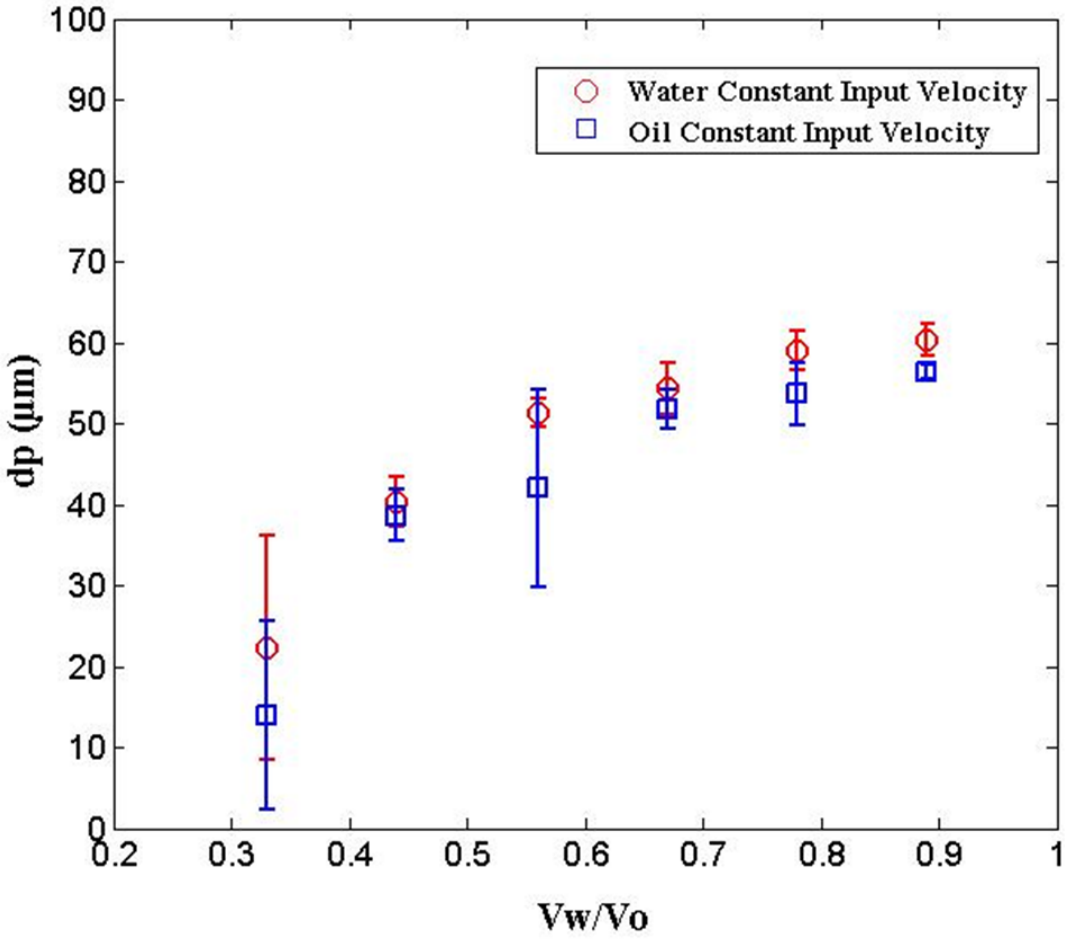

Figure 4.4. Droplets size (dp) based on the ratio of input velocities.

The variation in the sizes of generated droplets and consequently different standard deviation in each simulation stems from the measuring method and also the accuracy in measuring the sizes.

Both sets of simulations indicate similar droplet sizes for same ratio of input velocities. In other words, the results demonstrate that the average sizes for the droplets appear in the closely same position for each velocity ratio. Therefore, as the result it can be concluded that the velocity ratio of two phases is the key factor determining the size of the droplets. It can be also claimed that the velocity of either phase has nothing to do with the size of

generated droplets, but the ratio between them is the parameter which determines the droplets size.

To investigate this issue further, additional simulations with different oil and water input velocity ranges might be accomplished to proof the idea with more precision. Moreover, this work could be extended to investigate the polydispersity of droplets and the effect of varying the device geometry, with for example different expansion angles near the nozzle. Also, generating the experimental results for a microfluidic device with the same geometry as of the one used in simulations and comparison to the simulation results can technically verify the obtained conclusion.

5 DESIGN OF A TAYLOR-COUETTE DEVICE FOR DROPLET GENERATION

5.1 Principles of the Taylor-Couette Flow Device

As it was explained earlier in the section 2.2.4 the second approach to generate the microdroplets is to utilize a concentric double-cylinder undergoing Taylor-Couette flow pattern. As the matter of fact, the main aspect of this device is based on the rotation. Regarding its principle, the device contains two concentric cylinders located one into another that depending on their orientation, they may be categorized as horizontal or vertical device.[176] A sample of vertical device has been schematically illustrated in Figure 2.14.

The outer cylinder, which is typically made of a transparent substance, is fixed and the inner one that is normally made of steel is rotatable. The gap area between two cylinders, that is the actual working area, is initially filled with the fluid (that is actually the continuous phase) and subsequently when the gap is thoroughly filled with continuous phase, the inner cylinder starts rotating to reach the desired rotational speed. The desired rotational speed is determined according to the conditions of the system and the types of fluids used to generate the droplets. During the rotation of the inner cylinder, the fluid filling the gap undergoes the Taylor-Couette flow pattern. Once the inner cylinder reached the desired rotational speed, the second fluid (that is the disperse phase) is injected to the gap through a separate inlet and due to the immiscibility of the phases, the second fluids appears as the droplets into the first fluids. According to the pattern of the pattern of the flow in the device (i.e. Taylor-Couette flow) the droplets are transferred along the cylinders axis moving forward toward the outlet of the device.

Depending on the dimensions and geometries of the device, in particular, the gap area, the rotational speed of the inner cylinder and the flow rate of the dispersed phase (that is injected later) the size and generation rate of the droplets may vary. The main deal in designing a Taylor-Couette flow device to determine the optimum dimensions of the

cylinder device according the purpose and desired droplet specifications. In this approach, the actual size is not as of high importance, but the throughput of the system and the monodispersity of the generated droplets are the main goal parameters which are investigated.

5.2 Set-up Design

In this work, a set-up is needed to be designed and constructed as illustrated in Figure 5.1 which consists of a cylinder device, two pumps and a motor. The cylinder device that is actually a Taylor-Couette flow device is a horizontal type which consists of two concentric cylinders. The whole assembly of the two cylinders device is located inside another larger concentric cylinder box containing a solution circulating around the Taylor-Couette flow device to keep the working temperature constant for the device.

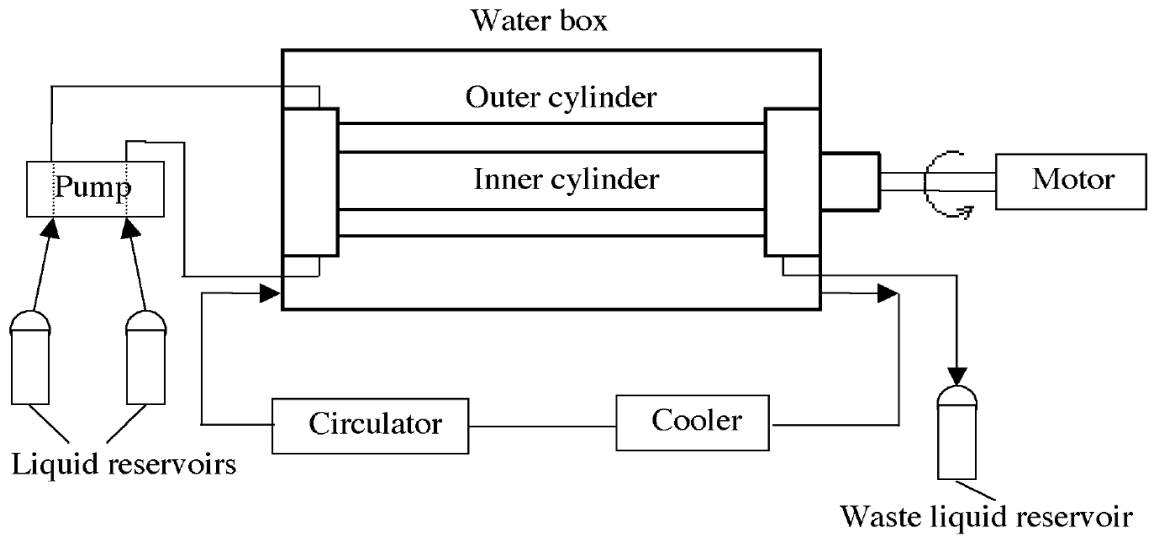

Figure 5.1. Schematice view of set-up for Taylor-Couette device.[95]

The experimental set-up to be designed and constructed will have the following specifications:

- The set-up consists of three main equipment parts including two pumps, one motor, and a double cylinder device.
- The outer cylinder is fixed and the inner one is driven.

- Two immiscible liquids are used as the fluids for droplet generation. One of them is water and another is oil.

- The gap is initially filled with and inner cylinder is accelerated from rest to reach the desired speed. Then, the inlet pump is started and the droplets are formed.

- The entire assembly of double-cylinder is placed inside a transparent box containing a cooling substance circulating around the double-cylinder to keep the temperature constant.

Pumps and motor may be carefully selected and ordered from the specialized companies; however, the specific double-cylinder device is not likely to be commercially available; thus, it has to be fully designed and subsequently constructed by technicians in the workshops (in this case by the technicians at the central workshop of ETH Zurich, campus of Honggerberg). To purchase the most appropriate pumps and motor, a comprehensive online search is fulfilled followed by establishing an extensive communication with the companies through submitting inquiry to about 40 companies for electric motor as well as about 25 companies for pumps. Eventually, the most appropriate peristaltic pumps and electric motor are ordered and purchased as explained through the following sections separately.

5.2.1 Pumps

To inject the two fluids into the system, two similar pumps are needed. Since high precision is required, and also regarding that the fluids to be pumped are clean fluids, the peristaltic pumps are selected as the most appropriate options because in that case the cross contamination with the components of the exposed pump does not occur. Therefore, two peristaltic pumps are needed. Since these pumps are supposed to operate under a very low flow rates about 10 ml/min, they should be very accurate and precise. Also, in order to minimize the human error and increase the precision, they are recommended to be controllable by a LabVIEW program. Also, due to the small amount of fluids to be pumped and the scale of the system, the outlet pressure of the pump will not be more than 1 bar.

Eventually, two peristaltic pumps are purchased which can pump the fluids with the with low flow rate down to around 10 ml/min. In fact, the main specifications of the purchased pumps are enlisted below:

- Manufacturing company: Lambda Instrument GmbH, Switzerland.
- Effective applicable flow rate range: 0 - 600 ml/h (0 - 10 ml/min).
- Both pumps are capable of being programmed and controlled by a PC/LABVIEW or also alternatively they might be operated in ON/OFF mode
- In addition, a RS-interface for PC control as well as a RS-connection kit is also included.

Figure 5.2 illustrates one of the two purchased identical peristaltic pumps at front and up view.

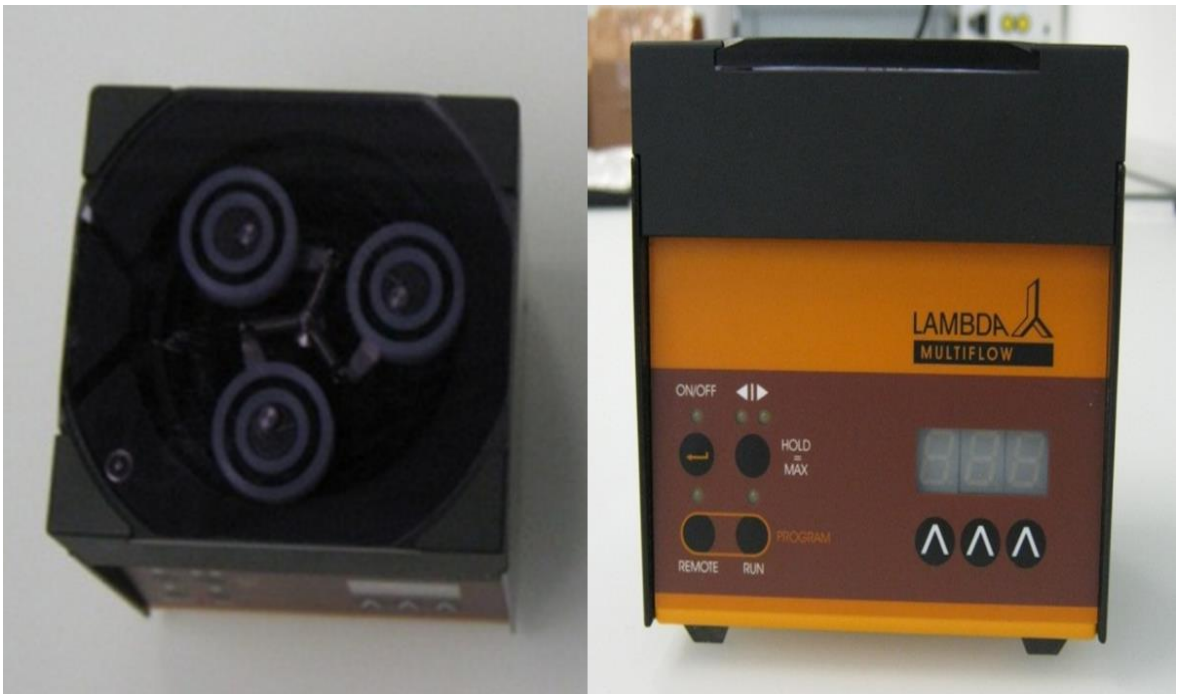

Figure 5.2. Purchased peristaltic pumps from front and up view.

Also, Appendix IX represents the purchased peristaltic pumps as well as all their accessories including RS-interface, RS-connection kit, adaptors and tubing.

5.2.2 Motor

In order to drive the inner cylinder an electric motor is needed. Also, to have more possibilities to operate the motor at different speeds, the motor is decided to be a variable speed motor. The same as the pumps, the motor must be also capable of being controlled and programmed by a PC/LabVIEW in order to comply with the needs of a high precision and sensitive system. Eventually a servo motor, as represented in Figure 5.3, is ordered and purchased as well as the accessories (refer to Appendix X).

Figure 5.3. Purchased servo motor and the copley control xenus servo drive/controller.

The detailed specifications of the purchased servo motor are as follows:

- Manufacturing company: MotionUSA, Ohio, USA.

- Applicable range for rotational speed: up to 5000 rpm.
- The motor is able to put out a torque of about 0.45 Nm (231 Watts) at the rotational speed of 5000 rpm.
- The servo motor is capable of being controlled and programmed by a PC/LabVIEW thanks to the interface and LabVIEW program.
- A Copley Control Xenus Servo Drive/Controller is also included for PC/LabVIEW control.

5.2.3 Cylinders (Taylor-Couette Device)

The third and the most important part of the set-up is double-cylinder device what has to be designed and further constructed. In order to construct the whole assembly including double-cylinder and the transparent box containing the cooling fluid, a proper, comprehensive and detailed design of the device is required. To that end, also the specifications of pumps and motor that are supposed to be mounted to the device as well as construction limitations and considerations should be taken into account. Therefore, the specifications of the device might be enlisted as below:

- Fluidic fittings for the liquid input and output must be super flangeless 1/16" fittings such as Upchurch Scientific®[207]. The outlet should be 1/4" tubing, again with a standard of Upchurch Scientific® low pressure fitting.
- The inner cylinder is made of stainless-steel and is rotatable whereas the outer cylinder, that is actually a fixed cylinder, is made of a transparent polymer like PC or PMMA.
- The entire assembly of double-cylinder is surrounded by a transparent cylinder box, which contains a circulating constant temperature water-ethylene glycol bath to keep the temperature of process constant.

- Pressure at outlet of the double-cylinder is expected to be less than three bars.
- Fluids to be used for the experiments are water and FC-40 oil.

All the specifications for the construction are determined except for the dimensions of the device, in particular, the radius of the inner cylinder, the gap width between the two cylinders and the length of the device. According to the desired application of the device, these may be optimized.

5.3 Optimization of the Cylinders Device

In order to finalize the design and make it ready to send further for the construction, all the specifications including the precise dimensions are required. The dimensions must be accurately and carefully optimized. The most critical part of optimization is to determine the optimum radius of the inner cylinder as well as the gap width. To this end, the correlation so-called Haas correlation [95, 176, 208] (equation (5)), which relates the mean droplet diameter to the surface tension, is applied to carry out the further optimization computations.

$$\frac{d_p}{D} = 150 \cdot N_{We}{}^{-0.65} \cdot N_{\mathrm{Re}\theta}{}^{-0.2} \cdot \left(\frac{\mu_p \cdot (r_o - r_i)}{\mu_c \cdot r_i} \right)^{0.5} \tag{5}$$

where d_p (m) is the mean droplet diameter and N_{We} and N_{Re} are Weber and azimuthal Reynolds dimensionless numbers respectively and are calculated as

$$N_{We} = \left(\frac{D\, \Omega_i^2\, r_i^2\, \rho_c}{\gamma} \right) \tag{6}$$

$$N_{\mathrm{Re}} = \left(\frac{D\, \Omega_i\, r_i\, \rho_c}{2\, \mu_c} \right) \tag{7}$$

where D (m) is hydraulic diameter of the Taylor-Couette cell that is equal to two times of gap width, μ_p (Pa.s) is viscosity of disperse phase, r_i and r_o (m) stand for inner and outer cylinder radius respectively, ρ_c (kg/m^3) is density of continuous phase, and Ω_i (rad/s) stands for rotational speed.

Then, utilizing MATLAB R2013a®, the Haas correlation is optimized. To that end, some initial parameters are needed to fulfill the optimization process, which are mean droplet diameter, rotational speed and interfacial surface tension. The mean droplet diameter is assumed 70 µm that is 0.00007 m and the rotational speed should be in the range of 0 to 5000 rpm; thus, to be in the safe side, halfway and three-fourths of the speed range that are 2500 and 3750 rpm (equal to 41.67 and 62.50 rad/s). For interfacial surface tension, since adding the surfactant is very likely to stabilize the droplets and avoid merging, two values is considered that stand for interfacial surface tension of oil with and without surfactant with water.

Table 5.1. Interfacial surface tension of FC-40 oil with and without surfactant.[209]

Dispersed Phase	Continuous Phase	σ (N/m)
FC-40	Water	**0.05206**
FC-40 with 5% EA	Water	**0.00285**

Then to fulfill the optimization, different values for the radius of inner cylinder are considered and the calculations are accomplished to find the optimum value for gap width and inner cylinder radius. The reasonable range for the inner cylinder radius is considered to be in the range of 1 to 10 cm. And regarding the construction limitations for the gap width, the reasonable and accepted range for the gap width is considered as 1.0 to 2.0 mm. Finally, the optimization process is accomplished and a couple of sets of optimum results are obtained that are required to be screened to select the most appropriate one. The initial sets of obtained data are represented at Appendix XI.

However, due to the limitation of the size of available PMMA tubes (which is supposed to be the outer cylinder) some modifications are necessary. The available standard measurements for PMMA tube, close to the appropriate range for this work, are 32 and 34 mm in inner diameter. To this end, some modifications are needed to be applied to the optimization to obtain new set of optimum result meeting one of the available standard measurements. Thus, utilizing the MATLAB R2013a® coding again, a few new sets of potentially acceptable sets of results are obtained taking into account the inner radius of PMMA tube to match to 32 or 34 mm as illustrated in Table 5.2.

Table 5.2. New sets of acceptable dimensions for the cylinder device.

Droplet size (μm)	Radius of inner cylinder, S-S (mm)	Gap width (mm)	Inner radius of PMMA Tube (mm)
70	30.35	1.636	31.986
70	30.4	1.644	32.044
70	32.1	1.944	34.044
70	32.0	1.925	33.925

Finally, due to the large gap width for the last two sets of results at Table 5.2 (corresponding to the PMMA tube size of 34 mm), the last two sets are eliminated from the choices and between the first two, the first set of result (gap width of 1.636 mm) is selected regarding that the obtained inner radius of PMMA tube is slightly smaller than 32 mm (31.986 mm).

And regarding the length of cylinders, there is no specific correlation for calculation of the exact length; however, the ratio of cylinder length to the gap width, that is so-called aspect ratio, is recommended to be larger than 10 to avoid length effects in the Taylor-Couette

device.[176, 177] In different investigations, the aspect ratio of 11.5 [176], 16 [177] and even 250 [95] have been reported. In this work, the aspect ratio is considered to be about 150; therefore, the length of the cylinders is calculated to be 25 cm.

Thus, the optimum dimensions for the double-cylinder (Taylor-Couette) device may be enlisted as:

- Radius of inner cylinder: 30.35 mm,
- Gap width: 1.636 mm,
- Length of cylinders: 20 cm.

Having these optimum dimensions, the double-cylinder device might be constructed by the technicians.

5.4 Construction Procedure

Once the optimization process is fulfilled and the optimum dimensions are determined, the cylinder device is constructed by the technicians at central workshop in ETH Zurich, campus of Honggerberg. To that end, a detailed 3D design of the device is needed. The design should comply with the limitations in the actual construction, as well as, the obtained precise dimensions for the device. Take for instance, due to the high rotational speed of the inner cylinder, a cooling system is vital and regarding the availability of the cooling system for the double-cylinder device to keep the temperature constant, these two cooling systems are combined. In a simple word, the cooling system for the double-cylinder device is designed so that the bath of cooling agent would surround the bearing and sealing parts of the motor as well. And regarding the large amount of the fluid as well as its circulation possibility, it does not affect the performance of the cooling system of double-cylinder device. To this end, two different drawings are designed for the device with the slight deference in the inlet parts, in particular, in the angle of the inlet positions. Finally, the perpendicular angel is chosen as the best design and the design is completely fulfilled as depicted in Figure 5.4.

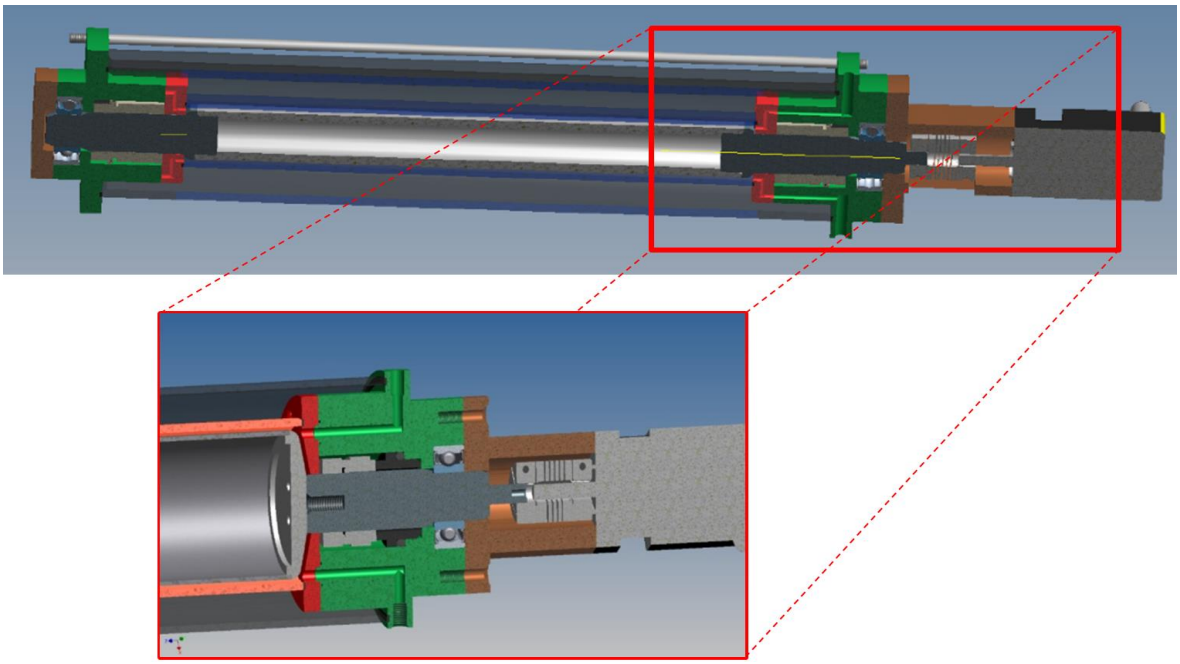

Figure 5.4. The final schematic design of the Taylor-Couette device approved for the construction.

Also, the more detailed view of the design has been illustrated in Figure 5.5.

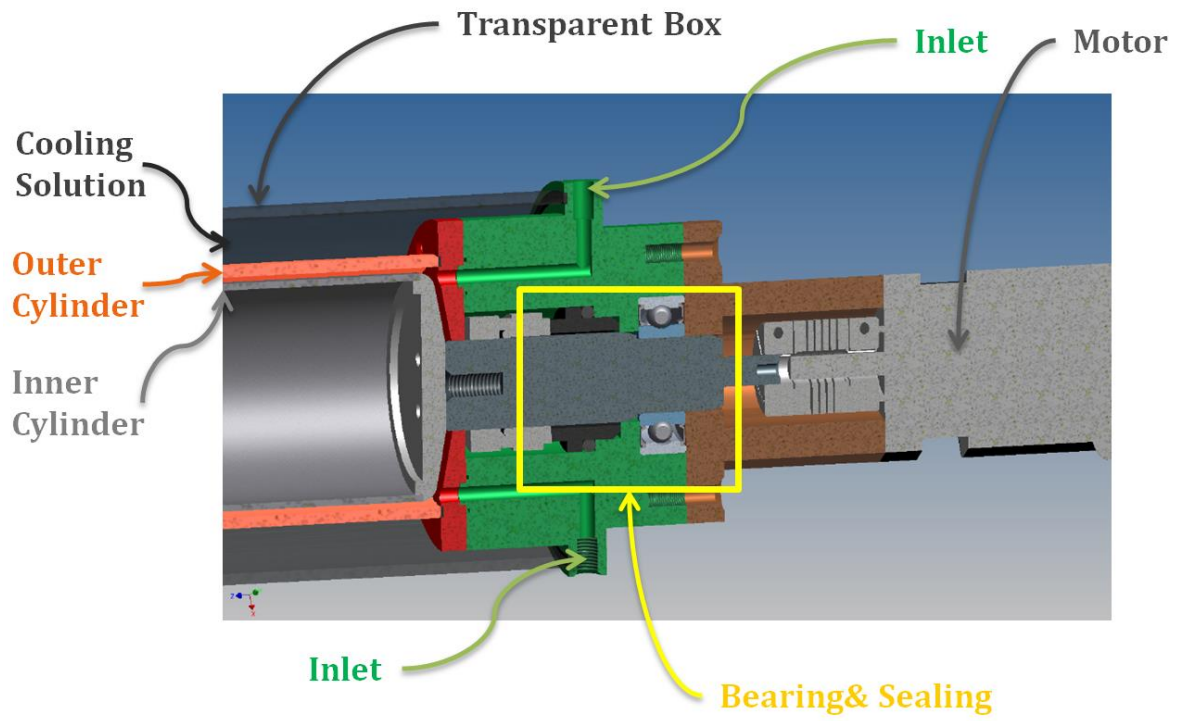

Figure 5.5. The detailed view of the final design for Taylor-Couette device.

Having the approved design, the device is constructed. To that end, some pieces such as the polymeric tube, bearings and sealing are directly ordered and purchased accordingly, in addition to some pieces like the connectors, metal discs and metal tubes that are fabricated in the workshop. In the end, all the fabricated and purchased items and pieces are assembled together to construct the actual device. All these parts are depicted in Appendix XII.

This device is aimed to be used for the droplet generation using water and FC-40 oil as the two immiscible phases. In particular, the experiments will be carried out mainly focusing on the generation rate and the monodispersity of the generated droplets with less focus on the actual size of the droplets. Figure 5.6 represents the constructed desired Taylor-Couette device ready for the experimental tests. Moreover, Appendix XIII includes the supplementary pictures of the device.

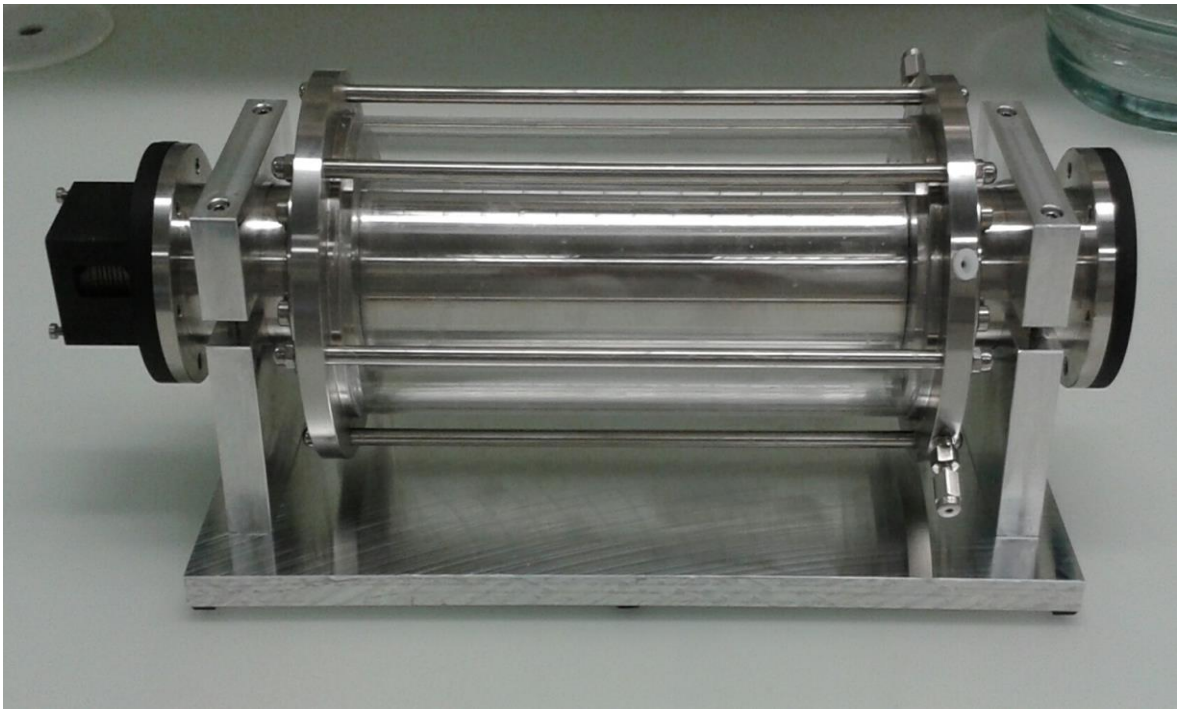

Figure 5.6. The constructed Taylor-Couette double-cylinder device ready to undergo the experiments.

6 CONCLUSION

Due to the emerging applications of the microdroplets, this work has endeavored to achieve the best and functional methods capable of generating microdroplets of water in FC-40 oil in extremely high production rate (i.e. over a million droplets per second). To that end, various methods were investigated and finally a most suitable method was selected for replication which was fabrication of the microdroplets through a multi-layer module. Through the experiment investigations, the proper protocol for fabrication of a multi-layer PDMS device was recognized. Moreover, the optimum and correct design for a multi-array microfluidic module equipped with eight identical and simultaneous flow-focusing devices was obtained. Carrying out many different experimental attempts, a couple of major drawbacks and problems for fabrication of a multi-layer microfluidic device were identified what were resolved accordingly.

In addition, the effective exploitation of a 3D printer for the direct fabrication of a multi-layer microfluidic device from a three dimensional design was investigated. Subsequently, the proper design and configurations for fabricating a particular multi-layer microfluidic module by the 3D printer were successfully achieved. However, due to the lack of time, neither the PDMS multi-layer device (fabricated through the final troubleshot protocol), nor the 3D printed multi-layer module were not experimentally tested.

Furthermore, modeling and simulation of a microfluidic device concentrating on the droplet generation phenomenon was also studied. Fulfilling that, the right procedure for the simulation of a droplet generation phenomenon utilizing the software COMSOL Multiphysics® was studied and determined. In the following, the simulation of a particular flow-focusing droplet generator (as a sample) utilizing COMSOL Multiphysics® was carried out, through which effect of the input velocities ratio on droplet size in the desired microfluidic device was numerically investigated.

And finally, as an alternative method for the bulk generation of microdroplets, a double-cylinder device was designed and carefully optimized. The designed and optimized device

was later mechanically constructed for the experimental tests. This device is supposed to be used for the experimental investigations further.

7 REFERENCES

[1] B. J. Kirby, Micro- and nanoscale fluid mechanics transport in microfluidic devices. Cambridge: Cambridge University Press, 2010.

[2] G. Karniadakis, A. Beskok, and N. Aluru, Microflows and nanoflows fundamentals and simulation. New York, NY: Springer, 2005.

[3] M. Koch, A. Evans, and A. Brunnschweiler, Microfluidic technology and applications. Baldock, Hertfordshire: Research Studies Press, 2000.

[4] W. C. Tian and E. Finehout, "Introduction to Microfluidics," in Microfluidics for Biological Applications, ed: Springer, 2009, pp. 1-34.

[5] P. Tabeling, Introduction to microfluidics, [Paperback ed. Oxford: Oxford University Press, 2010.

[6] E. Kumacheva and P. Garstecki, Microfluidic reactors for polymer particles. Hoboken, N.J.: Wiley, 2011.

[7] J. Kong, N. R. Franklin, C. Zhou, M. G. Chapline, S. Peng, K. Cho, et al., "Nanotube molecular wires as chemical sensors," Science, vol. 287, pp. 622-5, Jan 28 2000.

[8] Y. Koc, A. J. de Mello, G. McHale, M. I. Newton, P. Roach, and N. J. Shirtcliffe, "Nano-scale superhydrophobicity: suppression of protein adsorption and promotion of flow-induced detachment," Lab Chip, vol. 8, pp. 582-6, Apr 2008.

[9] G. M. Whitesides, "The 'right' size in nanobiotechnology," Nat Biotechnol, vol. 21, pp. 1161-5, Oct 2003.

[10] H. A. Stone and S. Kim, "Microfluidics: Basic issues, applications, and challenges," Aiche Journal, vol. 47, pp. 1250-1254, Jun 2001.

[11] F. Habbal and A. Vitti, "Fundamentals of Microfabrication with Applications to BioMEMS," vol. 12, ed. Harvard University Extension School: Harvard University, 2008.

[12] J. Melin and S. R. Quake, "Microfluidic large-scale integration: the evolution of design rules for biological automation," Annu Rev Biophys Biomol Struct, vol. 36, pp. 213-31, 2007.

[13] T. M. Squires and S. R. Quake, "Microfluidics: Fluid physics at the nanoliter scale," Reviews of Modern Physics, vol. 77, pp. 977-1026, Jul 2005.

[14] E. Livak-Dahl, I. Sinn, and M. Burns, "Microfluidic chemical analysis systems," Annu Rev Chem Biomol Eng, vol. 2, pp. 325-53, 2011.

[15] W. C. Tian and E. Finehout, Microfluidics for Biological Applications: Springer Publishing Company, Incorporated, 2008.

[16] K. A. Addae-Mensah, Z. Wang, H. Parsa, S. Y. Chin, T. Laksanasopin, and S. K. Sia, "Fundamentals of Microfluidics Devices," in Microfluidic Devices in Nanotechnology, ed: John Wiley & Sons, Inc., 2010, pp. 1-38.

[17] G. M. Whitesides, "The origins and the future of microfluidics," Nature, vol. 442, pp. 368-73, Jul 27 2006.

[18] M. A. McClain, C. T. Culbertson, S. C. Jacobson, N. L. Allbritton, C. E. Sims, and J. M. Ramsey, "Microfluidic devices for the high-throughput chemical analysis of cells," Anal Chem, vol. 75, pp. 5646-55, 2003.

[19] Y. Cheng, H. Chen, Y. Li, X. Chen, and Z. Hu, "Separation and determination of aloperine, sophoridine, matrine and oxymatrine by combination of flow injection with microfluidic capillary electrophoresis," Talanta, vol. 63, pp. 491-6, 2004.

[20] A. de Mello, "On-chip chromatography: the last twenty years," Lab Chip, vol. 2, pp. 48N-54N, 2002.

[21] Y. Ueno, T. Horiuchi, T. Morimoto, and O. Niwa, "Microfluidic device for airborne BTEX detection," Anal Chem, vol. 73, pp. 4688-93, 2001.

[22] H. Yin, K. Killeen, R. Brennen, D. Sobek, M. Werlich, and T. van de Goor, "Microfluidic chip for peptide analysis with an integrated HPLC column, sample enrichment column, and nanoelectrospray tip," Anal Chem, vol. 77, pp. 527-33, 2005.

[23] J. Xie, Y. Miao, J. Shih, Y. C. Tai, and T. D. Lee, "Microfluidic platform for liquid chromatography-tandem mass spectrometry analyses of complex peptide mixtures," Anal Chem, vol. 77, pp. 6947-53, 2005.

[24] A. R. de Boer, B. Bruyneel, J. G. Krabbe, H. Lingeman, W. M. Niessen, and H. Irth, "A microfluidic-based enzymatic assay for bioactivity screening combined with capillary liquid chromatography and mass spectrometry," Lab Chip, vol. 5, pp. 1286-92, 2005.

[25] C. C. Lee, G. Sui, A. Elizarov, C. J. Shu, Y. S. Shin, A. N. Dooley, et al., "Multistep synthesis of a radiolabeled imaging probe using integrated microfluidics," Science, vol. 310, pp. 1793-6, Dec 16 2005.

[26] J. P. Murrihy, M. C. Breadmore, A. Tan, M. McEnery, J. Alderman, C. O'Mathuna, et al., "Ion chromatography on-chip," J Chromatogr A, vol. 924, pp. 233-8, Jul 27 2001.

[27] X. Zhang and S. J. Haswell, "Materials Matter in Microfluidic Devices," MRS Bulletin, vol. 31, pp. 95-99, 2006.

[28] H. A. Stone, A. D. Stroock, and A. Ajdari, "ENGINEERING FLOWS IN SMALL DEVICES," Annual Review of Fluid Mechanics, vol. 36, pp. 381-411, 2004.

[29] U. Attia, S. Marson, and J. Alcock, "Micro-injection moulding of polymer microfluidic devices," Microfluidics and Nanofluidics, vol. 7, pp. 1-28, 2009/07/01 2009.

[30] J. B. Hutchison, K. T. Haraldsson, B. T. Good, R. P. Sebra, N. Luo, K. S. Anseth, et al., "Robust polymer microfluidic device fabrication via contact liquid photolithographic polymerization (CLiPP)," Lab on a Chip, vol. 4, pp. 658-662, 2004.

[31] D. R. Link, S. L. Anna, D. A. Weitz, and H. A. Stone, "Geometrically mediated breakup of drops in microfluidic devices," Phys Rev Lett, vol. 92, p. 054503, Feb 6 2004.

[32] J. C. McDonald and G. M. Whitesides, "Poly(dimethylsiloxane) as a material for fabricating microfluidic devices," Acc Chem Res, vol. 35, pp. 491-9, Jul 2002.

[33] N. Maluf, <<An>> introduction to microelectromechanical systems engineering. Boston: Artech House, 2000.

[34] J. Friend and L. Yeo, "Fabrication of microfluidic devices using polydimethylsiloxane," Biomicrofluidics, vol. 4, 2010.

[35] S. K. Sia and G. M. Whitesides, "Microfluidic devices fabricated in poly(dimethylsiloxane) for biological studies," Electrophoresis, vol. 24, pp. 3563-76, Nov 2003.

[36] M. Ogura, Y. Agata, K. Watanabe, R. M. McCormick, Y. Hamaguchi, Y. Aso, et al., "RNA chip: quality assessment of RNA by microchannel linear gel electrophoresis in injection-molded plastic chips," Clin Chem, vol. 44, pp. 2249-55, Nov 1998.

[37] H. Bayer and H. Engelhardt, "Capillary electrophoresis in organic polymer capillaries," Journal of Microcolumn Separations, vol. 8, pp. 479-484, 1996.

[38] M. A. Roberts, J. S. Rossier, P. Bercier, and H. Girault, "UV Laser Machined Polymer Substrates for the Development of Microdiagnostic Systems," Anal Chem, vol. 69, pp. 2035-42, Jun 1 1997.

[39] J. C. McDonald, D. C. Duffy, J. R. Anderson, D. T. Chiu, H. Wu, O. J. A. Schueller, et al., "Fabrication of microfluidic systems in poly(dimethylsiloxane)," ELECTROPHORESIS, vol. 21, pp. 27-40, 2000.

[40] D. Ogonczyk, J. Wegrzyn, P. Jankowski, B. Dabrowski, and P. Garstecki, "Bonding of microfluidic devices fabricated in polycarbonate," Lab Chip, vol. 10, pp. 1324-7, May 21 2010.

[41] H. Becker and C. Gartner, "Polymer microfabrication technologies for microfluidic systems," Anal Bioanal Chem, vol. 390, pp. 89-111, Jan 2008.

[42] H. Becker and L. E. Locascio, "Polymer microfluidic devices," Talanta, vol. 56, pp. 267-287, Feb 11 2002.

[43] C.-W. Tsao and D. DeVoe, "Bonding of thermoplastic polymer microfluidics," Microfluidics and Nanofluidics, vol. 6, pp. 1-16, 2009/01/01 2009.

[44] Y. N. Xia, E. Kim, X. M. Zhao, J. A. Rogers, M. Prentiss, and G. M. Whitesides, "Complex optical surfaces formed by replica molding against elastomeric masters," Science, vol. 273, pp. 347-349, Jul 19 1996.

[45] Y. N. Xia, E. Kim, and G. M. Whitesides, "Micromolding of polymers in capillaries: Applications in microfabrication," Chemistry of Materials, vol. 8, pp. 1558-1567, Jul 1996.

[46] E. Kim, Y. N. Xia, and G. M. Whitesides, "Polymer Microstructures Formed by Molding in Capillaries," Nature, vol. 376, pp. 581-584, Aug 17 1995.

[47] B. Y. Jeon and S. M. Kim, "Non-stick ceramic coating composition and process," ed: Google Patents, 2011.

[48] T. Fujii, "PDMS-based microfluidic devices for biomedical applications," Microelectronic Engineering, vol. 61-2, pp. 907-914, Jul 2002.

[49] G. Li, Q. Chen, and J. Zhao, "A simple and economical holder for casting PDMS chips," Chips & Tips (Lab on a Chip), Nov. 20th, 2009.

[50] M. Svoboda, Z. Slouka, W. Schrott, P. Cervenka, M. Pribyl, and D. Snita, "Fabrication of plastic microchips with gold microelectrodes using techniques of sacrificed

substrate and thermally activated solvent bonding," Microelectronic Engineering, vol. 87, pp. 1590-1593, May-Aug 2010.

[51] W. Schrott, M. Svoboda, Z. Slouka, M. Přibyl, and D. Šnita, "PDMS microfluidic chips prepared by a novel casting and pre-polymerization method," Microelectronic Engineering, vol. 87, pp. 1600-1602, 5// 2010.

[52] A. Tan, K. Rodgers, J. Murrihy, C. O'Mathuna, and J. D. Glennon, "Rapid fabrication of microfluidic devices in poly(dimethylsiloxane) by photocopying," Lab Chip, vol. 1, pp. 7-9, Sep 2001.

[53] G. V. Kaigala, S. Ho, R. Penterman, and C. J. Backhouse, "Rapid prototyping of microfluidic devices with a wax printer," Lab Chip, vol. 7, pp. 384-7, Mar 2007.

[54] N. Bao, Q. Zhang, J. J. Xu, and H. Y. Chen, "Fabrication of poly(dimethylsiloxane) microfluidic system based on masters directly printed with an office laser printer," J Chromatogr A, vol. 1089, pp. 270-5, Sep 30 2005.

[55] A. W. Martinez, S. T. Phillips, G. M. Whitesides, and E. Carrilho, "Diagnostics for the developing world: microfluidic paper-based analytical devices," Anal Chem, vol. 82, pp. 3-10, Jan 1 2010.

[56] T. Songjaroen, W. Dungchai, O. Chailapakul, and W. Laiwattanapaisal, "Novel, simple and low-cost alternative method for fabrication of paper-based microfluidics by wax dipping," Talanta, vol. 85, pp. 2587-93, Oct 15 2011.

[57] A. W. Grant, Q. H. Hu, and B. Kasemo, "Transmission electron microscopy 'windows' for nanofabricated structures," Nanotechnology, vol. 15, pp. 1175-1181, Sep 2004.

[58] S. D. Minteer, Microfluidics and microfabrication, Reviews and Protocols. Totowa, New Jersey: Humana Press Inc, 2006.

[59] T. Adam and U. Hashim, "Micro/Nanowires Fabrication: Design Consideration for Reliable and Repeatability in Pattern Transfer," in Computational Intelligence, Modelling and Simulation (CIMSiM), 2012 Fourth International Conference on, 2012, pp. 48-53.

[60] J. Siegrist, M. Amasia, and M. Madou, "Fast-iteration prototyping and bonding of complex plastic microfluidic devices," Chips & Tips (Lab on a Chip), May 17th, 2010.

[61] B. S. Rao and U. Hashim, "Microfluidic Photomask Design Using CAD Software for Application in Lab-On-Chip Biomedical Nanodiagnostics," Advanced Materials Research, vol. 795, pp. 388-392, 2013.

[62] M. D. Levenson, "Wavefront Engineering for Photolithography," Physics Today, vol. 46, pp. 28-36, July 1993 1993.

[63] C. Chen, D. Hirdes, and A. Folch, "Gray-scale photolithography using microfluidic photomasks," Proc Natl Acad Sci U S A, vol. 100, pp. 1499-504, Feb 18 2003.

[64] B. Wu, "Photomask plasma etching: A review," Journal of Vacuum Science & Technology B: Microelectronics and Nanometer Structures, vol. 24, pp. 1-15, 2006.

[65] M. Fujimura, T. Sohmura, and T. Suhara, "Fabrication of domain-inverted gratings in MgO:LiNbO₃ by applying voltage under ultraviolet irradiation through photomask at room temperature," Electronics Letters, vol. 39, pp. 719-721, 2003.

[66] D. Rittman and M. Oren, "Photomask for eliminating antenna effects in an integrated circuit and integrated circuit manufacture with same," United States Patent US 6978437 B1, 2005.

[67] D. Rittman and M. Oren, "Photomask for reducing power supply voltage fluctuations in an integrated circuit and integrated circuit manufactured with the same," United Stated Patent US 6904582 B1 2005.

[68] L. Che-Hsin, L. Gwo-Bin, L. Yen-Heng, and C. Guan-Liang, "A fast prototyping process for fabrication of microfluidic systems on soda-lime glass," Journal of Micromechanics and Microengineering, vol. 11, p. 726, 2001.

[69] A. Azioune, M. Storch, M. Bornens, M. Thery, and M. Piel, "Simple and rapid process for single cell micro-patterning," Lab Chip, vol. 9, pp. 1640-2, Jun 7 2009.

[70] H. Hwang, G. Kang, J. H. Yeon, Y. Nam, and J. K. Park, "Direct rapid prototyping of PDMS from a photomask film for micropatterning of biomolecules and cells," Lab Chip, vol. 9, pp. 167-70, Jan 7 2009.

[71] J. Dingley, "The Photo-Mask Guide," ed. United Kingdom: JD Photo-Tools & Photo Data Ltd, 2011, pp. 9-22.

[72] A. Tselev, K. Hatton, M. S. Fuhrer, M. Paranjape, and P. Barbara, "A photolithographic process for fabrication of devices with isolated single-walled carbon nanotubes," Nanotechnology, vol. 15, pp. 1475-1478, Nov 2004.

[73] C. G. J. Schabmueller, M. Koch, A. G. R. Evans, and A. Brunnschweiler, "Design and fabrication of a microfluidic circuitboard," Journal of Micromechanics and Microengineering, vol. 9, pp. 176-179, Jun 1999.

[74] A. Tourovskaia, X. Figueroa-Masot, and A. Folch, "Differentiation-on-a-chip: A microfluidic platform for long-term cell culture studies," Lab on a Chip, vol. 5, pp. 14-19, 2005.

[75] S. Pun Pang, G. K. Knopf, M. Ostojic, and S. Nikumb, "Rapid Fabrication of Micromolds for Polymeric Microfluidic Devices," in Electrical and Computer Engineering, 2007. CCECE 2007. Canadian Conference on, 2007, pp. 8-11.

[76] P. P. Shiu, G. K. Knopf, and M. Ostojic, "Fabrication of metallic micromolds by laser and electro-discharge micromachining," Microsystem Technologies-Micro-and Nanosystems-Information Storage and Processing Systems, vol. 16, pp. 477-485, Mar 2010.

[77] P. P. Shiu, G. K. Knopf, M. Ostojic, and S. Nikumb, "Rapid fabrication of tooling for microfluidic devices via laser micromachining and hot embossing," Journal of Micromechanics and Microengineering, vol. 18, p. 025012, 2008.

[78] F. Brizuela, Y. Wang, C. A. Brewer, F. Pedaci, W. Chao, E. H. Anderson, et al., "Microscopy of extreme ultraviolet lithography masks with 13.2 nm tabletop laser illumination," Opt Lett, vol. 34, pp. 271-3, Feb 1 2009.

[79] A. Bardea and R. Naaman, "Magnetolithography: from bottom-up route to high throughput," Small, vol. 5, pp. 316-9, Mar 2009.

[80] S. Y. Chou, P. R. Krauss, and P. J. Renstrom, "Imprint lithography with 25-nanometer resolution," Science, vol. 272, pp. 85-87, Apr 5 1996.

[81] B. D. Gates, Q. Xu, M. Stewart, D. Ryan, C. G. Willson, and G. M. Whitesides, "New approaches to nanofabrication: molding, printing, and other techniques," Chem Rev, vol. 105, pp. 1171-96, Apr 2005.

[82] J. C. McDonald, M. L. Chabinyc, S. J. Metallo, J. R. Anderson, A. D. Stroock, and G. M. Whitesides, "Prototyping of microfluidic devices in poly(dimethylsiloxane) using solid-object printing," Anal Chem, vol. 74, pp. 1537-45, Apr 1 2002.

[83] A. Carrión, "Technology forecast on ink-jet head technology applications in rapid prototyping," Rapid Prototyping Journal, vol. 3, pp. 99-115, 1997.

[84] R. M. Guijt and M. C. Breadmore, "Maskless photolithography using UV LEDs," Lab Chip, vol. 8, pp. 1402-4, Aug 2008.

[85] R. Menon, A. Patel, D. Gil, and H. I. Smith, "Maskless lithography," Materials Today, vol. 8, pp. 26-33, 2// 2005.

[86] T. H. P. Chang, M. Mankos, K. Y. Lee, and L. P. Muray, "Multiple electron-beam lithography," Microelectronic Engineering, vol. 57–58, pp. 117-135, 9// 2001.

[87] M. Krogh and P. Asberg, My Little Guide to Soft Lithography (Soft Lithography for Dummies) Sweden: Linkoping University, 2003.

[88] A. del Campo and C. Greiner, "SU-8: a photoresist for high-aspect-ratio and 3D submicron lithography," Journal of Micromechanics and Microengineering, vol. 17, pp. R81-R95, Jun 2007.

[89] H. Lorenz, M. Despont, N. Fahrni, N. LaBianca, P. Renaud, and P. Vettiger, "SU-8: a low-cost negative resist for MEMS," Journal of Micromechanics and Microengineering, vol. 7, pp. 121-124, Sep 1997.

[90] M. Rabarot, J. Bablet, M. Ruty, M. Kipp, I. Chartier, and C. Dubarry, "Thick SU-8 photolithography for BioMEMS," Micromachining and Microfabrication Process Technology Viii, vol. 4979, pp. 382-393, 2003.

[91] K. Huikko, P. Ostman, K. Grigoras, S. Tuomikoski, V. M. Tiainen, A. Soininen, et al., "Poly(dimethylsiloxane) electrospray devices fabricated with diamond-like carbon-poly(dimethylsiloxane) coated SU-8 masters," Lab Chip, vol. 3, pp. 67-72, May 2003.

[92] M. B. Chan-Park, J. Zhang, Y. H. Yan, and C. Y. Yue, "Fabrication of large SU-8 mold with high aspect ratio microchannels by UV exposure dose reduction," Sensors and Actuators B-Chemical, vol. 101, pp. 175-182, Jun 15 2004.

[93] A. Kroetch, "NanoFab's PDMS Microfluidic Device Fabrication Manual " University of Alberta, nanoFAB Resource librarySeptember 2004 2004.

[94] M. R. Kendall, D. Bardin, R. Shih, P. A. Dayton, and A. P. Lee, "Scaled-Up Production of Monodisperse, Dual Layer Microbubbles Using Multi-Array Microfluidic Module for Medical Imaging and Drug Delivery," Bubble Sci Eng Technol, vol. 4, pp. 12-20, May 2012.

[95] X. Zhu and R. D. Vigil, "Banded liquid–liquid Taylor-Couette-Poiseuille flow," AIChE Journal, vol. 47, pp. 1932-1940, 2001.

[96] W. H. Henley, P. J. Dennis, and J. M. Ramsey, "Fabrication of microfluidic devices containing patterned microwell arrays," Anal Chem, vol. 84, pp. 1776-80, Feb 7 2012.

[97] M. U. Kopp, A. J. Mello, and A. Manz, "Chemical amplification: continuous-flow PCR on a chip," Science, vol. 280, pp. 1046-8, May 15 1998.

[98] K. Sun, A. Yamaguchi, Y. Ishida, S. Matsuo, and H. Misawa, "A heater-integrated transparent microchannel chip for continuous-flow PCR," Sensors and Actuators B: Chemical, vol. 84, pp. 283-289, 5/15/ 2002.

[99] N. Park, S. Kim, and J. H. Hahn, "Cylindrical compact thermal-cycling device for continuous-flow polymerase chain reaction," Anal Chem, vol. 75, pp. 6029-33, Nov 1 2003.

[100] I. Schneegass, R. Brautigam, and J. M. Kohler, "Miniaturized flow-through PCR with different template types in a silicon chip thermocycler," Lab Chip, vol. 1, pp. 42-9, Sep 2001.

[101] C. S. Effenhauser, G. J. Bruin, A. Paulus, and M. Ehrat, "Integrated capillary electrophoresis on flexible silicone microdevices: analysis of DNA restriction fragments and detection of single DNA molecules on microchips," Anal Chem, vol. 69, pp. 3451-7, Sep 1 1997.

[102] P. Jiang, L. Ma, J. Pan, Y. Chun, Q. H. Xu, and J. L. Dong, "Preparation of Amphiphilic HZSM-5 Zeolite by Chemical Vapor Deposition of Trimethylchlorosilane," Chinese Journal of Catalysis, vol. 30, pp. 503-508, Jun 2009.

[103] L. Rösch, P. John, and R. Reitmeier, "Silicon Compounds, Organic," in Ullmann's Encyclopedia of Industrial Chemistry, ed: Wiley-VCH Verlag GmbH & Co. KGaA, 2000.

[104] A. Mata, A. J. Fleischman, and S. Roy, "Characterization of polydimethylsiloxane (PDMS) properties for biomedical micro/nanosystems," Biomed Microdevices, vol. 7, pp. 281-93, Dec 2005.

[105] Dow Corning Corporation. Material Safety Data Sheet: Sylgard (R) 184 Silicone Elastomer Kit [Online]. Available: http://www1.dowcorning.com/DataFiles/090007b281d34c26.pdf

[106] W. W. Chow, K. F. Lei, G. Shi, W. J. Li, and Q. Huang, "Microfluidic channel fabrication by PDMS-interface bonding," 2004, pp. 141-148.

[107] E. J. Wong, "Modeling and control of rapid cure in polydimethylsiloxane (PDMS) for microfluidic device applications," Ph D, Massachusetts Institute of Technology, 2010.

[108] J. Gilbertson, M. Hemling, and G. Lisensky. (2013, July 2nd). Microfluidic Devices. [Video]. Available: http://chemlinks.beloit.edu/Edetc/nanolab/shrink/index.html

[109] Z. Jatoi. (2013, February 21st). Latest Top 10 Medical Inventions - A Chip Designed To Diagnose Flu. Available: http://thefactworl.blogspot.fi/2013/02/latest-top-10-medical-inventions.html

[110] A. Jafar and M. Burhanuddin Yeop, "A new UV-curing elastomeric substrate for rapid prototyping of microfluidic devices," Journal of Micromechanics and Microengineering, vol. 22, p. 035006, 2012.

[111] L. Millet and M. Collens, "Microfluidics and Enabling Tchnology Lab Module: Fabrication of PDMS-based Microfluidics " presented at the Bionanotechnology Summer Institute 2011, IL, USA, 2011.

[112] A. C. Rowat and D. A. Weitz, "See where to punch holes easily in a PDMS microfluidic device," Chips & Tips (Lab on a Chip), pp. 1-2, May 29th, 2008.

[113] A. E. Mark, A. J. Michael, and K. G. Bruce, "Determining the optimal PDMS–PDMS bonding technique for microfluidic devices," Journal of Micromechanics and Microengineering, vol. 18, p. 067001, 2008.

[114] K. Kim, S. W. Park, and S. S. Yang, "The optimization of PDMS-PMMA bonding process using silane primer," Biochip Journal, vol. 4, pp. 148-154, Jun 20 2010.

[115] K. S. Lee and R. J. Ram, "Plastic-PDMS bonding for high pressure hydrolytically stable active microfluidics," Lab on a Chip, vol. 9, pp. 1618-1624, 2009.

[116] W. H. Zhang, S. C. Lin, C. M. Wang, J. Hu, C. Li, Z. X. Zhuang, et al., "PMMA/PDMS valves and pumps for disposable microfluidics," Lab on a Chip, vol. 9, pp. 3088-3094, 2009.

[117] S. H. Tan, N. T. Nguyen, Y. C. Chua, and T. G. Kang, "Oxygen plasma treatment for reducing hydrophobicity of a sealed polydimethylsiloxane microchannel," Biomicrofluidics, vol. 4, p. 32204, 2010.

[118] K. Haubert, T. Drier, and D. Beebe, "PDMS bonding by means of a portable, low-cost corona system," Lab Chip, vol. 6, pp. 1548-9, Dec 2006.

[119] S. H. Ng, Y. X. Wu, Z. F. Wang, and Z. P. Wang, "Rapid thermal bonding of polymer microfluidic devices assisted by corona discharge," in Design, Test, Integration & Packaging of MEMS/MOEMS, 2009. MEMS/MOEMS '09. Symposium on, 2009, pp. 343-348.

[120] H. Wu, B. Huang, and R. N. Zare, "Construction of microfluidic chips using polydimethylsiloxane for adhesive bonding," Lab on a Chip, vol. 5, pp. 1393-1398, 2005.

[121] PPG Industries. Material Safety Data Sheet: Aquapel Glass Windshield Cleaner [Online]. Available: http://www.aquapel.com/PDF/SP050PPGGlass_MSDS.pdf

[122] A. R. Abate, D. Lee, T. Do, C. Holtze, and D. A. Weitz, "Glass coating for PDMS microfluidic channels by sol-gel methods," Lab Chip, vol. 8, pp. 516-8, Apr 2008.

[123] C. H. Schmitz, A. C. Rowat, S. Koster, and D. A. Weitz, "Dropspots: a picoliter array in a microfluidic device," Lab Chip, vol. 9, pp. 44-9, Jan 7 2009.

[124] J. Atencia and D. J. Beebe, "Controlled microfluidic interfaces," Nature, vol. 437, pp. 648-55, Sep 29 2005.

[125] S. Y. Teh, R. Lin, L. H. Hung, and A. P. Lee, "Droplet microfluidics," Lab Chip, vol. 8, pp. 198-220, Feb 2008.

[126] R. Seemann, M. Brinkmann, T. Pfohl, and S. Herminghaus, "Droplet based microfluidics," Rep Prog Phys, vol. 75, p. 016601, Jan 2012.

[127] A. Huebner, S. Sharma, M. Srisa-Art, F. Hollfelder, J. B. Edel, and A. J. Demello, "Microdroplets: a sea of applications?," Lab Chip, vol. 8, pp. 1244-54, Aug 2008.

[128] A. B. Theberge, F. Courtois, Y. Schaerli, M. Fischlechner, C. Abell, F. Hollfelder, et al., "Microdroplets in microfluidics: an evolving platform for discoveries in chemistry and biology," Angew Chem Int Ed Engl, vol. 49, pp. 5846-68, Aug 9 2010.

[129] G. F. Christopher and S. L. Anna, "Microfluidic methods for generating continuous droplet streams," Journal of Physics D-Applied Physics, vol. 40, pp. R319-R336, Oct 7 2007.

[130] L. Tzu-Chun and J. A. Yeh, "Microdroplet application in protein sensing," in Optical MEMS and Nanophotonics (OMN), 2011 International Conference on, 2011, pp. 123-124.

[131] K. Iwai, R. D. Sochol, L. P. Lee, and L. Lin, "Finger-powered bead-in-droplet microfluidic system for point-of-care diagnostics," in Micro Electro Mechanical Systems (MEMS), 2012 IEEE 25th International Conference on, 2012, pp. 949-952.

[132] K. Shigeta, H. Traub, U. Panne, A. Okino, L. Rottmann, and N. Jakubowski, "Application of a micro-droplet generator for an ICP-sector field mass spectrometer - optimization and analytical characterization," Journal of Analytical Atomic Spectrometry, vol. 28, pp. 646-656, 2013.

[133] P. S. Dittrich and A. Manz, "Lab-on-a-chip: microfluidics in drug discovery," Nat Rev Drug Discov, vol. 5, pp. 210-8, Mar 2006.

[134] H. Song, J. D. Tice, and R. F. Ismagilov, "A microfluidic system for controlling reaction networks in time," Angew Chem Int Ed Engl, vol. 42, pp. 768-72, Feb 17 2003.

[135] T. W. Hofmann, S. H. Anselmann, J. W. Janiesch, A. Rademacher, and C. H. J. Bohm, "Applying microdroplets as sensors for label-free detection of chemical reactions," Lab on a Chip, vol. 12, pp. 916-922, 2012.

[136] N. J. Carroll, S. B. Rathod, E. Derbins, S. Mendez, D. A. Weitz, and D. N. Petsev, "Droplet-based microfluidics for emulsion and solvent evaporation synthesis of monodisperse mesoporous silica microspheres," Langmuir, vol. 24, pp. 658-61, Feb 5 2008.

[137] L. H. Hung, S. Y. Teh, J. Jester, and A. P. Lee, "PLGA micro/nanosphere synthesis by droplet microfluidic solvent evaporation and extraction approaches," Lab Chip, vol. 10, pp. 1820-5, Jul 21 2010.

[138] A. D. Griffiths and D. S. Tawfik, "Miniaturising the laboratory in emulsion droplets," Trends Biotechnol, vol. 24, pp. 395-402, Sep 2006.

[139] X. Casadevall i Solvas, M. Srisa-Art, A. J. deMello, and J. B. Edel, "Mapping of fluidic mixing in microdroplets with 1 micros time resolution using fluorescence lifetime imaging," Anal Chem, vol. 82, pp. 3950-6, May 1 2010.

[140] J. Park, A. Kerner, M. A. Burns, and X. N. Lin, "Microdroplet-enabled highly parallel co-cultivation of microbial communities," PLoS One, vol. 6, p. e17019, 2011.

[141] S. Xu, Z. Nie, M. Seo, P. Lewis, E. Kumacheva, H. A. Stone, et al., "Generation of monodisperse particles by using microfluidics: control over size, shape, and composition," Angew Chem Int Ed Engl, vol. 44, pp. 724-8, Jan 21 2005.

[142] M. Najah, A. D. Griffiths, and M. Ryckelynck, "Teaching single-cell digital analysis using droplet-based microfluidics," Anal Chem, vol. 84, pp. 1202-9, Feb 7 2012.

[143] P. J. Day, Y. Zhang, and A. Manz, Microdroplet Technology: Principles and Emerging Applications in Biology and Chemistry: Springer, 2012.

[144] T. Nisisako, S. Okushima, and T. Torii, "Controlled formulation of monodisperse double emulsions in a multiple-phase microfluidic system," Soft Matter, vol. 1, pp. 23-27, Jun 14 2005.

[145] H. Song, D. L. Chen, and R. F. Ismagilov, "Reactions in droplets in microflulidic channels," Angewandte Chemie-International Edition, vol. 45, pp. 7336-7356, 2006.

[146] S. L. Anna and H. C. Mayer, "Microscale tipstreaming in a microfluidic flow focusing device," Physics Of Fluids, vol. 18, // 2006.

[147] R. M. Lorenz, J. S. Edgar, G. D. Jeffries, and D. T. Chiu, "Microfluidic and optical systems for the on-demand generation and manipulation of single femtoliter-volume aqueous droplets," Anal Chem, vol. 78, pp. 6433-9, Sep 15 2006.

[148] E. Quevedo, J. Steinbacher, and D. T. McQuade, "Interfacial polymerization within a simplified microfluidic device: capturing capsules," J Am Chem Soc, vol. 127, pp. 10498-9, Aug 3 2005.

[149] S. J. Kim, Y. A. Song, P. L. Skipper, and J. Han, "Electrohydrodynamic generation and delivery of monodisperse picoliter droplets using a poly(dimethylsiloxane) microchip," Anal Chem, vol. 78, pp. 8011-9, Dec 1 2006.

[150] X. Casadevall i Solvas and A. deMello, "Droplet microfluidics: recent developments and future applications," Chem Commun (Camb), vol. 47, pp. 1936-42, 2011.

[151] P. B. Umbanhowar, V. Prasad, and D. A. Weitz, "Monodisperse Emulsion Generation via Drop Break Off in a Coflowing Stream," Langmuir, vol. 16, pp. 347-351, 1999.

[152] S. Sugiura, M. Nakajima, and M. Seki, "Prediction of Droplet Diameter for Microchannel Emulsification: Prediction Model for Complicated Microchannel Geometries," Industrial & Engineering Chemistry Research, vol. 43, pp. 8233-8238, 2004/12/01 2004.

[153] J. D. Tice, H. Song, A. D. Lyon, and R. F. Ismagilov, "Formation of Droplets and Mixing in Multiphase Microfluidics at Low Values of the Reynolds and the Capillary Numbers," Langmuir, vol. 19, pp. 9127-9133, 2003/10/01 2003.

[154] T. Ward, M. Faivre, M. Abkarian, and H. A. Stone, "Microfluidic flow focusing: Drop size and scaling in pressure versus flow-rate-driven pumping," Electrophoresis, vol. 26, pp. 3716-3724, Oct 2005.

[155] J. K. Nunes, S. S. Tsai, J. Wan, and H. A. Stone, "Dripping and jetting in microfluidic multiphase flows applied to particle and fiber synthesis," J Phys D Appl Phys, vol. 46, Mar 20 2013.

[156] C. Cramer, P. Fischer, and E. J. Windhab, "Drop formation in a co-flowing ambient fluid," Chemical Engineering Science, vol. 59, pp. 3045-3058, Aug 2004.

[157] T. Beatus, R. H. Bar-Ziv, and T. Tlusty, "The physics of 2D microfluidic droplet ensembles," Physics Reports-Review Section of Physics Letters, vol. 516, pp. 103-145, Jul 2012.

[158] A. B. Subramaniam, M. Abkarian, and H. A. Stone, "Controlled assembly of jammed colloidal shells on fluid droplets," Nat Mater, vol. 4, pp. 553-6, Jul 2005.

[159] A. J. Ribeiro, R. J. Neufeld, P. Arnaud, and J. C. Chaumeil, "Microencapsulation of lipophilic drugs in chitosan-coated alginate microspheres," Int J Pharm, vol. 187, pp. 115-23, Sep 30 1999.

[160] Y. Yamanishi, L. Feng, and F. Arai, "On-demand Production of Emulsion Droplets Over a Wide Range of Sizes," Advanced Robotics, vol. 24, pp. 2005-2018, 2010.

[161] Y. C. Tan and A. P. Lee, "Microfluidic separation of satellite droplets as the basis of a monodispersed micron and submicron emulsification system," Lab on a Chip, vol. 5, pp. 1178-1183, 2005.

[162] Y. Yamanishi, Y. Kihara, S. Sakuma, and F. Arai, "Active Size Controlled On-chip Droplet Dispensing by Magnetically Driven Microtool," 2009 Ieee-Rsj International Conference on Intelligent Robots and Systems, pp. 522-527, 2009.

[163] A. Golberg, M. L. Yarmush, and T. Konry, "Picoliter droplet microfluidic immunosorbent platform for point-of-care diagnostics of tetanus," Microchimica Acta, vol. 180, pp. 855-860, Jul 2013.

[164] J. J. Agresti, E. Antipov, A. R. Abate, K. Ahn, A. C. Rowat, J. C. Baret, et al., "Ultrahigh-throughput screening in drop-based microfluidics for directed evolution," Proc Natl Acad Sci U S A, vol. 107, pp. 4004-9, Mar 2 2010.

[165] I. Schrauwen, M. Sommen, J. J. Corneveaux, R. A. Reiman, N. J. Hackett, C. Claes, et al., "A sensitive and specific diagnostic test for hearing loss using a microdroplet PCR-based approach and next generation sequencing," Am J Med Genet A, vol. 161A, pp. 145-52, Jan 2013.

[166] D. Bardin, M. R. Kendall, P. A. Dayton, and A. P. Lee, "Parallel generation of uniform fine droplets at hundreds of kilohertz in a flow-focusing module," Biomicrofluidics, vol. 7, pp. -, 2013.

[167] S. Cho, D.-K. Kang, S. Sim, F. Geier, J.-Y. Kim, X. Niu, et al., "Droplet-Based Microfluidic Platform for High-Throughput, Multi-Parameter Screening of Photosensitizer Activity," Analytical Chemistry, vol. 85, pp. 8866-8872, 2013/09/17 2013.

[168] W. Li, J. Greener, D. Voicu, and E. Kumacheva, "Multiple modular microfluidic (M3) reactors for the synthesis of polymer particles," Lab Chip, vol. 9, pp. 2715-21, Sep 21 2009.

[169] S. L. Anna, N. Bontoux, and H. A. Stone, "Formation of dispersions using “flow focusing” in microchannels," Applied Physics Letters, vol. 82, pp. 364-366, 2003.

[170] N. Blow, "Microfluidics: in search of a killer application," Nature Methods, vol. 4, pp. 665-668, Aug 2007.

[171] J.-u. Shim, R. T. Ranasinghe, C. A. Smith, S. M. Ibrahim, F. Hollfelder, W. T. S. Huck, et al., "Ultrarapid Generation of Femtoliter Microfluidic Droplets for Single-Molecule-Counting Immunoassays," ACS Nano, vol. 7, pp. 5955-5964, 2013/07/23 2013.

[172] D. Bardin, T. D. Martz, P. S. Sheeran, R. Shih, P. A. Dayton, and A. P. Lee, "High-speed, clinical-scale microfluidic generation of stable phase-change droplets for gas embolotherapy," Lab Chip, vol. 11, pp. 3990-8, Dec 7 2011.

[173] D. Bardin, T. Martz, P. A. Dayton, and A. P. Lee, "High-speed microfluidic production of phase-change droplets for gas embolotherapy and as a novel on-chip pump," presented at the 15th International Conference on Miniaturized Systems for Chemistry and Life Sciences, Seattle, Washington, USA, 2011.

[174] M. Joanicot and A. Ajdari, "Applied physics. Droplet control for microfluidics," Science, vol. 309, pp. 887-8, Aug 5 2005.

[175] J. Hong, J. B. Edel, and A. J. deMello, "Micro- and nanofluidic systems for high-throughput biological screening," Drug Discov Today, vol. 14, pp. 134-46, Feb 2009.

[176] M. J. Sathe, S. S. Deshmukh, J. B. Joshi, and S. B. Koganti, "Computational Fluid Dynamics Simulation and Experimental Investigation: Study of Two-Phase Liquid-Liquid Flow in a Vertical Taylor-Couette Contactor," Industrial & Engineering Chemistry Research, vol. 49, pp. 14-28, Jan 6 2010.

[177] K. W. Moser, L. G. Raguin, A. Harris, H. D. Morris, J. Georgiadis, M. Shannon, et al., "Visualization of Taylor-Couette and spiral Poiseuille flows using a snapshot FLASH spatial tagging sequence," Magn Reson Imaging, vol. 18, pp. 199-207, Feb 2000.

[178] T. Nisisako and T. Torii, "Microfluidic large-scale integration on a chip for mass production of monodisperse droplets and particles," Lab Chip, vol. 8, pp. 287-93, Feb 2008.

[179] C. G. Yang, Z. R. Xu, A. P. Lee, and J. H. Wang, "A microfluidic concentration-gradient droplet array generator for the production of multi-color nanoparticles," Lab Chip, vol. 13, pp. 2815-20, Jul 21 2013.

[180] G. T. Vladisavljevic, I. Kobayashi, and M. Nakajima, "Production of uniform droplets using membrane, microchannel and microfluidic emulsification devices," Microfluidics and Nanofluidics, vol. 13, pp. 151-178, Jul 2012.

[181] L. Mazutis, A. F. Araghi, O. J. Miller, J. C. Baret, L. Frenz, A. Janoshazi, et al., "Droplet-Based Microfluidic Systems for High-Throughput Single DNA Molecule Isothermal Amplification and Analysis," Analytical Chemistry, vol. 81, pp. 4813-4821, Jun 15 2009.

[182] B. M. Paegel and G. F. Joyce, "Microfluidic compartmentalized directed evolution," Chem Biol, vol. 17, pp. 717-24, Jul 30 2010.

[183] Y. Zeng, R. Novak, J. Shuga, M. T. Smith, and R. A. Mathies, "High-performance single cell genetic analysis using microfluidic emulsion generator arrays," Anal Chem, vol. 82, pp. 3183-90, Apr 15 2010.

[184] J. Haun, J. Leonhardt, C. Portner, T. Hetzel, J. Tuerk, T. Teutenberg, et al., "Online and Splitless NanoLC x CapillaryLC with Quadrupole/Time-of-Flight Mass Spectrometric Detection for Comprehensive Screening Analysis of Complex Samples," Anal Chem, vol. 85, pp. 10083-90, Nov 5 2013.

[185] Macherey-Nagel Co.©, "CHROMAFIL® - Disposable filters from Macherey-Nagel," ed. Germany: Macherey-Nagel Co.©, 2013, pp. 17-18.

[186] C. N. Baroud, F. Gallaire, and R. Dangla, "Dynamics of microfluidic droplets," Lab Chip, vol. 10, pp. 2032-45, Aug 21 2010.

[187] H. Gu, M. H. Duits, and F. Mugele, "Droplets formation and merging in two-phase flow microfluidics," Int J Mol Sci, vol. 12, pp. 2572-97, 2011.

[188] Harvard Apparatus©, "Harvard Apparatus Pumps, legendary performance for every application," in Syringe Pumps, Pump 11 Elite, ed. United States: Harvard Apparatus©, 2013, pp. 11-14.

[189] (2013, 17th of November). ImageJ® (Image Processing and Analysis in Java) (Version 1.48g ed.) [Free software]. Available: http://rsbweb.nih.gov/ij/index.html

[190] Huntsman Advanced Materials GmBH©, "Araldite® 2012 Two component epoxy paste adhesive," in Advanced Materials, ed. Switzerland: Huntsman Advanced Materials GmBH©, 2012, pp. 1-5.

[191] P. J. Kitson, M. H. Rosnes, V. Sans, V. Dragone, and L. Cronin, "Configurable 3D-Printed millifluidic and microfluidic 'lab on a chip' reactionware devices," Lab Chip, vol. 12, pp. 3267-71, Sep 21 2012.

[192] Y. Cheng, X. Luo, C. Y. Tsao, H. C. Wu, J. Betz, G. F. Payne, et al., "Biocompatible multi-address 3D cell assembly in microfluidic devices using spatially programmable gel formation," Lab Chip, vol. 11, pp. 2316-8, Jul 21 2011.

[193] D. Therriault, S. R. White, and J. A. Lewis, "Chaotic mixing in three-dimensional microvascular networks fabricated by direct-write assembly," Nat Mater, vol. 2, pp. 265-71, Apr 2003.

[194] M. D. Symes, P. J. Kitson, J. Yan, C. J. Richmond, G. J. Cooper, R. W. Bowman, et al., "Integrated 3D-printed reactionware for chemical synthesis and analysis," Nat Chem, vol. 4, pp. 349-54, May 2012.

[195] "ProJetTM HD 3000 Technical Specifications," in High Definition 3-D Modeling, ed: 3D Systems Corporation, 2009, pp. 1-2.

[196] Dow Corning Corporation. Material Safety Data Sheet: Sylgard (R) 170 Silicone Elastomer Kit [Online]. Available: http://www1.dowcorning.com/DataFiles/090007b2817dde67.pdf

[197] W. Lee, L. M. Walker, and S. L. Anna, "Role of geometry and fluid properties in droplet and thread formation processes in planar flow focusing," Physics of Fluids, vol. 21, Mar 2009.

[198] Z. H. Nie, M. S. Seo, S. Q. Xu, P. C. Lewis, M. Mok, E. Kumacheva, et al., "Emulsification in a microfluidic flow-focusing device: effect of the viscosities of the liquids," Microfluidics and Nanofluidics, vol. 5, pp. 585-594, Nov 2008.

[199] P. Garstecki, H. A. Stone, and G. M. Whitesides, "Mechanism for flow-rate controlled breakup in confined geometries: A route to monodisperse emulsions," Physical Review Letters, vol. 94, Apr 29 2005.

[200] V. Cristini and Y. C. Tan, "Theory and numerical simulation of droplet dynamics in complex flows - a review," Lab on a Chip, vol. 4, pp. 257-264, 2004.

[201] Y. Li, M. Jain, and K. Nandakumar, "Numerical Study of Droplet Formation inside a Microfluidic Flow-Focusing Device," in COMSOL Conference, Boston, United States, 2012, pp. 1-6.

[202] P. He, H. Kim, D. Luo, and Z. Cheng, "Numerical Study of Droplet Formation Patterns in Flow Focusing Microfluidics," in The 2008 Spring National Meeting, 2008.

[203] P. He, H. Kim, D. Luo, and Z. Cheng, "Numerical Simulation on the Modes of Droplet Formation in Flow Focusing Microfluidics Device," in The 2007 Annual Meeting, 2007.

[204] R. Bhardwaj, X. H. Fang, and D. Attinger, "Pattern formation during the evaporation of a colloidal nanoliter drop: a numerical and experimental study," New Journal of Physics, vol. 11, Jul 31 2009.

[205] S. Bashir, J. M. Rees, and W. B. Zimmerman, "Simulations of microfluidic droplet formation using the two-phase level set method," Chemical Engineering Science, vol. 66, pp. 4733-4741, 10/15/ 2011.

[206] T. Fu, Y. Wu, Y. Ma, and H. Z. Li, "Droplet formation and breakup dynamics in microfluidic flow-focusing devices: From dripping to jetting," Chemical Engineering Science, vol. 84, pp. 207-217, 12/24/ 2012.

[207] "Super Flangeless™ Fittings," in Upchurch Scientific Fittings, ed: IDEX Health & Science Web Store, 2013, pp. 21-23.

[208] E. Lobry, F. Theron, C. Gourdon, N. Le Sauze, C. Xuereb, and T. Lasuye, "Turbulent liquid-liquid dispersion in SMV static mixer at high dispersed phase concentration," Chemical Engineering Science, vol. 66, pp. 5762-5774, Dec 1 2011.

[209] L. Mazutis and A. D. Griffiths, "Selective droplet coalescence using microfluidic systems," Lab on a Chip, vol. 12, pp. 1800-1806, 2012.

8 APPENDICES

Appendix I: The four-stage layout design of the main chip

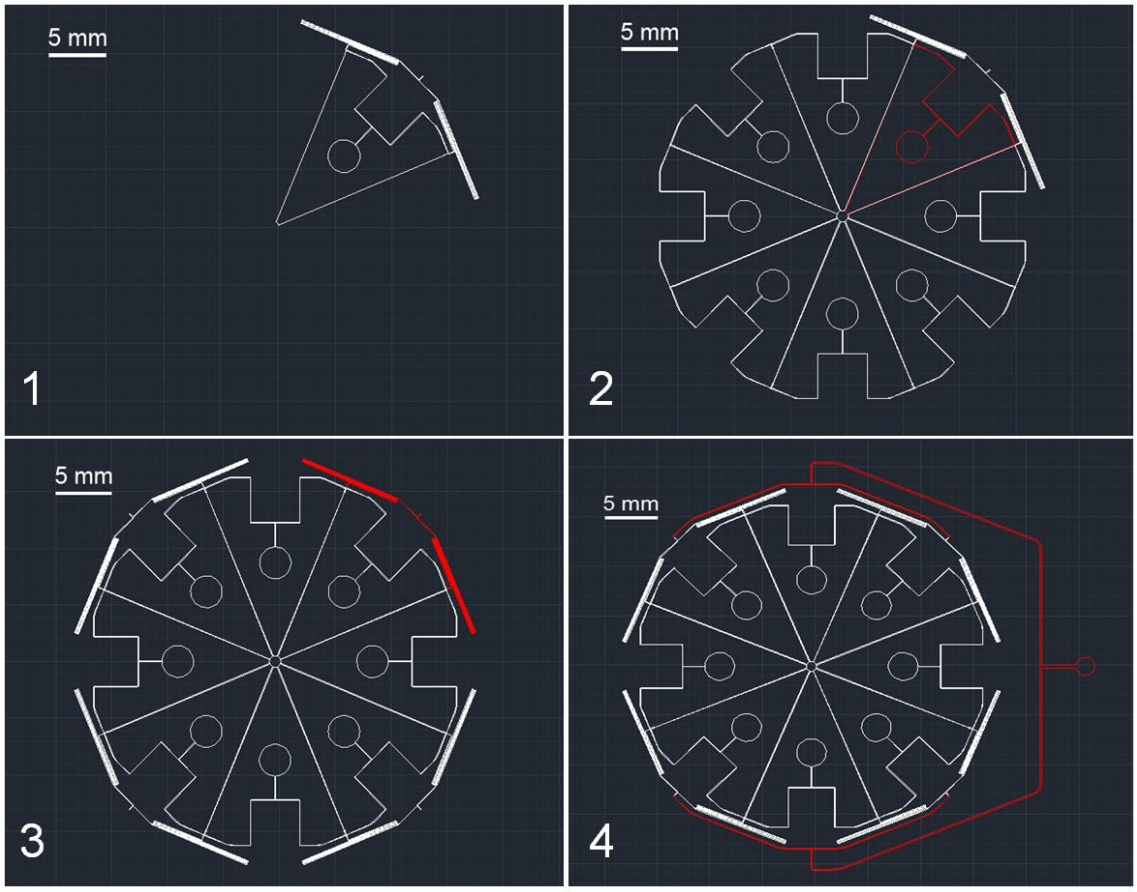

Figure 8.1. The procedure for drawing the layout of main chip utilizing AutoCAD® through circular array command. (1) Drawing an entire sector of the design, (2) utilization of "polar array" command in AutoCAD® and creating eight symmetric sectors making a whole circular device, (3) again utilization of "polar array" for serpentines and making four serpentine systems, and (4) adding remaining channels.

Appendix II: Width details of the initial main chip layout

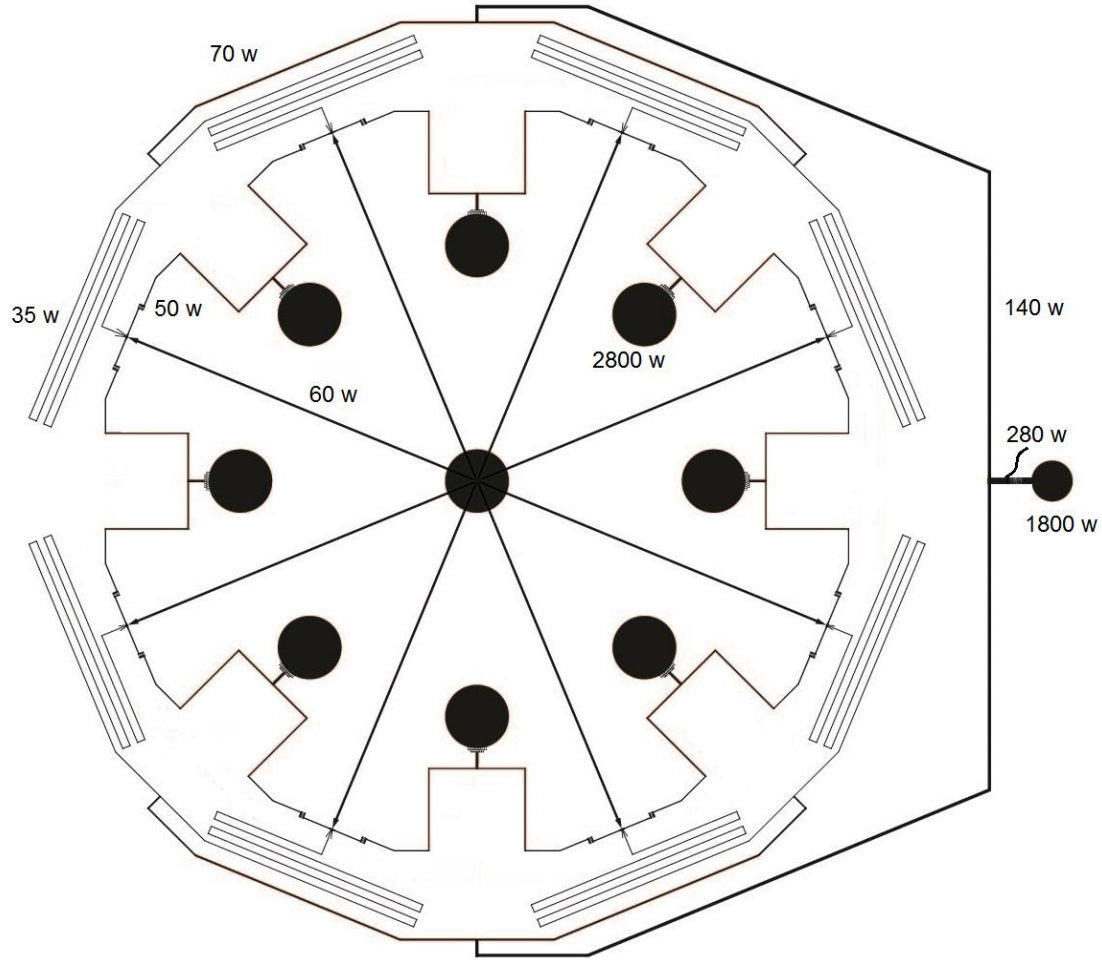

Figure 8.2. Detailed initial layout of the main chip indicating the width of every channel.

Appendix III: Technical issues of the fabricated masters

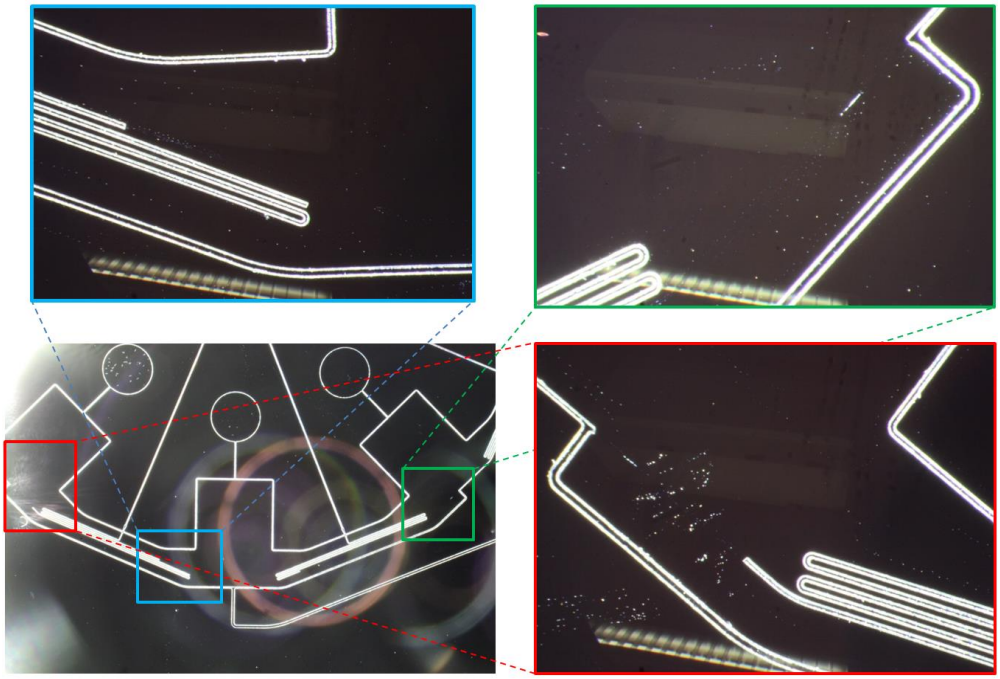

Figure 8.3. A closed-up view of the master for the main chip after first try of fabrication at showing the issues, fractionas and missing channels.

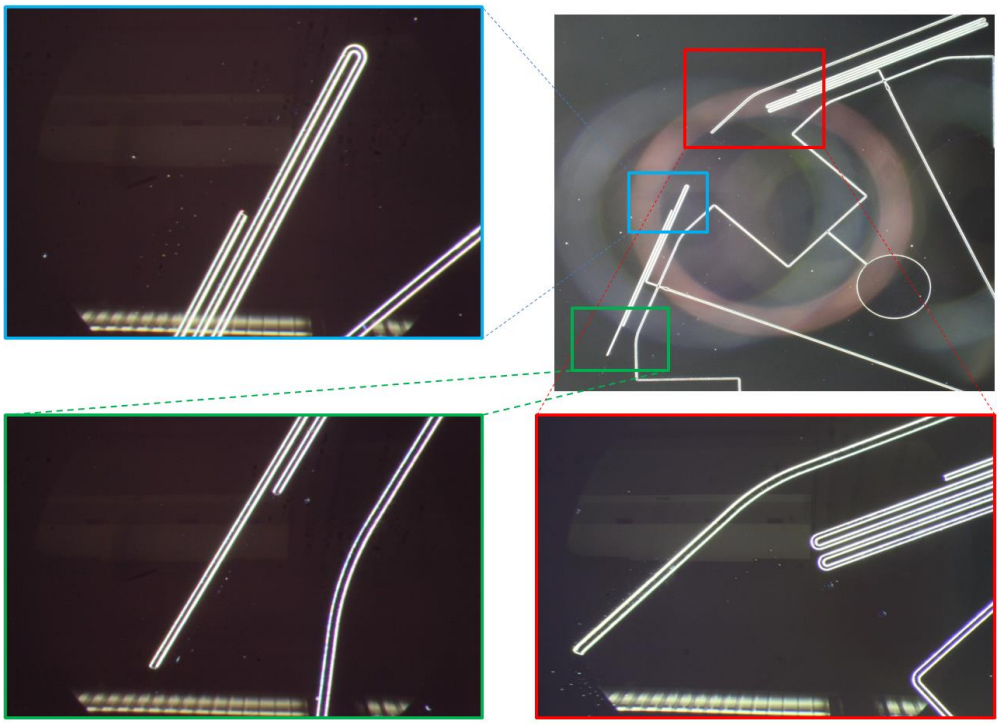

Figure 8.4. A closed-up view of the master for the main chip after second try of fabrication showing the issues, fractionas and missing channels.

Appendix IV: First fabricated multi-layer PDMS device

In this module, a simple blank PDMS slab is used as the substrate and the entire three-layer PDMS device is bonded (stuck) against a glass slide.

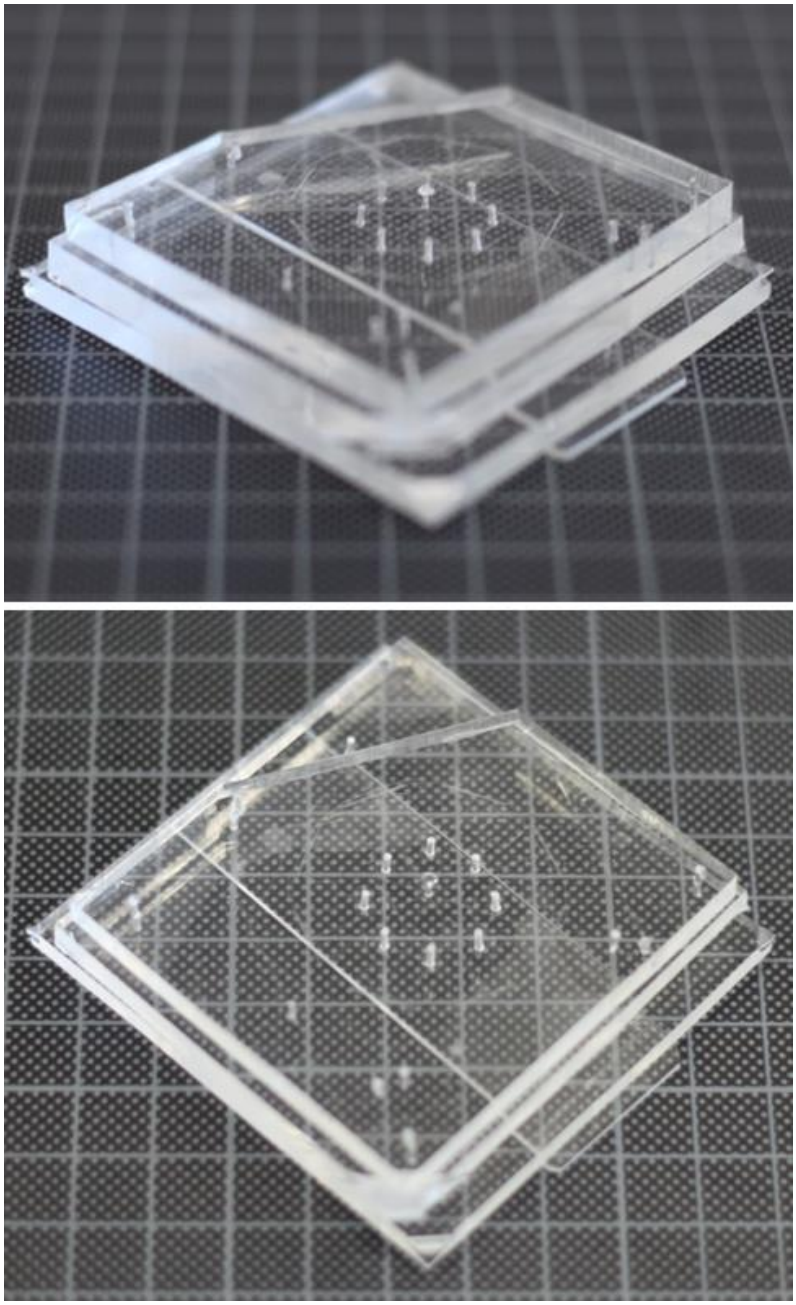

Figure 8.5. First fabricated three-layer device having the substrate of a PDMS slab.

Appendix V: Filtration of the fluids prior to inject into the microfluidic device

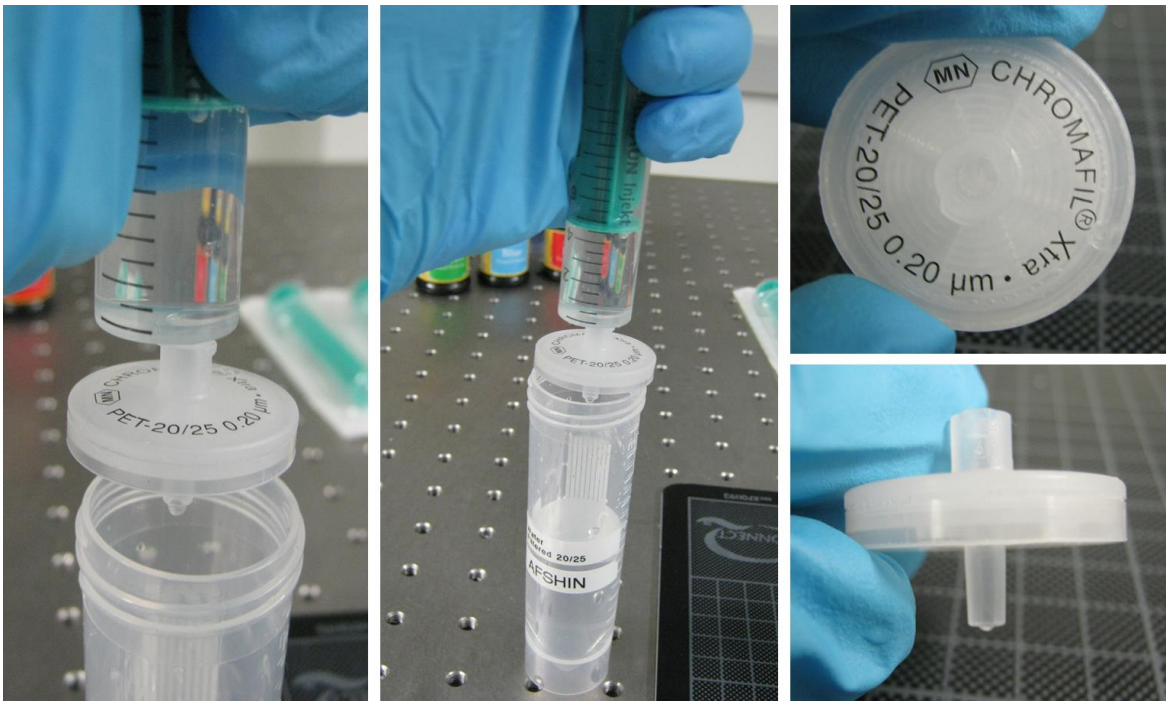

Figure 8.6. Filtration of the fluids: test operation and a sample of used filter.

Appendix VI: High-speed camera apparatus and related sections

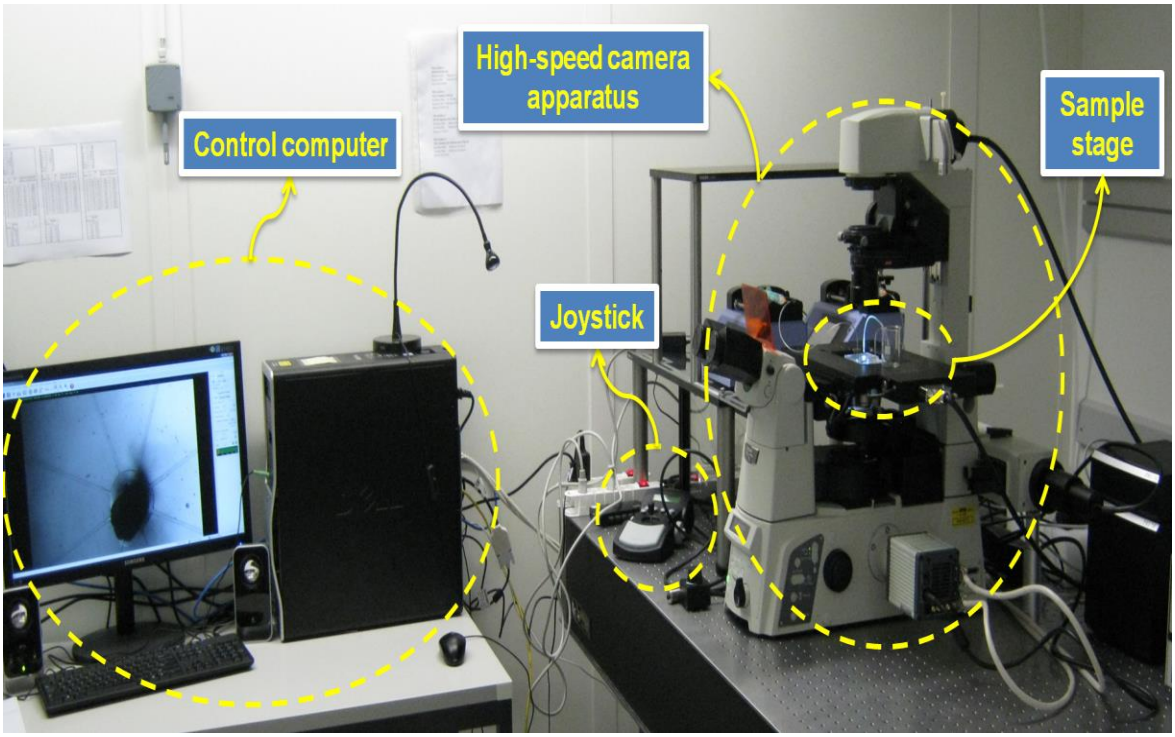

Figure 8.7. High-speed camera apparatus and related belongings and sections.

Appendix VII: Fabricated devices with fixed inlet pins and tubing

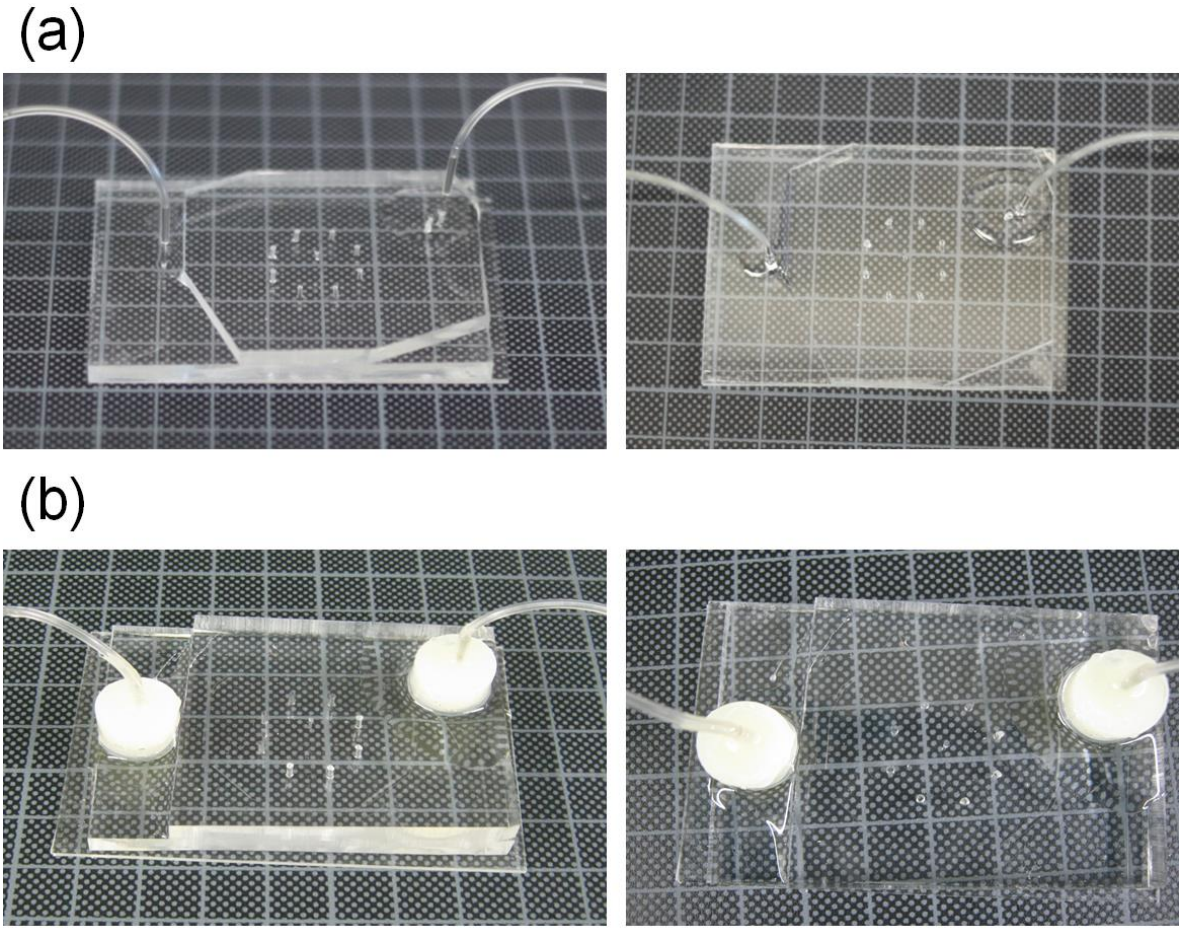

Figure 8.8. Fabricated devices as the result of new protocols for fixing the inlet pins (a) applying uncured PDMS, and (b) applying glue and uncured PDMS over it.

Appendix VIII: 3D printed holding frame, belongings and species

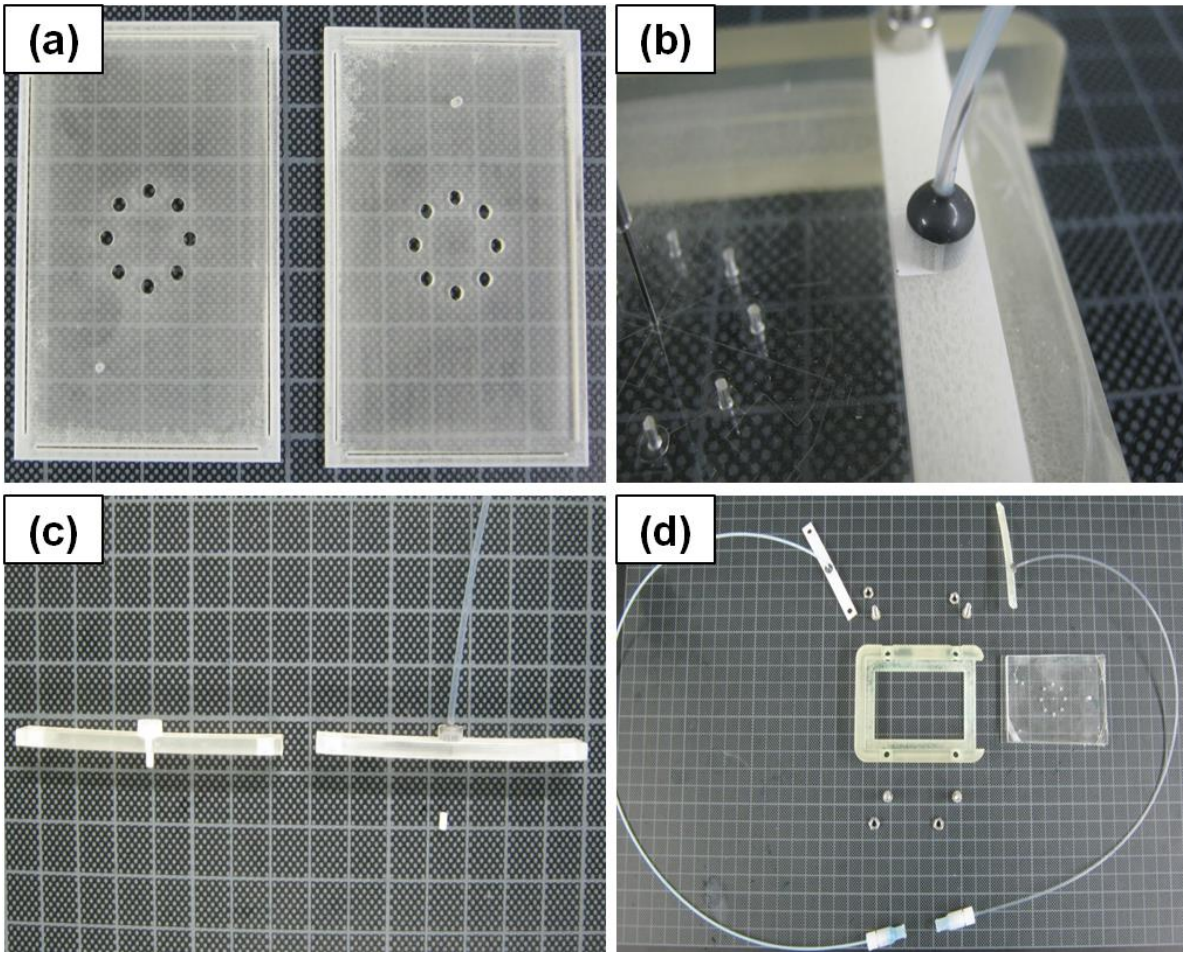

Figure 8.9. (a) Measuring assistant sheets for cutting the PDMS devices, (b) special fitting reinforced by Sylgard-170® for a 3D printed holding frame, (c) a healthy and a damaged bar of a 3D printed holding frames, and (d) all the required pieces prior to installation of a PDMS device into a 3D printed holding frame.

Appendix IX: Purchased peristaltic pumps along with all the accessories.

Figure 8.10. Two purchased identical peristaltic pumps and their accessories.

Appendix X: Purchased servo motor as well as all the accessories.

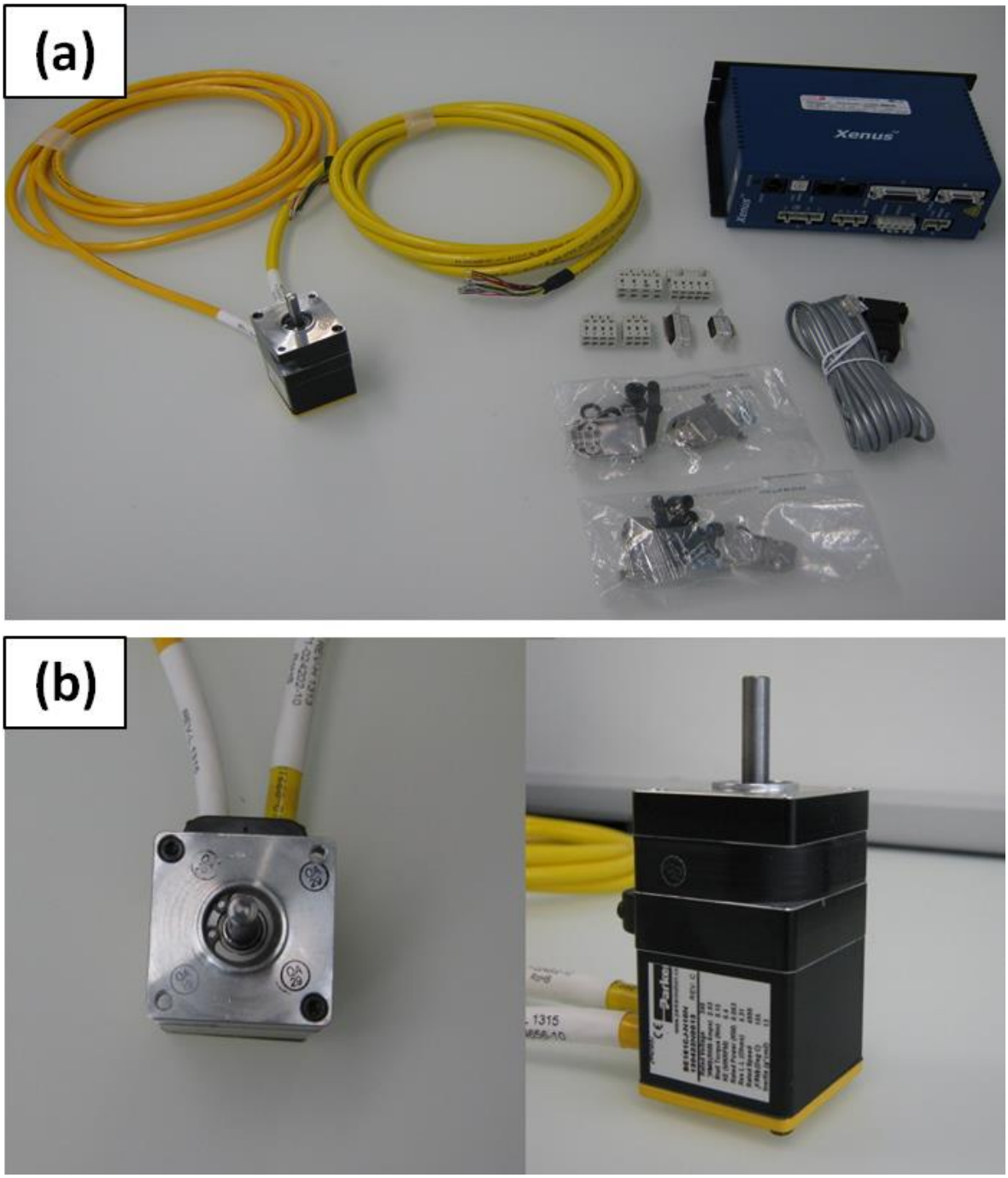

Figure 8.11. (a) The purchased servo motor with all the accessories, and (b) the motor from side and up view.

Appendix XI: The initial results of optimization for the gap width and also inner cylinder radius.

Table 8.1. The results of optimization for gap width where the cells marked with green and red indicate the acceptable and rejected set of results.

d_p (m)	μ_p (Pa.S)	μ_c (Pa.S)	ρ_c (kg/m^3)	Ω_i (rad/s)	σ (N/m)	r_i (m)	Gap width (mm)
0.00007	$4.65 \cdot 10^3$	$1.002 \cdot 10^3$	998.2	41.67	0.05206	0.03	0.01
0.00007	$4.65 \cdot 10^3$	$1.002 \cdot 10^3$	998.2	41.67	0.05206	0.05	0.03
0.00007	$4.65 \cdot 10^3$	$1.002 \cdot 10^3$	998.2	41.67	0.05206	0.07	0.08
0.00007	$4.65 \cdot 10^3$	$1.002 \cdot 10^3$	998.2	41.67	0.05206	0.09	0.17
0.00007	$4.65 \cdot 10^3$	$1.002 \cdot 10^3$	998.2	41.67	0.00285	0.03	0.10
0.00007	$4.65 \cdot 10^3$	$1.002 \cdot 10^3$	998.2	41.67	0.00285	0.05	0.51
0.00007	$4.65 \cdot 10^3$	$1.002 \cdot 10^3$	998.2	41.67	0.00285	0.07	1.44
0.00007	$4.65 \cdot 10^3$	$1.002 \cdot 10^3$	998.2	41.67	0.00285	0.09	3.13
0.00007	$4.65 \cdot 10^3$	$1.002 \cdot 10^3$	998.2	62.50	0.05206	0.03	0.01
0.00007	$4.65 \cdot 10^3$	$1.002 \cdot 10^3$	998.2	62.50	0.05206	0.05	0.07
0.00007	$4.65 \cdot 10^3$	$1.002 \cdot 10^3$	998.2	62.50	0.05206	0.07	0.20
0.00007	$4.65 \cdot 10^3$	$1.002 \cdot 10^3$	998.2	62.50	0.05206	0.09	0.43
0.00007	$4.65 \cdot 10^3$	$1.002 \cdot 10^3$	998.2	62.50	0.00285	0.03	0.27
0.00007	$4.65 \cdot 10^3$	$1.002 \cdot 10^3$	998.2	62.50	0.00285	0.05	1.30
0.00007	$4.65 \cdot 10^3$	$1.002 \cdot 10^3$	998.2	62.50	0.00285	0.07	3.68
0.00007	$4.65 \cdot 10^3$	$1.002 \cdot 10^3$	998.2	62.50	0.00285	0.09	7.98

Appendix XII: All the pieces, parts and the accessories of the Taylor-Couette device prior to assembling.

Figure 8.12. The parts of Taylor-Couette device ready for assembling.

Appendix XIII: The constructed Taylor-Couette double-cylinder device.

Figure 8.13. The constructed optimized Taylor-Couette device for droplet generation.